Steam Flow Distribution in Air-Cooled Condenser for Power Plant Application

Werner Honing

Thesis presented in partial fulfillment of the requirements for the degree of Master of Science in Engineering (Mechanical) at Stellenbosch University

Thesis Supervisor: Prof D.G. Kröger

September 2009

Declaration

By submitting this thesis electronically, I declare that the entirety of the work contained therein is my own, original work, that I am the owner of the copyright thereof (unless to the extent explicitly otherwise stated) and that I have not previously in its entirety or in part submitted it for obtaining any qualification.

Signature: .....

Abstract

Air-cooled steam condensers are used in arid regions where adequate cooling water is not available or very expensive. In this thesis the effect of steam-side and air-side effects on the condenser performance, steam distribution and critical dephlegmator length is investigated for air-cooled steam condensers as found in power plants. Solutions are found so that no backflow is present in the condenser. Both single and two-row condensers are investigated.

The tube inlet loss coefficients have the largest impact on the critical dephlegmator tube length in both the single and two-row condensers. The critical dephlegmator tube lengths were determined for different dividing header inlet geometries and it was found that a step at the inlet to the dividing header resulted in the shortest tubes.

Different ambient conditions were found to affect the inlet steam temperature, the steam flow distribution, heat rejection distribution and the critical dephlegmator length for the single and two-row condensers. There were differences in the steam mass flow distributions for the single and two-row condensers with opposite trends being present in parts of the condenser. The single-row condenser's critical dephlegmator tube lengths were shorter than those of the two-row condenser for the same ambient conditions. Areas of potential backflow change with different ambient conditions and also differ between a single and two-row condenser. The two-row condenser always have an area of potential backflow for the first row at the first condenser fan unit.

Opsomming

Droë lug-verkoelde stoom kondensors word gebruik in droë gebiede waar genoegsame verkoelingswater nie beskikbaar is nie of baie duur is. In hierdie tesis word die effek van stoomkant en lugkant effekte op die vermoë van die kondensor, die stoomvloeiverdeling en kritiese deflegmator lengte ondersoek vir lug-verkoelde stoom kondensors soos gevind in kragstasies. Dit word opgelos sodat daar geen terugvloei in enige van die buise is nie. ’n Enkel- en dubbelry kondensor word ondersoek.

Die inlaatverlieskoëffisiënte van die buise het die grootste impak op die lengte van die kritiese deflegmator buise in beide die enkel- en dubbelry kondensors. Die kritiese deflegmator buis lengtes is bereken vir verskillende verdeelingspyp inlaat geometrië en dit is gevind dat ’n trap by die inlaat van die verdeelingspyp die kortste buise lewer.

Dit is gesien dat verskillende omgewingskondisies die inlaat stoom temperatuur, die stoomvloeiverdeling, die warmteoordrag verdeling en die kritiese lengte van die deflegmator buise vir die enkel- en dubbelry kondensor. Daar was verskille tussen die stoomvloeiverdelings vir die enkel- en dubbelry met teenoorgestelde neigings in dele van die kondensor. Die kritiese deflegmator buis lengte vir die enkelry kondensor was korter as die vir die dubbelry kondensor vir dieselfde omgewingskondisies. Die areas in die kondensor waar terugvloei moontlik kan plaasvind in die kondensor verander met ongewingskondisies en verskil vir die enkel- en dubbelry kondensers. Die dubbelry kondensor het altyd ’n area van moontlike terugvloei vir die eerste buisry by die eerste kondensor waaiereenheid.

Acknowledgements

To Prof Kröger, thank you for all your patience and support, for your hard words and those of encouragement. Without your support this would not have been possible.

To my parents who supported me throughout the course of my thesis. Thank you for all that you have done.

To everyone who supported me during the course of my thesis, I appreciate the support that was given to me. There are those who contributed more towards the completion of my thesis and I would like to thank them very much for the effort that was given so freely.

To Dr A van Heerden, thank you for listening.

Table of Contents

Nomenclature

A	Area, m^2
a	Coefficient, or length, m, or relaxation factor
b_T	Exponent
c	Constant for directional use in manifold theory
c_p	Specific heat at constant pressure, J/kgK
c_v	Specific heat at constant volume, J/kgK
DALR	Dry adiabatic lapse rate, K/m
d	Diameter, m
d_e	Hydraulic diameter, m
e	Effectiveness
F	Force, N
f	Friction factor
G	Mass velocity, kg/sm^2
g	Gravitational acceleration, m/s^2
H	Height, m
h	Heat transfer coefficient, W/m^2K
i	Enthalpy, J/kg
i_{vw}	Latent heat, J/kg
I	Integral
K	Loss coefficient
k	Thermal conductivity, W/mK
L	Length, m
m	Mass flow rate, kg/s
N	Revolutions per minute, $minute^{-1}$
n	Number or exponent
Ny	Characteristic heat transfer parameter, m^{-1}
P	Power, W
P_e	Perimeter, m
p	Pressure, N/m^2
Q	Heat transfer rate, W
r	Recirculation factor
R	Thermal resistance m^2K/W
Ry	Characteristic flow parameter, m^{-1}
r	Radius, m, or recirculation factor
T	Temperature, °C or K
U	Overall heat transfer coefficient, W/m^2K
V	Volume flow rate, m^3/s
v	Speed, m/s
W	Width, m
x	Quality
z	Elevation, m

Greek symbols

α	Void fraction, momentum velocity distribution correction factor, or overall momentum correction factor
γ	Specific heat ratio
Δ	Differential
δ	Film thickness, m
ε	Surface roughness, m
η	Efficiency
θ	Angle, °
μ	Dynamic viscosity, kg/ms
ρ	Density, kg/m^3
Σ	Summation
σ	Area ratio, or surface tension, N/m^2
τ	Shear stress, N/m^2
ϕ	Angle, °

Subscripts

a	Air, or based on air side
amb	Ambient
b	Bundle, or bend, or exponent
bm	Miter bend
c	Combining header, or casing, or condensate, or contraction
cs	Cross section
D	Darcy
d	Dividing header, or dephlegmator
do	Downstream
ds	Steam duct
e	Effective, or expansion
F	Fan
f	Fin, fluid, or friction
fr	Frontal
h	Homogeneous, or header
he	Heat exchanger
i	Inlet, or inside
id	Ideal
ir	Recirculation inlet temperature
j	Jet, or junction
L	Left hand side
l	Liquid, or tube length, or lateral
m	Mean, middle or momentum
n	Normal
o	Outlet
or	Recirculation outlet temperature
p	Constant pressure, or plume, or passes
pl	Plenum chamber
R	Right hand side
r	Root, or rounded, or rejected, or recirculation, or reducer, or reference
red	Reducer
s	Static, or steam

si	Inlet shroud
T	Total
t	Tube
tp	Two-phase
ts	Tube cross section, or tower support
v	Vapor
w	Water, or windwall
wb	Wet-bulb
z	Co-ordinate
θ	Inclined

Dimensionless groups

Fr	Froude number, $\mathrm{Fr} = \frac{v^2}{dg}$
Fr_{Dw}	Densimetric Froude number, $\frac{\rho v^2}{\Delta\rho dg}$
Oh	Ohnesorge number, $\frac{\mu}{\sigma\rho d_e^{\,0.5}}$
Pr	Prandtl number, $\frac{\mu c_p}{k}$
Re	Reynolds number, $\frac{\rho vL}{\mu}$ for plate, $\frac{\rho vd}{\mu}$ for a tube

Constants

$g = 9.8\ m/s^2$ Gravitational acceleration

$R = 287.08\ J/kgK$ Gas constant for air

Chapter 1: Introduction

Air-cooled heat exchangers are used in arid regions where adequate cooling water is not available or very expensive. Air is used to cool the process fluid and the heat is rejected to the atmosphere. Different configurations of air-cooled heat exchangers are used in the industry (Kröger 2004). In this study the A-frame forced draft configuration will be used.

In direct air-cooled steam condensers (ACC), as found in power plants, the process fluid is steam. Figure 1.1 is a schematic of a power plant cycle using a direct air-cooled steam condenser. Steam is generated by the boiler and then passes through the turbine. At the low pressure side of the turbine the steam enters the exhaust steam duct system and directs the steam to the condenser where it is distributed into finned tubes configured in A-frames where the steam condenses. The condensate is collected in a tank and pumped back to the boiler. The A-frame configuration is used to minimize the ground surface area and to help with condensate drainage. A fan is situated underneath the A-frame and forces air over the finned tubes.

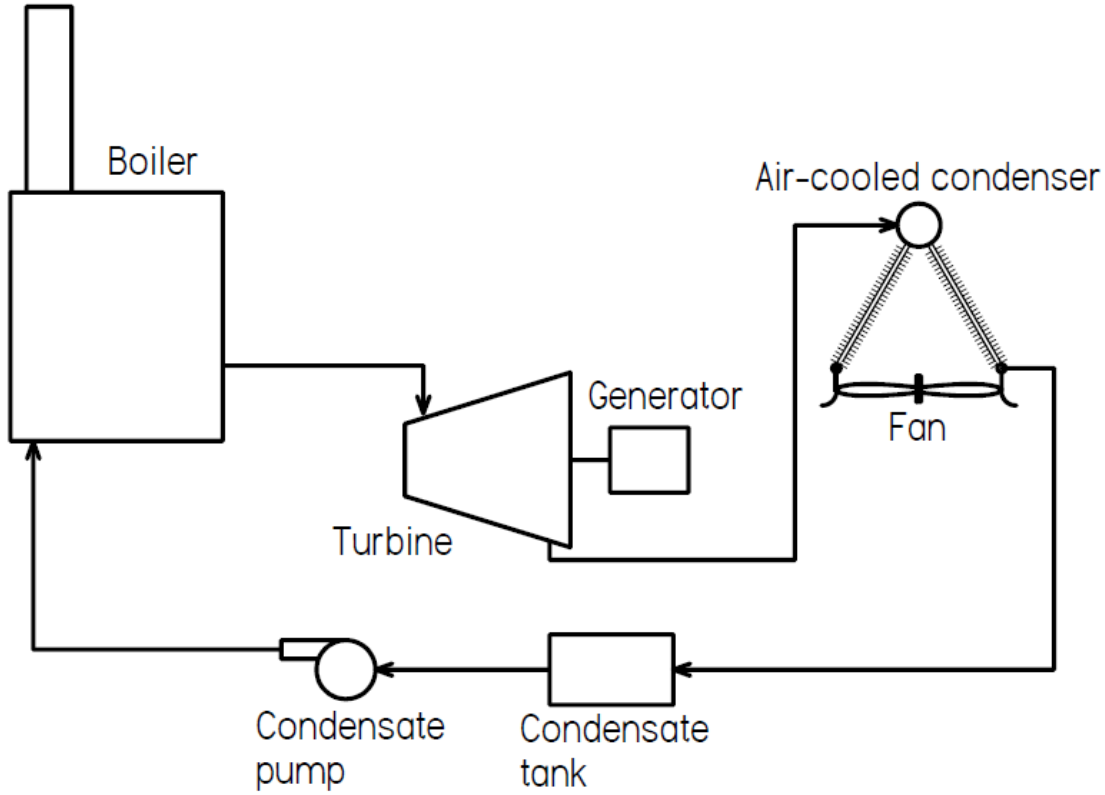

Figure 1.1: Cycle for a power plant incorporating a direct air-cooled steam condenser

There are several ambient effects that have a detrimental effect on the performance of the condenser. These include ambient temperature distributions, wind speed, wind direction and recirculation of hot plume air. Similarly steam side effects include variation in lateral or finned tube inlet loss coefficients and overall

momentum correction factor effects. The effect of these parameters on the performance of the condenser, the steam distributions and the corresponding critical dephlegmator tube lengths are investigated in this thesis.

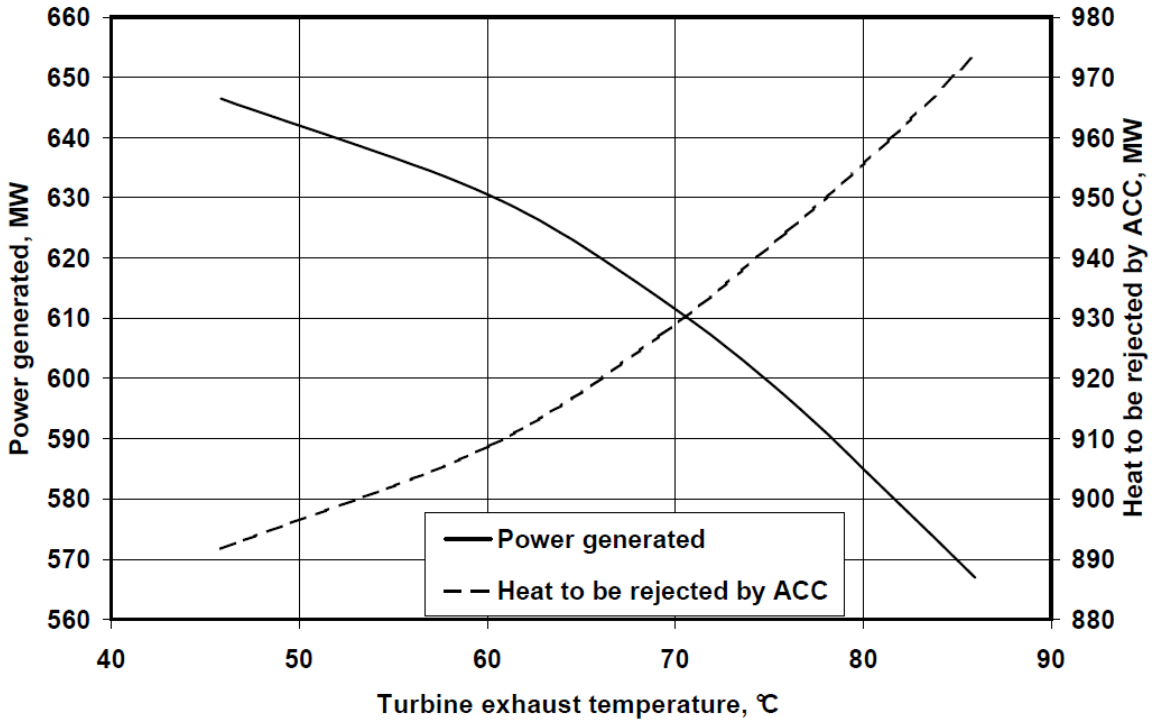

Figure 1.2: Characteristic curves of turbine

The characteristic of a particular power station turbine is shown in figure 1.2. The air-cooled condenser must be sized according to the turbine and the ambient conditions to ensure that sufficient heat can be rejected under all operating conditions.

As the turbine exhaust temperature increases the power generated decreases and the heat that must be rejected increases. This is due to the reduction in efficiency of the turbine. When ambient conditions reduce the effectiveness of the condenser, the steam temperature must increase to reject the needed heat and less power will be generated. A better understanding of these effects on the ACC will result in better design specifications for ACC's.

Chapter 2: Flow analysis of steam in air-cooled condenser

2.1 Introduction

In figure 1.1 steam exits the turbine and flows to the condenser. A turbine unit, with characteristics as seen in figure 1.2, exhausts into two symmetrical ducts which leads to an air-cooled condenser unit. An example of one of these ducts and half of an air-cooled condenser unit is shown in figure 2.1. The steam flows through the steam duct to the dividing header. The header distributes the steam to the finned tubes where condensation takes place. The condensate and excess steam is collected in the combining header. The excess steam is condensed in the dephlegmator fan unit and the non-condensable gasses are extracted by a vacuum pump.

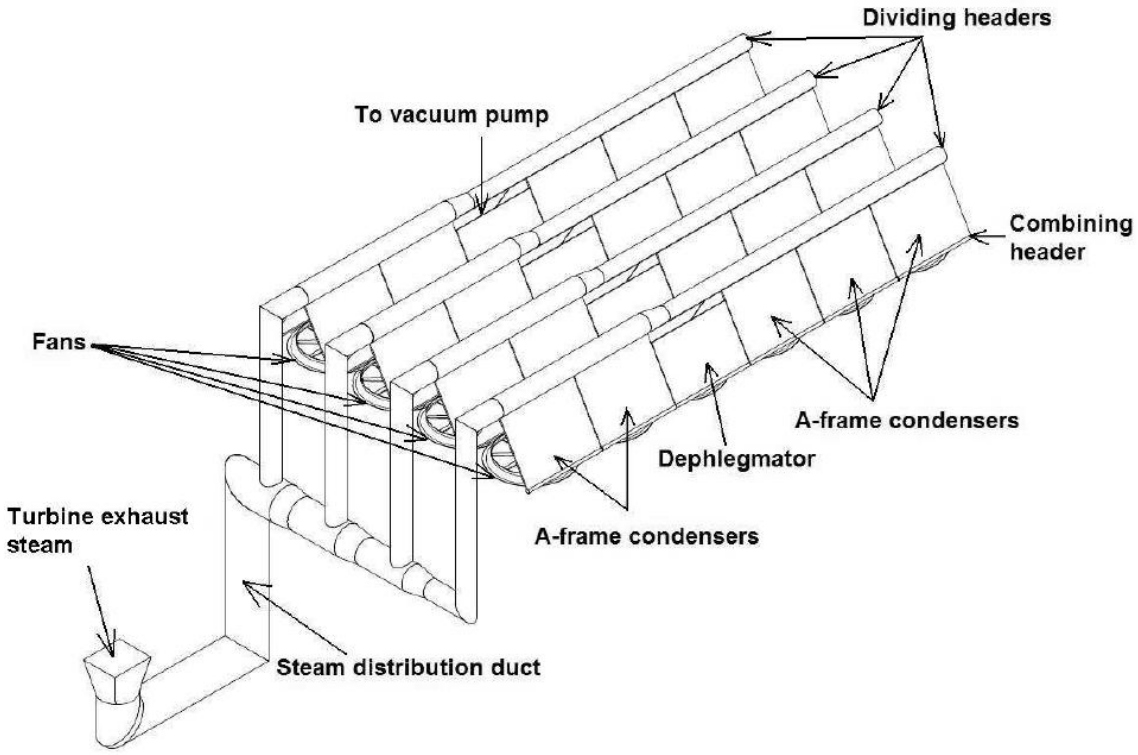

Figure 2.1: Schematic of an air-cooled condenser

In this chapter a thermal-flow analysis of an air-cooled steam condenser is presented. Initially a thermal-flow analysis of the steam duct is presented after which the condenser and dephlegmator units are analyzed.

2.2 Supply steam duct

The steam duct system in an air-cooled steam condenser connects the turbine exhaust and the air-cooled steam condenser. In the steam duct there are pressure changes due to friction, elevation changes, pipe components and momentum changes. These pressure changes cause the steam temperature to change. It is

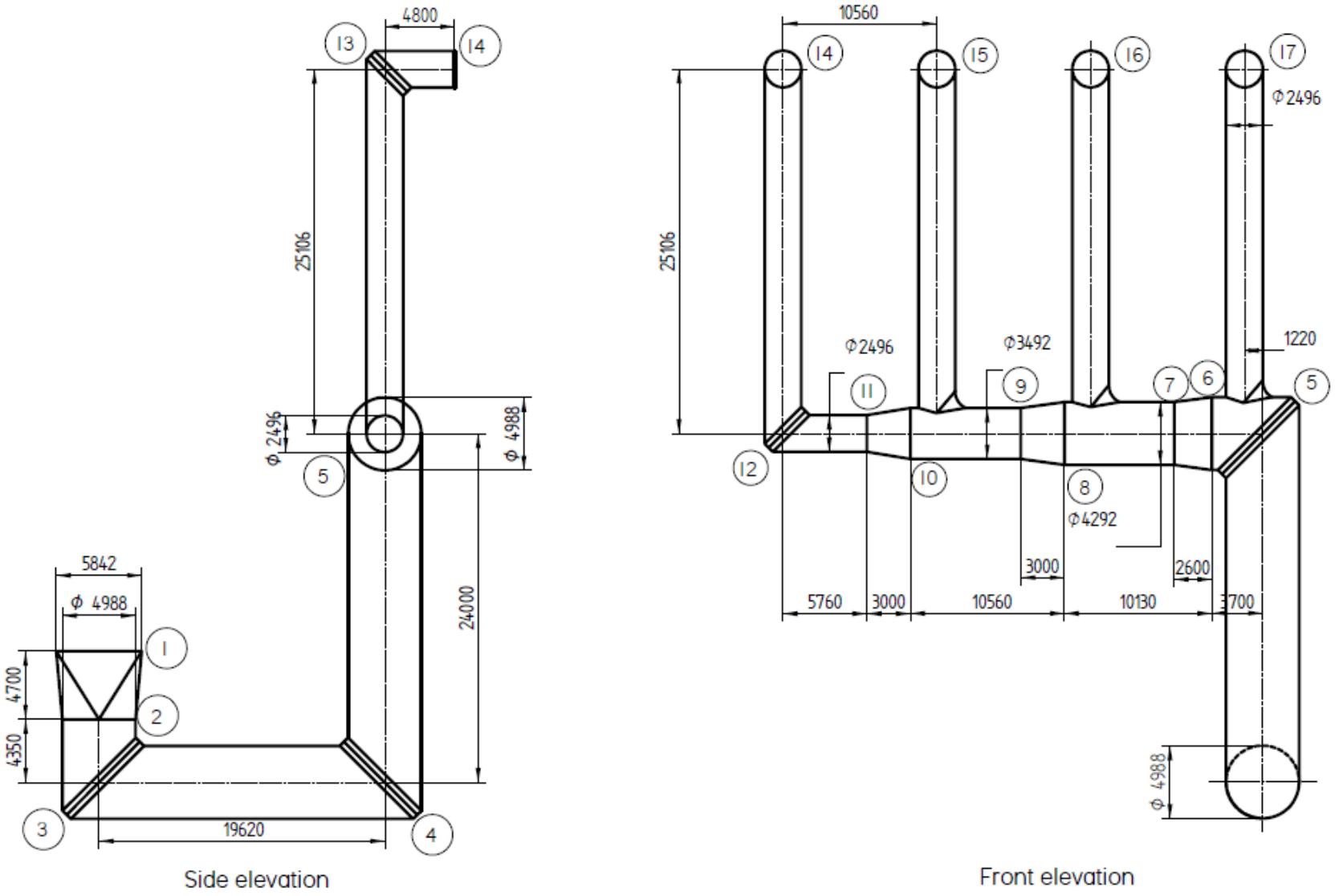

Figure 2.2: Schematic drawing of a steam duct system

therefore necessary to determine the pressure change in the duct system so that the steam temperature in the condenser can be determined in order to determine the ability of the condenser to reject heat. The flow characteristics of the different duct sections will be analyzed. It will be assumed that the flow is essentially incompressible and that the velocity distribution is uniform in each section. For purposes of illustration consider the steam duct system shown in figure 2.2.

2.2.1 Momentum theorem

Real flows in ducts are usually not isentropic because of frictional effects.

Consider steady upward flow through the elementary control volume of a vertical duct as shown in figure 2.3.

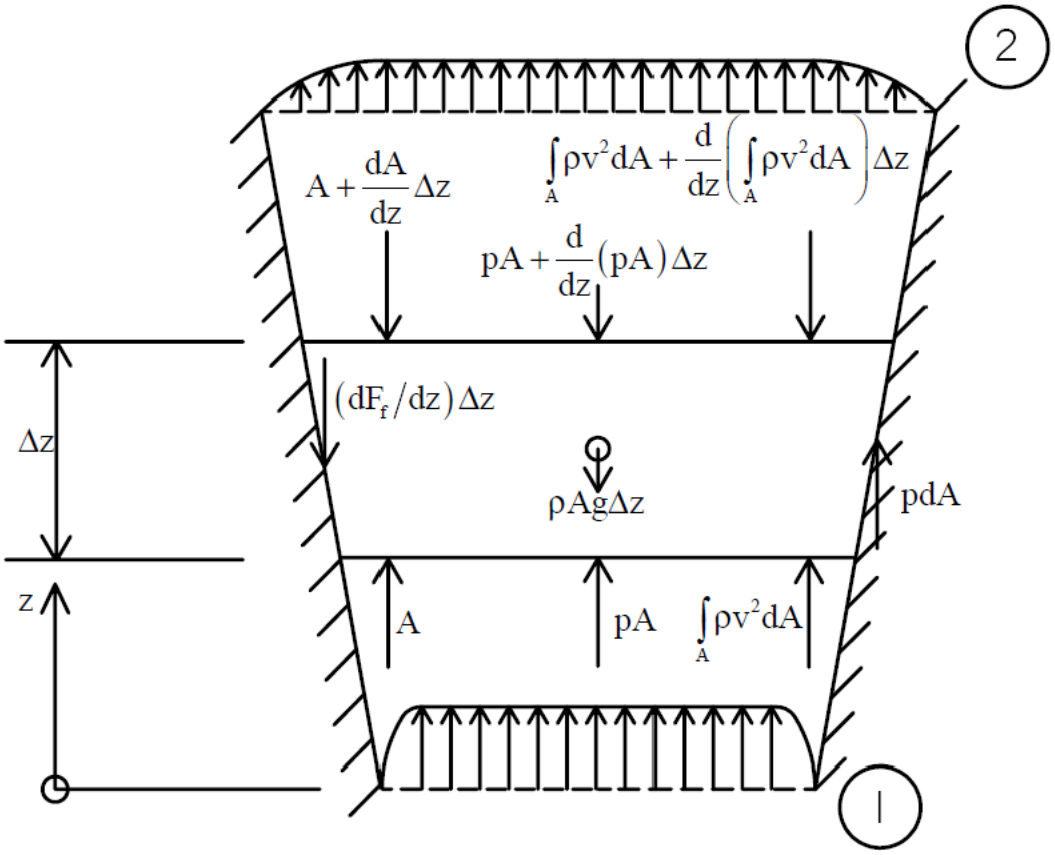

Figure 2.3: Elementary control volume in a vertical duct

It follows from Newton's second law of motion that the net force due to pressure, friction and gravity acting on the fluid within the elementary control volume, is equal to the difference in momentum between the outgoing and incoming flow, i.e.

$$pdA-\frac{d\ pA}{dz}\Delta z-\frac{dF_f}{dz}\Delta z-\rho gA\Delta z=\frac{d}{dz}\left(\int_A \rho v^2 dA\right)\Delta z$$

$$-A\frac{dp}{dz}\Delta z-\frac{dF_f}{dz}\Delta z-\rho gA\Delta z=\frac{d}{dz}\ \alpha_m \rho v^2 A\ \ \Delta z \qquad (2.1)$$

where the momentum velocity distribution correction factor is defined as

$$\alpha_m = \int v^2 dA \Big/ v_m^2 A \qquad (2.2)$$

If the velocity distribution at any cross-section of the duct is uniform then $\alpha_m = 1$.

With $\alpha_m = 1$ integrate equation (2.1) between sections 1 and 2 to find the pressure differential

$$p_2 - p_1 = -\int_1^2 \frac{dF_f}{A} - \int_1^2 \rho g dz - \left(\frac{\rho_2 v_2^2}{2} - \frac{\rho_1 v_1^2}{2} \right) \qquad (2.3)$$

If the duct is horizontal the gravity pressure change would be left out and equation (2.3) would become

$$p_2 - p_1 = -\int_1^2 \frac{dF_f}{A} - \left(\frac{\rho_2 v_2^2}{2} - \frac{\rho_1 v_1^2}{2} \right) \qquad (2.4)$$

For incompressible flow, in a duct of uniform area, equations (2.3) becomes

$$p_2 - p_1 = -\int_1^2 \frac{dF_f}{A} - \int_1^2 \rho g dz = -\int_1^2 \frac{dF_f}{A} - \rho g \ (z_2 - z_1) \qquad (2.5)$$

and equation (2.4) becomes

$$p_2 - p_1 = -\int_1^2 \frac{dF_f}{A} \qquad (2.6)$$

2.2.2 Straight pipe section pressure change

For a straight section of pipe having a cross-sectional area A and of uniform diameter equations (2.5) and (2.6) are used to calculate the pressure change between two sections. The first term that is found on the right-hand side of these equations is the frictional pressure change. This integral can also be written as

$$p_2 - p_{1\ f} = -\int_1^2 \frac{dF_f}{A} = -\int_1^2 \frac{\tau P_e dz}{A} = -\frac{1}{2} \frac{f_D L}{d} \rho v^2 \qquad (2.7)$$

where d is the diameter of the pipe section, L is the section length, f_D is the Darcy friction factor, v is the average steam speed and ρ is the steam density.

Haaland (1983) proposes two correlations for the calculation of friction factors in round ducts. Where $\varepsilon/d < 10^{-4}$ the correlation is

$$f_D = \frac{2.77776}{\left[\log \left\{ \left(\frac{7.7}{Re} \right)^3 + \left(\frac{\varepsilon/d}{3.75} \right)^{3.333} \right\} \right]^2} \qquad (2.8)$$

and where $\varepsilon/d > 10^{-4}$

$$f_D = \frac{0.30864}{\left[\log\left\{\left(\frac{6.9}{Re}\right)+\left(\frac{\varepsilon/d}{3.7}\right)^{1.11}\right\}\right]^2} \qquad (2.9)$$

where ε is the surface roughness, d is the duct diameter and the Reynolds number is

$$Re = \frac{\rho d v}{\mu} \qquad (2.10)$$

2.2.3 Miter bend pressure change

A schematic of a miter bend as found in the steam duct system is shown in figure 2.4. The bend has guide vanes to reduce the pressure loss over the turn. Jorgenson (1968) states that the loss coefficient of such a bend is $K_{bm} = 0.28$.

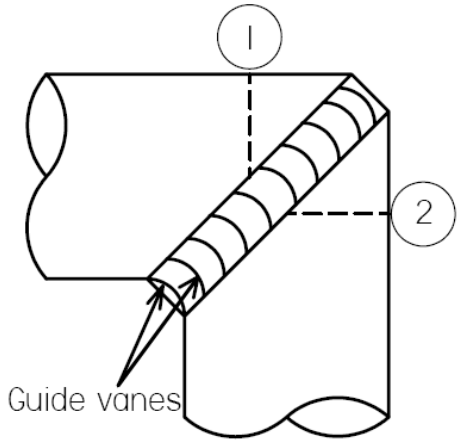

Figure 2.4: Miter bend with guide vanes

The pressure change over the miter bend is given by

$$p_2 - p_{1\ b} = -\frac{K_{bm}\rho v^2}{2} \qquad (2.11)$$

where v is the inlet speed to the bend. The pressure after the miter bend can now be calculated,

$$p_2 = p_1 - \frac{K_{bm}\rho v^2}{2} \qquad (2.12)$$

2.2.4 Conical reducers pressure change

In the steam duct system there are conical reducers to keep the steam speed close to constant throughout the system. A schematic of such a reducer is shown in figure 2.5.

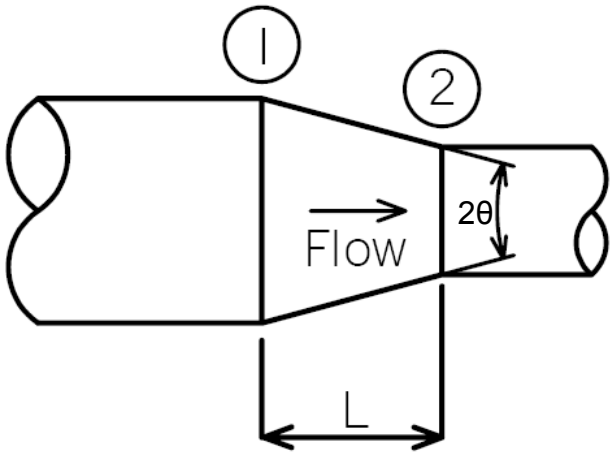

Figure 2.5: Schematic of a conical reducer

In figures 2.1 and 2.2 it can be seen that the duct system branches into four separate branches. Because of the branches in the steam duct the steam speed drops and a reducer is used to accelerate the steam to keep an approximately uniform steam speed distribution throughout the duct. Fried et al. (1989) give the loss coefficient for a conical reducer with $\mathrm{Re}_{v2} \geq 10^5$ as

$$\begin{aligned} K_{red} &= \frac{p_1 + \rho v_1^2/2 \; - \; p_2 + \rho v_2^2/2}{\rho v_2^2/2} \\ &= -0.0125\sigma_{21}^4 + 0.0224\sigma_{21}^3 - 0.00723\sigma_{21}^2 + 0.00444\sigma_{21} - 0.00745 \\ &\times \; 8\theta^3 - 8\pi\theta^2 - 20\theta \end{aligned} \qquad (2.13)$$

where $\sigma_{21} = A_2/A_1$ is the area ratio and θ is the half angle of the reducer and is given in radians. The pressure change over a reducer is

$$p_2 - p_{1\ r} = \rho\left(\frac{v_1^2}{2} - \frac{v_2^2}{2}\right) - \frac{K_{red}\rho v_2^2}{2} \qquad (2.14)$$

where $d_m = \left(d_1 + d_2\right)/2$ and $v_m = \left(v_1 + v_2\right)/2$.

There is also a friction pressure change over the reducer, so to find the total pressure change equation (2.7) is added to equation (2.14). The approximate friction pressure change is evaluated at the mean diameter with the corresponding speed. The pressure at the outlet of the reducer is then

$$p_2 = p_1 + \rho\left(\frac{v_1^2}{2} - \frac{v_2^2}{2}\right) - \frac{K_{red}\rho v_2^2}{2} - \frac{1}{2}\frac{f_D L}{d_m}\rho v_m^2 \qquad (2.15)$$

where $d_m = \left(d_1 + d_2\right)/2$ and $v_m = \left(v_1 + v_2\right)/2$.

2.2.5 T-junction pressure change

T-junctions are used in the duct system to divide the flow to the different branches. In the schematic drawing in figure 2.6 it can be seen that the branch diameter is smaller than the main duct's. There may be guide vanes in the inlet to the branch that help to turn the flow and reduce the loss coefficient.

Van Heerden (1991) did calculations for a similar T-junction and suggested that the guide vanes be modeled as a rounded inlet because correlations for this configuration exist. The assumed configuration is shown in figure 2.6 and does not include guide vanes. The rounded inlet radius, r_{31}, is 0.5 m.

The theory that is available for T-junction requires fully developed flow, but the distances in the duct system are too short for developed conditions to form. Kröger(2004) states that the T-junction theory can be used with minimal error if there are 15 diameters upstream and 4 diameters downstream of straight duct. This is not the case in the duct system and therefore the pressure change at the T-junctions is at best an approximation.

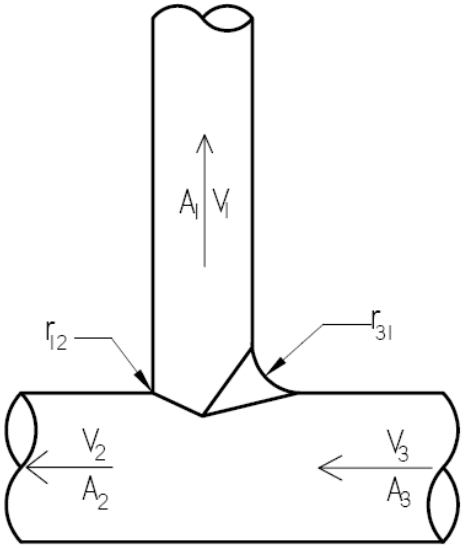

Figure 2.6: Schematic of T-junction actual geometry and assumed geometry

There are two pressure changes for each T-junction, one into the branch duct and one in the main duct. Figure 2.7 is a figure given by Kröger (2004) showing the loss coefficient versus the volume flow rate ratio and area ratio for a square edge T-junction.

It will be assumed that the volume flow ratio will not change significantly and therefore the loss coefficients for a uniform steam distribution is used for the calculation of the pressure change. Since the loss coefficients read off the figures are for square edged inlets, a correction must be made to the loss coefficient. The geometry of the branch has a negligible effect on the loss coefficient of the main duct. There are two correction equations. Each has a set of conditions for which it is valid. The first correction equation is used when $r_{12}/d_1 < 0.15$ and $r_{31}/d_1 < 0.15$

$$K_{31r} = K_{j90°} - 0.9\left(\frac{V_1/V_3}{A_1/A_3}\right)^2\left(\frac{r_{31}}{d_1}\right)^{0.5} - 0.26\left(\frac{V_1/V_3}{A_1/A_3}\right)^2\left(\frac{r_{12}}{d_1}\right)^{0.5} \quad (2.16)$$

where V is the volume flow rate and A is the area of the duct. The second equation is used when $r_{12}/d_1 > 0.15$ and $r_{31}/d_1 > 0.15$

$$K_{31r} = K_{j90°} - 0.45\left(\frac{V_1/V_3}{A_1/A_3}\right)^2 \quad (2.17)$$

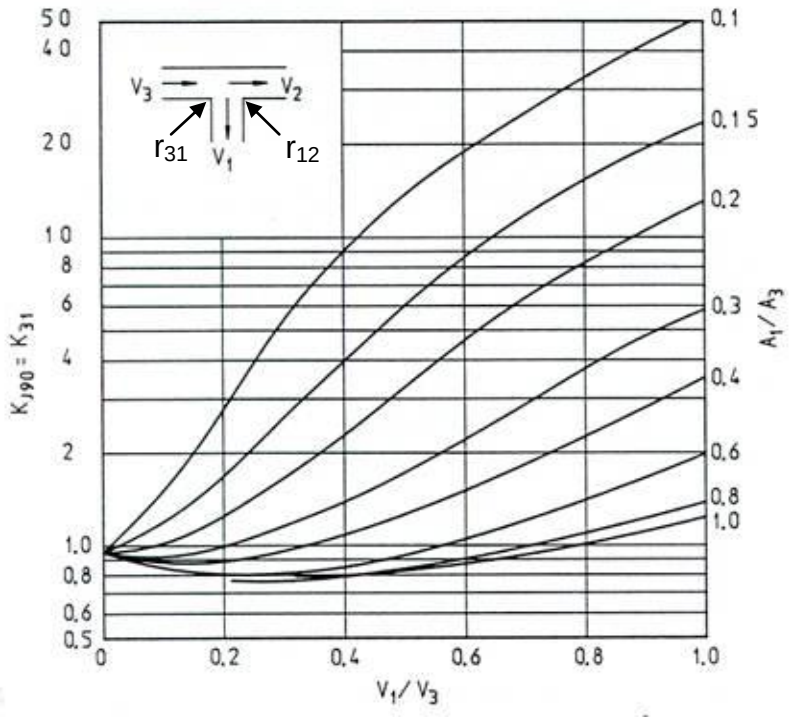

Figure 2.7: Loss coefficient for a 90° junction with square corners (Kröger 2004)

Equation (2.16) is used for the steam duct system under consideration. r_{12} is zero since it is a 90° edge. The pressure change over the T-junction is then

$$p_1 - p_3 = -\frac{K_{31r}\rho v_3^2}{2} + \rho\left(\frac{v_3^2}{2} - \frac{v_1^2}{2}\right) \quad (2.18)$$

The pressure change from 3 to 2 in figure 2.6 is read off figure 2.8 given by Kröger (2004). The pressure change from 3 to 2 is then

$$p_2 - p_3 = -\frac{K_{32}\rho v_3^2}{2} + \rho\left(\frac{v_3^2}{2} - \frac{v_2^2}{2}\right) \quad (2.19)$$

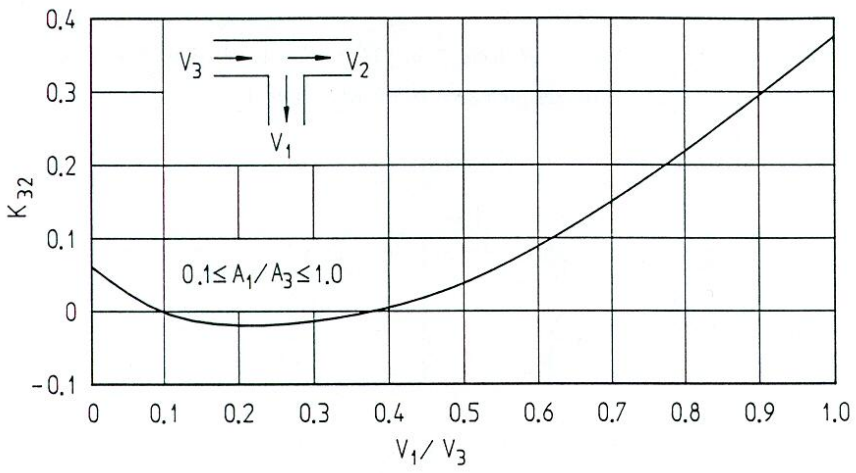

Figure 2.8: Loss coefficient K_{32} for a 90^{o} junction (Kröger 2004)

2.3 Steam properties

The steam in the steam duct is wet and therefore the quality will be less than 1.The flow regime at the exit of the turbine is called mist flow as the droplets are spread uniformly through the flow field. Carey (1992) states that the homogeneous flow model is a very good approximation for mist flows. In the homogeneous flow model the mixture of liquid and vapor are seen as one fluid and new properties are calculated for the homogeneous fluid. The homogeneous properties of interest for the duct system are given below.

Density (Whalley 1987):

$$\rho_{vw} = \left(\frac{x}{\rho_v} + \frac{1-x}{\rho_w} \right)^{-1}, kg/m^3 \qquad (2.20)$$

where x is the steam quality.

Enthalpy:

$$i_h = i_l + x i_{vw}, J/kg \qquad (2.21)$$

Dynamic viscosity:

Several different correlations to calculate the viscosity in mist flows are given in the literature (Isbin et al. 1958, Dukler et al. 1964, Beattie and Whalley 1981). Beattie and Whalley give the following correlation for dynamic viscosity in a homogenous flow,

$$\mu_{vw} = \mu_v \alpha + \mu_w \ (1-\alpha) \ (1+2.5\alpha), kg/ms \qquad (2.22)$$

where α is the void fraction. Whalley (1990) gives the following correlation for the void fraction,

$$\alpha = \frac{1}{1+\left(\frac{v_v}{v_w}\frac{1-x}{x}\frac{\rho_v}{\rho_w}\right)} \tag{2.23}$$

For a homogeneous flow the speed of the liquid and gas phases are equal and equation (2.23) simplifies to

$$\alpha = \frac{1}{1+\left(\frac{1-x}{x}\frac{\rho_v}{\rho_w}\right)} \tag{2.24}$$

The homogeneous dynamic viscosity can now be calculated. It was found however that the void fraction is practically unity for all conditions that were evaluated, since the steam is relatively dry and therefore the homogeneous and vapor dynamic viscosities are assumed to be equal.

An energy balance between any two sections in the duct is used to determine the quality of the steam in the duct. There is no work done on the steam and the process is assumed to be adiabatic, so the energy going into the steam duct will leave it again. The steady state energy equation is

$$i_1 + \frac{v_1^2}{2} + gz_1 = i_2 + \frac{v_2^2}{2} + gz_2 \tag{2.25}$$

Substituting equation (2.25) for i_2 and rearrange to find

$$x_2 = \frac{\left[i_1 - i_{w2} + 0.5\ \left(v_1^2 - v_2^2\right) + g\ \left(z_1 - z_2\right)\right]}{i_{vw2}} \tag{2.26}$$

It can be seen that the enthalpies are needed to calculate the quality. The inlet enthalpy, i_1, will be known, but the temperature of the steam is needed to calculate i_{w2} and i_{vw2}.

For saturated steam the relation between the temperature and pressure can be expressed as follows (Kröger 2004):

$$\begin{aligned} T_v = {} & 164.630366 + 1.832295x10^{-3}p_v + 4.27215x10^{-10}p_v^2 \\ & + 3.738954x10^{3}p_v^{-1} - 7.01204x10^{5}p_v^{-2} + 16.161488\ln\ p_v \\ & - 1.437169x10^{-4}p_v \ln\ p_v \end{aligned} \tag{A.2.1}$$

2.4 Results of numerical example of steam temperature and pressure change in steam duct

Changes in steam temperature and pressure in a steam duct under different operating conditions are determined in Appendix B for the system shown in figure 2.2.

During operating conditions, the air-cooled condenser will receive steam at different pressures. As the pressure decreases, the density decreases and for a constant mass flow rate the speed of the steam increases. This will cause a larger steam pressure drop in the steam duct system because the losses will increase with the increase in steam speed. In figure 2.9 the pressure drop is given as a function of the inlet steam temperature for a steam mass flow rate of 200 kg/s entering the steam duct system.

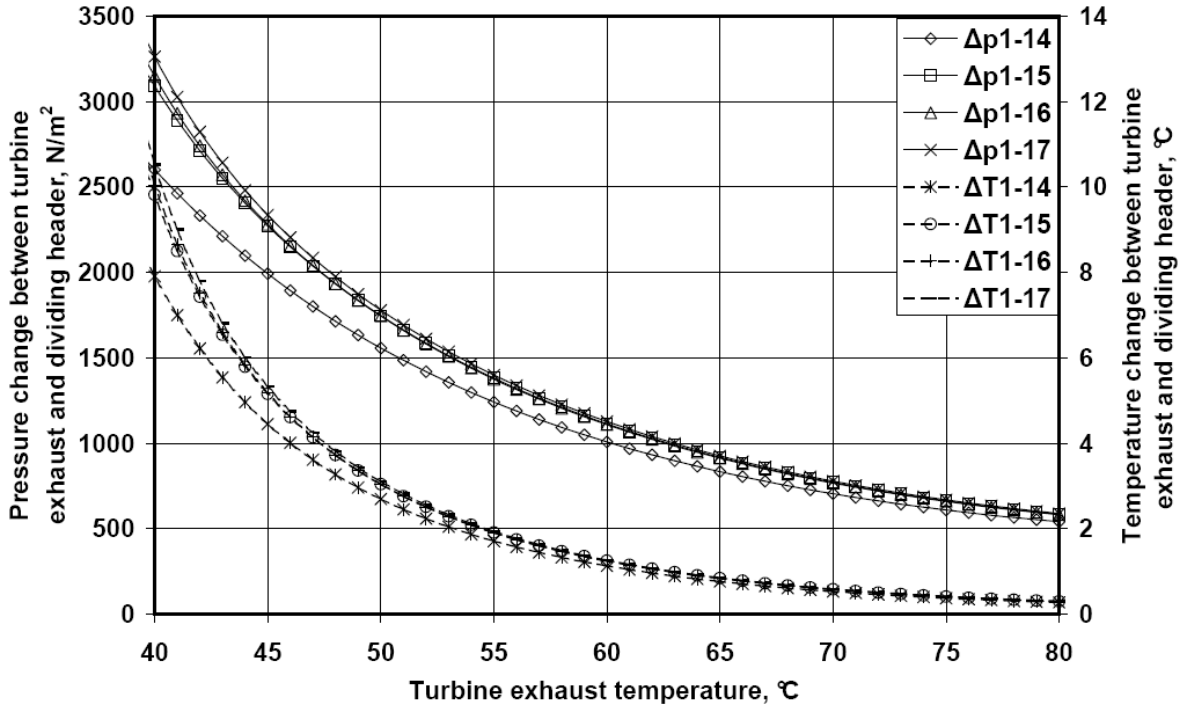

Figure 2.9: Steam pressure and temperature change for the four different branches in a typical steam duct system of an air-cooled steam condenser versus inlet steam temperature

The legend refers to the node points in figure 2.2 and is the pressure difference between the inlet to the duct and the inlet to the dividing headers. It is assumed that each header receives the same amount of steam. It can be seen that the pressure change is the largest when the inlet steam temperature is lowest. From figure 2.9 it can be seen that the steam pressure drop is lowest to node 14 and that the other branches are close to each other. The temperature change follows the same trend as the pressure drop.

2.5 Condenser headers

Headers, or manifolds, are used to divide flow into branching streams, or to combine different streams into one. Headers find application in an air-cooled condenser since the steam must divide into laterals, or finned tubes, and then the excess steam must be combined in the combining header. A schematic layout of an air-cooled condenser's headers is shown in figure 2.10.

Shown in figure 2.12 are two configurations of a dividing and combining header. These two headers are combined to distribute flow in the condenser. A co-current

configuration (Z-type) is used left of points 3 and 11 and a counter-current configuration (U-type) to the right of 5 and 12.

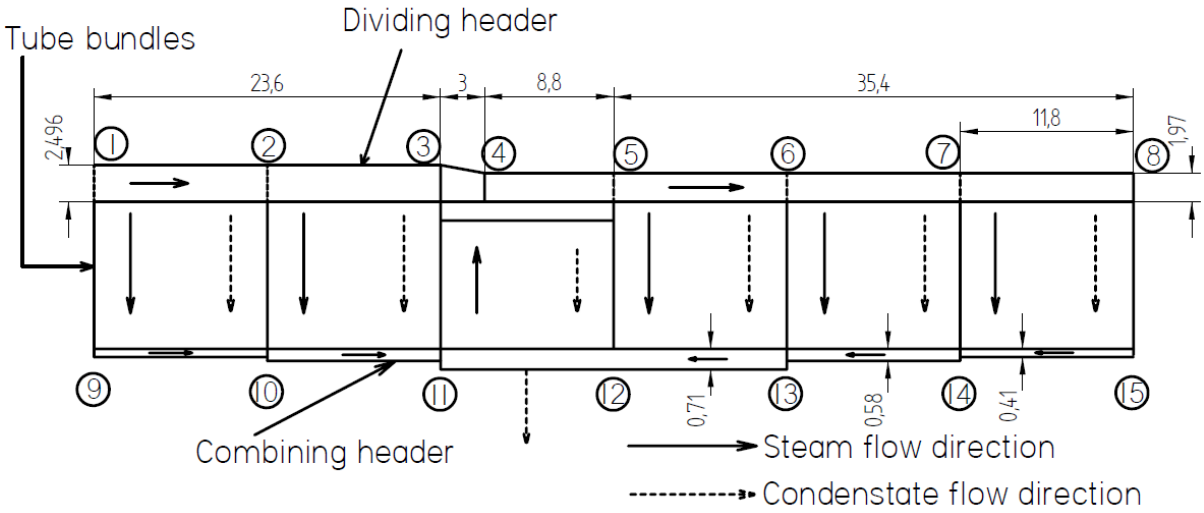

Figure 2.10: Schematic layout of the dividing and combining headers

Pressure changes in the headers are caused by frictional and momentum effects. The frictional pressure changes in the headers are normally much less than changes in pressure due to the momentum changes in the headers (Zipfel 1996). Zipfel (1996) give the following equation for the pressure change in a header

$$\Delta p_h = \frac{1}{2}\rho\alpha \left(v_{h0}^2 - v_{hL}^2 \right) - \Delta p_{hf} \qquad (2.27)$$

where α is the overall momentum correction factor and Δp_{hfr} is the frictional pressure change in the duct. Momentum effects will increase the pressure in the flow direction in the dividing header and decrease the pressure in the combining header. The flow in each section in figure 2.10 is assumed to be incompressible.

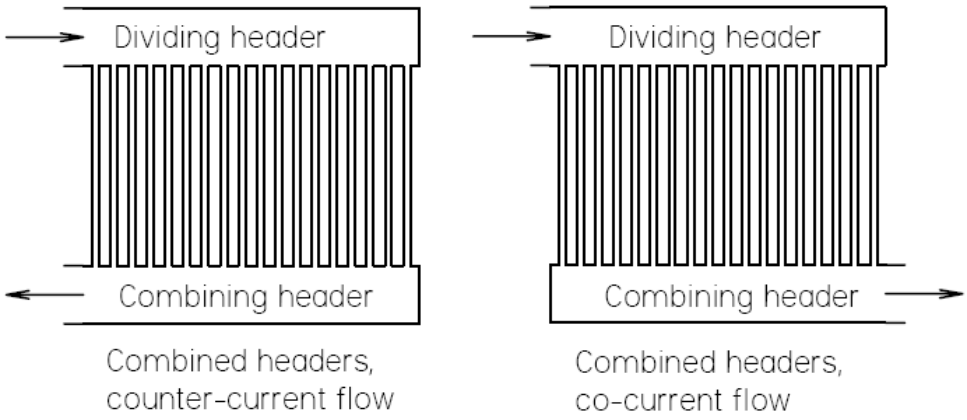

Figure 2.11: Schematic of co-current (Z-type) and counter-current (U-type) combined headers

The momentum correction factor accounts for non-uniformities in the steam speed distribution in the headers. A graphical representation for values of the overall

momentum correction coefficient for a particular duct is shown in figure 2.12. In an air-cooled condenser the lateral to diameter ratio is very small due to the small diameters of the finned tubes compared to the header diameters. The dividing header momentum correction factor is therefore $\alpha_d \approx 1$. In the combining header the curve stops at a diameter ratio of 0.1 and therefore the combining header momentum correction factor is assumed to be $\alpha_c \approx 2.6$.

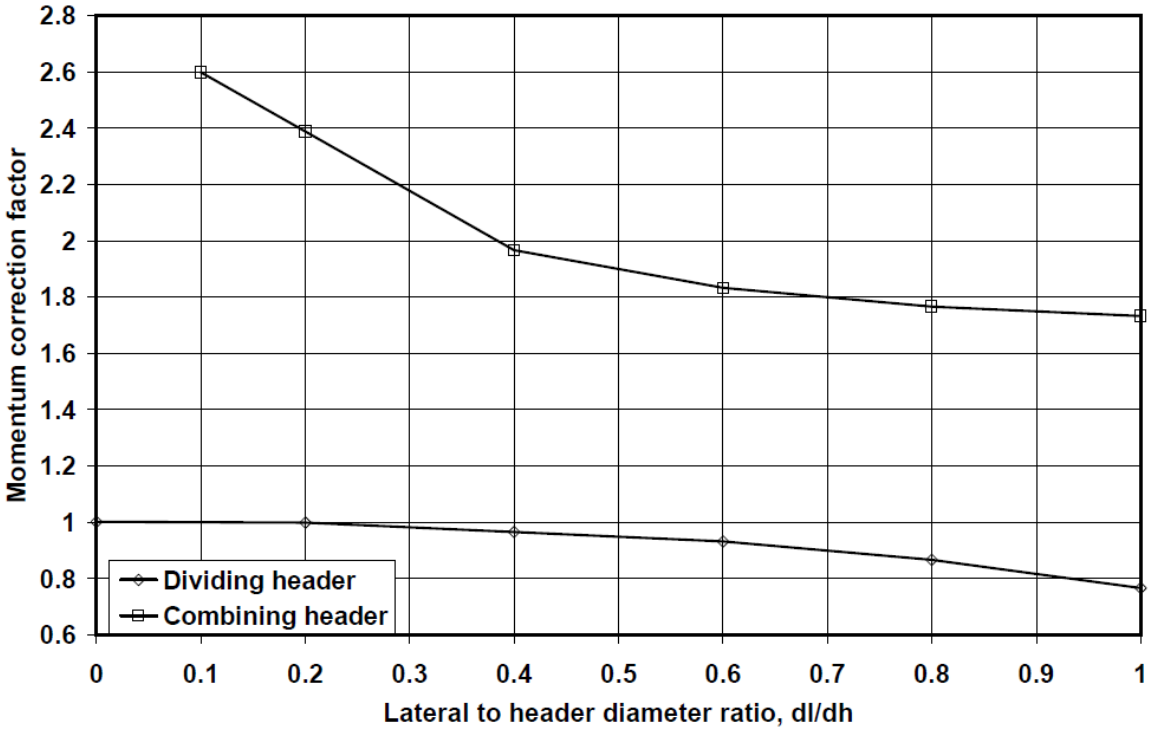

Figure 2.12: Momentum correction factors for dividing and combining header (Bajura, 1971)

2.5.1 Pressure distribution in the dividing header

The pressure distribution in a dividing header is calculated with equation (2.27). The amount of steam leaving the header after each fan unit is known and so the steam speed in the header can be calculated and the momentum pressure change can be calculated. The steam was considered incompressible in each section of the header. The inlet properties of each section are used to calculate the pressure change.

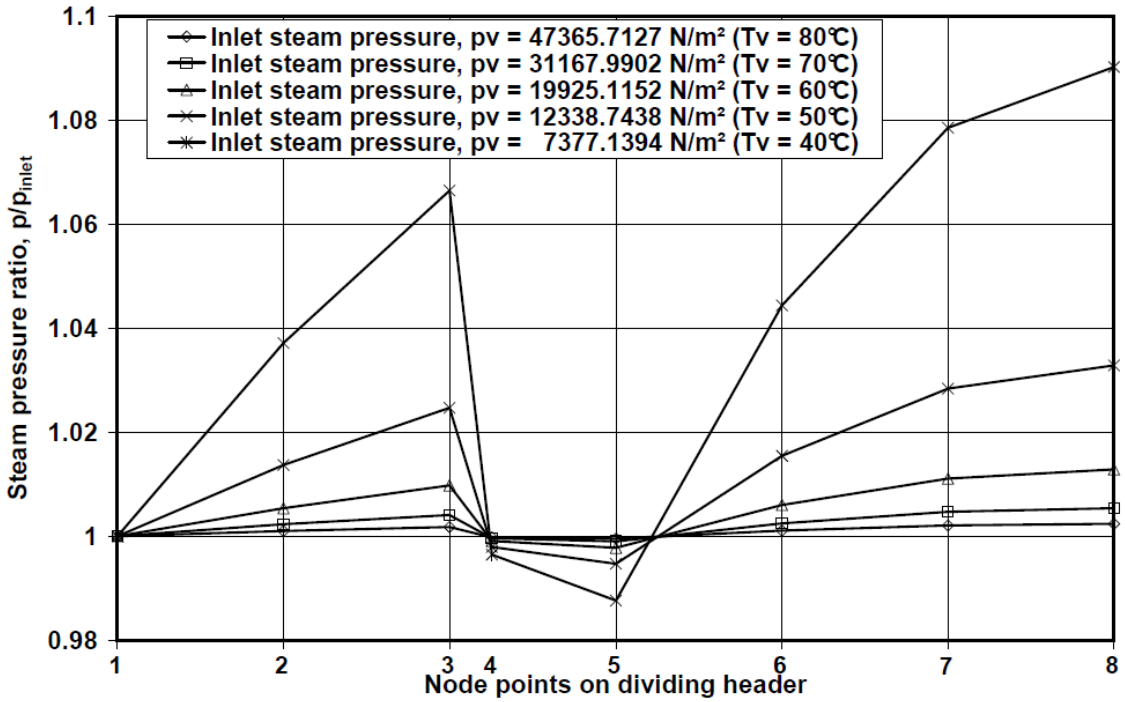

Figure 2.13: Scaled pressure distribution in the dividing header for different turbine exhaust pressures

In figure 2.10, the dividing header is between node points 1 and 8. Between nodes 3 and 4 there is a reducer and between 4 and 5 a straight section of pipe where no out flow occurs. The dephlegmator is located below this section.

Shown in figure 2.13 is the pressure distribution for different turbine exhaust temperatures. Each dividing header receives 47.5 kg/s of steam. It can be seen that at low temperatures the pressure change in the header is the biggest. As the turbine exhaust pressure and corresponding temperature increases the change in pressure in the header decreases, this due to the increase in steam density and the corresponding reduction in steam speed which reduces the frictional and momentum pressure changes. The pressure distribution has been scaled with the header inlet pressure for each temperature. Shown in figure 2.14 is the scaled temperature distribution.

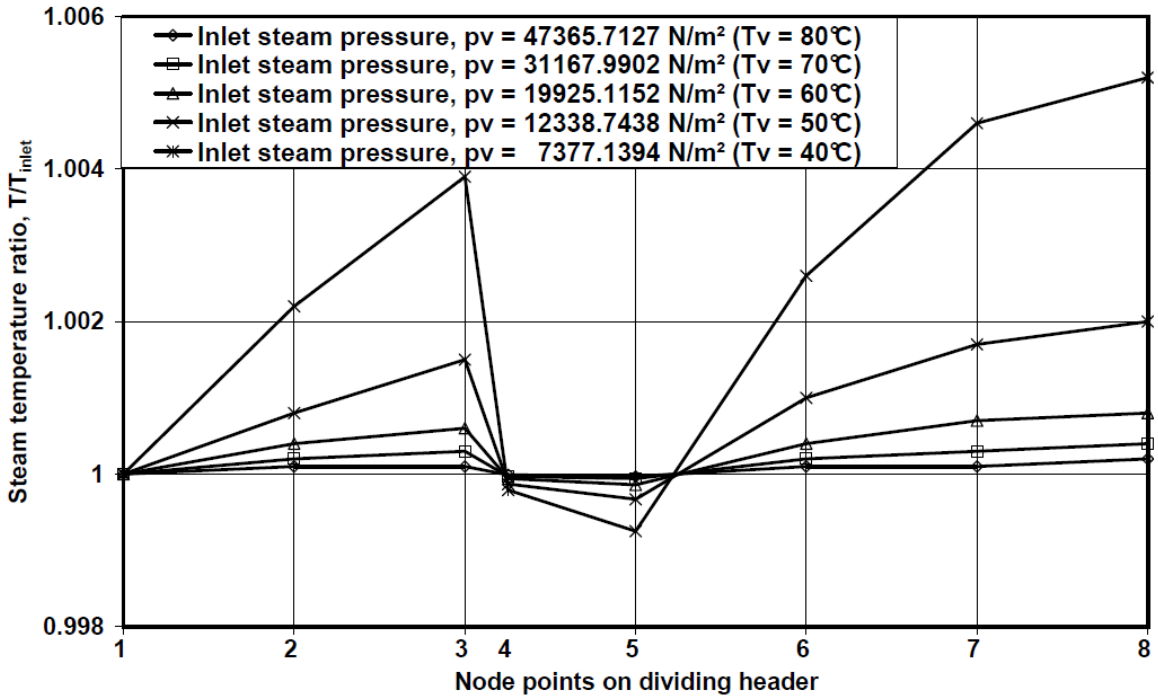

Figure 2.14: Scaled temperature (ºC) distribution in the dividing header for different turbine exhaust pressures

A sample calculation for the pressure change in a dividing header is included in the appendix C.

2.5.2 Pressure distribution in the combining header

In the combining header the steam flows to the dephlegmator where it is condensed. Between nodes 12 and 15 the steam flows in the opposite direction to that in the dividing header, whilst between 9 and 11 the flow is co-current. The pressure increases under the dephlegmator, which is situated between 11 and 12, as the steam is sucked into the finned tubes.

Figures 2.15 and 2.16 show the scaled pressure and temperature distribution for the combining header. It can be seen that the pressure reduces in the direction of steam flow until the dephlegmator is reached where the outflow of steam causes the pressure to increase in the header. As was seen in the dividing header the lowest steam temperature corresponds to the largest steam pressure and temperature changes. The discontinuities in the pressure distribution are due to the dividing header diameter changing.

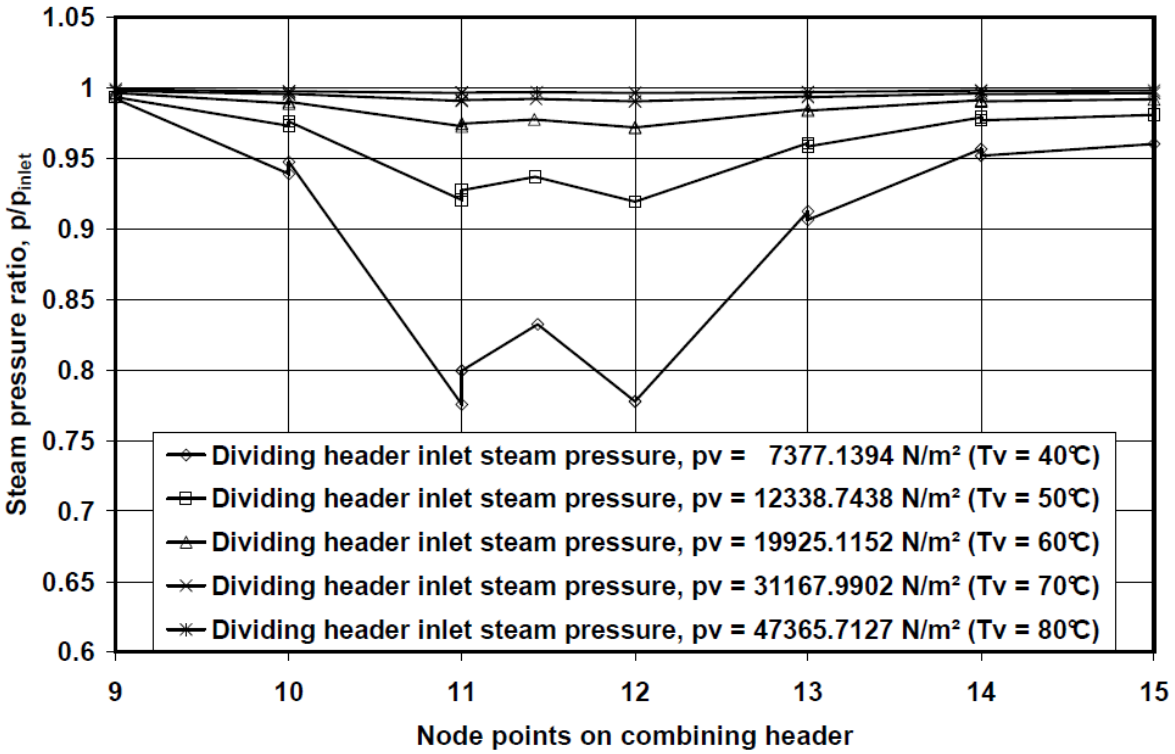

Figure 2.15: Scaled pressure distribution in the combining header for different dividing header inlet pressures

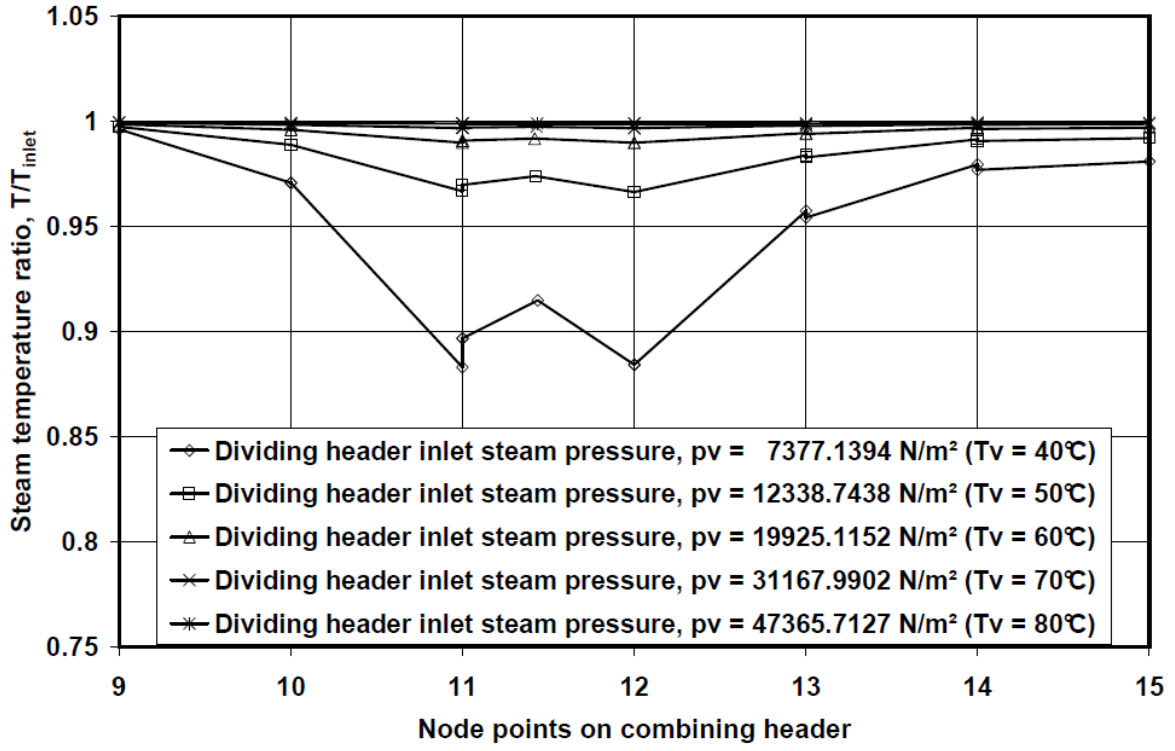

Figure 2.16: Scaled temperature (ºC) distribution in the combining header for different turbine exhaust pressures

A sample calculation is included in appendix E for the combining header.

2.6 Condensation in finned tubes

Figure 2.17 is a schematic of an A-frame condenser fan unit(K-type condenser fan unit). Ambient air, from 1, is sucked through the fan and blown across one or more rows of finned tubes wherein the steam condenses. The heated air is then released to the atmosphere. The governing equations for an A-frame condenser unit will be discussed below.

2.6.1 Heat transfer in an air-cooled condenser

The heat transfer in an air-cooled K-type condenser is given by

$$Q = m_a c_{pa} \left(T_{a6} - T_{a5} \right) = m_c i_{fg} \tag{2.28}$$

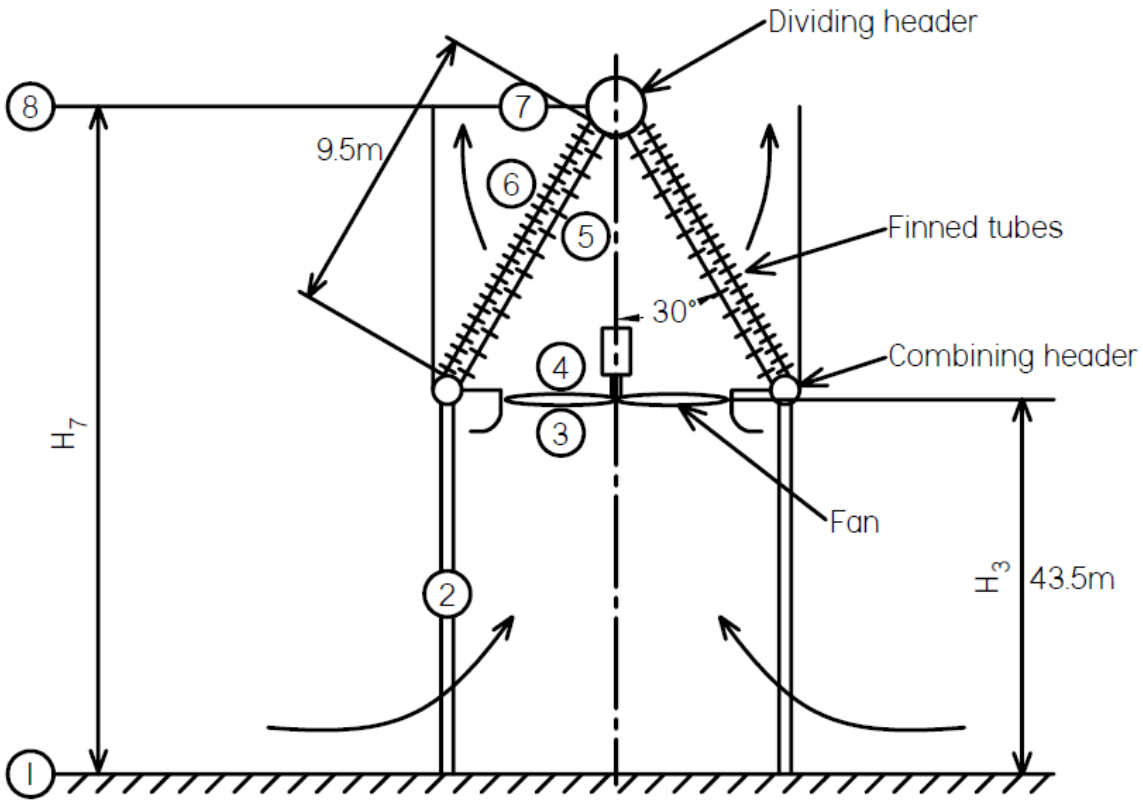

Figure 2.17 Schematic of K-type condenser fan unit

where m_a is the mass flow rate of air through the fan, m_c is the condensate mass flow rate and i_{fg} is the latent heat. The condenser under consideration has two tube rows. The heat transfer can be calculated for each tube row as long as the individual heat transfer characteristics of the tube rows are known. The heat transfer is then the sum of the heat transfer from the individual tube rows, and for n_r tube rows can be written as

$$Q = \sum_{i=1}^{n_r} m_a c_{pa\,i} \left(T_{ao\,1} - T_{ai\,i} \right) = \sum_{i=1}^{n_r} m_{c\,i}\, i_{fg} \tag{2.29}$$

Using the effectiveness of the condenser the heat transfer can be written as

$$Q = \sum_{i=1}^{n_r} e_{\,i}\, m_a c_{pa\,i} \left(T_s - T_{ai\,i} \right) \tag{2.30}$$

where T_s is the steam temperature in the finned tube and e is the heat exchanger effectiveness. The effectiveness of a heat exchanger where condensation takes place can be written as (Kröger 2004)

$$e_i = 1 - \exp\left[-U_i A_i \,/\, m_a c_{pa\,i} \right] \tag{2.31}$$

where $U_{(i)}A_{(i)}$ is the overall thermal conductance for a particular tube row and is given by

$$U_{(i)}A_{(i)} = \left(\frac{1}{h_{ae(i)}A_{a(i)}} + \frac{1}{h_{c(i)}A_{c(i)}} \right)^{-1} \tag{2.32}$$

The effective air-side thermal conductance can be expressed as

$$h_{ae(i)}A_{a(i)} = \left(\frac{1}{h_{a(i)}e_{f(i)}A_{a(i)}} + \sum_n \frac{R_n}{A_n} \right)^{-1} \tag{2.33}$$

The summation term accounts for the thermal resistances of effects like contact resistance and fouling. The air-side thermal conductance for a specific finned tube can be determined experimentally and presented in the form proposed by Kröger (2004),

$$h_{ae(i)}A_{a(i)} = Ny_{(i)}k_{a(i)}\,Pr_{a(i)}^{1/3}\,A_{fr(i)} \tag{2.34}$$

Ny is the characteristic heat transfer parameter and is determined experimentally and given in the following form

$$Ny_{(i)} = aRy_{(i)}^{b}, m^{-1} \tag{2.35}$$

and Ry, the characteristic flow parameter, is given by

$$Ry_{(i)} = \frac{m_a}{\mu_{a(i)}A_{fr(i)}}, m^{-1} \tag{2.36}$$

A correlation for the condensation heat transfer coefficient for flattened tubes was developed by Groenewald (1993),

$$h_{c(i)} = 0.9245\left[\frac{L_t k_{c(i)}^3 \rho_{c(i)}^2 g \cos\ \phi\ i_{fg(i)}}{\mu_{c(i)} m_{al(i)} c_{pa(i)}\ \ T_{vm(i)} - T_{ai(i)}\ \left[1 - \exp\ -\ U_{c(i)} H_t L_t \,/\, m_{al} c_{pa(i)}\right]} \right] \tag{2.37}$$

where m_{al} is the mass flow rate of air flowing on one side of the finned tube and is given by

$$m_{al} = m_a / (2 \times n_{tb\,i} \times n_b) \tag{2.38}$$

The overall heat transfer coefficient based on the condensation surface area, ignoring the film resistance, can be approximated by

$$U_{c(i)} H_t L_t = h_{ae(i)} A_{a(i)} \Big/ 2 n_{tb} n_b \tag{2.39}$$

The condensation surface area can be calculated by

$$A_{c(i)} = n_b n_{tb(i)} A_{ti} L_t \tag{2.40}$$

The above equations can be used to solve the heat transfer of the condenser for a given inlet temperature, air mass flow rate and steam temperature.

The fan in an air-cooled condenser must overcome a series of flow resistances to deliver the required air flow so that the desired heat transfer rate can be obtained. Stationary air accelerates from 1, flows across the heat exchanger supports at 2. Before the air is drawn into the fan, there can be upstream losses at 3, like support structures and wire mesh guards. The air stream will experience an increase in pressure as it moves through the fan from 3 to 4. The air then leaves the fan at 4 and downstream losses are experienced in the plenum chamber. The air then flows through the heat exchanger bundles 5 and experience further losses when the air exits the bundles at 6.

If it is assumed that the temperature change with elevation follows the dry adiabatic lapse rate, then the pressure at any elevation is given by (Kröger 2004)

$$p = p_1 \left(1 - 0.00975 z / T_1\right)^{3.5} \tag{2.41}$$

The pressure difference between 1 and 7 can then be written as

$$\begin{aligned} p_{a1} - p_{a7} &= \left(p_{a1} - p_{a6}\right) + \left(p_{a6} - p_{a7}\right) \\ &\approx p_{a1}\left[1 - \left(1 - 0.00975 H_6 / T_{a1}\right)^{3.5}\right] \\ &+ p_{a1}\left[1 - \left(1 - 0.00975 \left(H_7 - H_6\right) / T_{a6}\right)^{3.5}\right] \end{aligned} \tag{2.42}$$

The draft equation derived by Kröger (2004) for the air-cooled condenser as in figure 2.17 is

$$\begin{aligned} p_{a1} - p_{a7} = {} & p_{a1}\left[1 - \left(1 - 0.00975 H_6 / T_{a1}\right)^{3.5}\right] + K_{ts} \left(m_a / A_2\right)^2 \Big/ 2\rho_{a2} \\ & + K_{up} \left(m_a / A_e\right)^2 \Big/ 2\rho_{a3} - \left[\Delta p_{Fs} + \alpha_{eF} \left(m_a / A_c\right)^2 \Big/ 2\rho_{a4}\right] \\ & + K_{pl} \left(m_a / A_c\right)^2 \Big/ 2\rho_{a4} + K_{do} \left(m_a / A_e\right)^2 \Big/ 2\rho_{a4} \\ & + K_{\theta t} \left(m_a / A_{fr}\right)^2 \Big/ 2\rho_{a56} + p_{a6}\left[1 - \left(1 - 0.00975 \left(H_7 - H_6\right) / T_{a6}\right)^{3.5}\right] \end{aligned} \tag{2.43}$$

Kröger (2004) further states that for a configuration as in figure 2.17 that $K_{pl} = \alpha_{eF}$ and it follows that

$$\begin{aligned} & -\left[\Delta p_{Fs} + \alpha_{eF} \left(m_a / A_c\right)^2 \Big/ 2\rho_{a4}\right] + K_{pl} \left(m_a / A_c\right)^2 \Big/ 2\rho_{a4} \\ & \approx -K_{Fs} \left(m_a / A_c\right)^2 \Big/ 2\rho_{a3} \end{aligned} \tag{2.44}$$

Upon substituting of equations (2.42) and (2.44) into equation (2.43) find

$$
\begin{aligned}
&p_{a1}\left[\ 1-0.00975\ \left(H_7-H_6\right)/T_{a6}\ ^{3.5}-\ 1-0.00975\ \left(H_7-H_6\right)/T_{a1}\ ^{3.5}\right] \\
&=K_{ts}\ \left(m_a/A_2\right)^2/\ 2\rho_{a1}\ +K_{up}\ \left(m_a/A_e\right)^2/\ 2\rho_{a3}\ -K_{Fs}\ \left(m_a/A_c\right)^2/\ 2\rho_{a3} \\
&+K_{do}\ \left(m_a/A_e\right)^2/\ 2\rho_{a3}\ +K_{\theta t}\ \left(m_a/A_{fr}\right)^2/\ 2\rho_{a56}
\end{aligned}
\qquad (2.45)
$$

For the derivation of equation (2.45) it was assumed that $\rho_{a2}\approx\rho_{a1},\rho_{a4}\approx\rho_{a3}$, $\rho_{a7}\approx\rho_{a6}$ and $p_{a6}\approx p_{a1}$. This is for a case where the dry adiabatic lapse rate is applicable. In cases where temperature inversions are present equation (2.48) can not be used as the draft equation. A different equation will be derived later to account for the case of local temperature profiles.

Equations (2.29), (2.30) and (2.45) must be solved simultaneously to generate a solution for the ideal air-cooled condenser. Appendix E shows a sample calculation for an ideal fan unit. The different loss coefficients are described in more detail by Kröger (2004).

2.6.2 Finned tube inlet loss coefficients

Shown in figure 2.18 is a schematic of the first 10 finned tubes, also referred to as laterals, in the steam dividing header. There is a region of separation at the inlet of the finned tube. This separation is caused by the main steam flow in the duct being perpendicular to the flow in the finned tubes. Zipfel (1996) states that the inlet loss coefficient for laterals (finned tubes) can be calculated from experimental data, ignoring frictional effects, as follows

$$K_c=\frac{p_h-p_l}{\frac{1}{2}\rho v_l^2}+\alpha_d\frac{v_h^2}{v_l^2}-1 \qquad (2.46)$$

Because the experimental overall momentum correction factor was not available, a new loss coefficient is defined by Zipfel (1996) as

$$K_i=K_c-\alpha_d\frac{v_h^2}{v_l^2} \qquad (2.47)$$

The inlet pressure change is then

$$
\begin{aligned}
p_l-p_h\ &=-K_i\rho\frac{v_l^2}{2}-\rho\frac{v_l^2}{2} \\
&=-\rho\frac{v_l^2}{2}\ K_i+1
\end{aligned}
\qquad (2.48)
$$

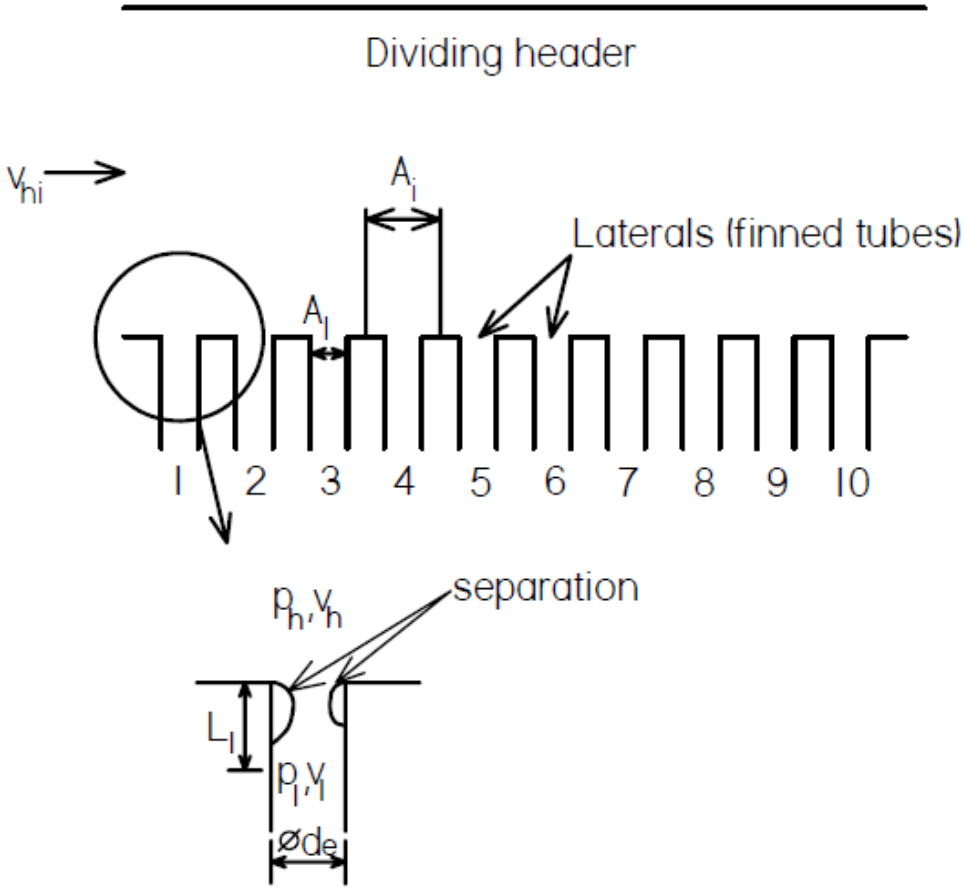

Figure 2.18: Schematic of first 10 tubes in the dividing header

The variation in the experimentally determined inlet loss coefficients for the ten tubes shown in figure 2.18, are shown in figure 2.19. The first tube has the largest inlet loss coefficient and it increases with an increase in speed ratio, v_{hi}/v_l. All the other tubes also experience an increase except for tubes 9 and 10 which experience a decrease in the inlet loss coefficient with an increase in the speed ratio. The different tubes in the header will therefore experience different inlet loss coefficients which will affect the steam distribution in the condenser. A large inlet loss coefficient can impede flow into the finned tubes.

The laterals used by Zipfel were 10mm wide and 190mm high and had a 40mm pitch. The results obtained were compared with those of Nosova (1959), who used laterals 40mm wide and 400mm high, and Van Heerden (1991), who had laterals 16mm wide and 182mm high. Good correlation was obtained between the different results. This suggests that the results obtained by Zipfel can be used for different tube geometries. The single tube row geometry is 17mm wide and 200mm high, while the two-row tubes are 17mm wide and 97mm high. Both have a pitch of 40mm.

Zipfel (1996) suggests a method to use the experimental inlet loss coefficients in the design of an air-cooled condenser. The first 3 tubes in the condenser have the inlet loss coefficient of the first 3 experimentally determined inlet loss coefficients. Zipfel then says that for the rest of the header the inlet loss coefficients are

determined by calculating the dimensionless header distance, z/L_h and the speed ratio. If the header is open at the end, then the experimentally determined inlet loss coefficients are used for the last two tubes, while if the header end is closed then the inlet loss coefficient for the second last tube is

$K_i = 0.316533$

and for the last tube

$K_i = 0.552367$

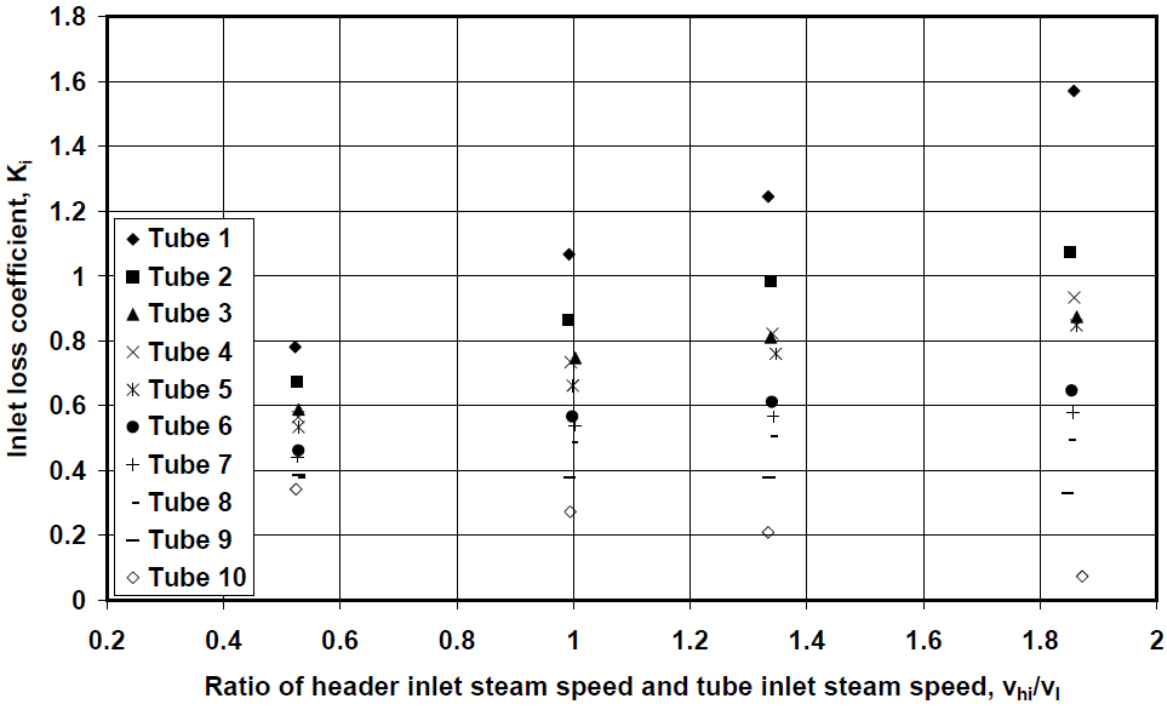

Figure 2.19: Inlet loss coefficient for first 10 tubes (straight inlet), see figure 2.18

It was decided to change the model slightly. The first 3 tubes' inlet loss coefficients are taken as the experimentally determined inlet loss coefficients. The dimensionless header length is calculated and used to determine which of tube of 4 to 10's inlet loss coefficient should be used at a certain location in the header. The end of the headers is treated in the same way as above. This prevents the first 3 tubes' inlet loss coefficient being used again in the header. The inlet loss coefficients for the two methods described above are shown in figure 2.20 for the second part of the dividing header, from 5 to 8 in figure 2.10, and for v_{hi} = 70 m/s and v_i = 50 m/s. This part of the dividing header is 35.4m long and has a closed end.

For the method proposed by Zipfel (1996) the inlet loss coefficient increases sharply again after the third tube while for the modified model this sharp increase is avoided. The trend is for the inlet loss to decrease down the header for the straight inlet as described in figure 2.18, and therefore the modification was made. Due to the closed end the inlet loss coefficients for the last two tubes are higher.

The condenser dividing header is divided into two headers because there is no steam suction from 3 to 5. The first dividing header starts at 1 and ends at 3, with

an open end, while the second dividing header starts at 5 and ends at 8, with a closed end. The model described above is therefore used from 1 to 3 and from 5 to 8. The header inlet steam speed is calculated at 1 and 5 for the two headers respectively.

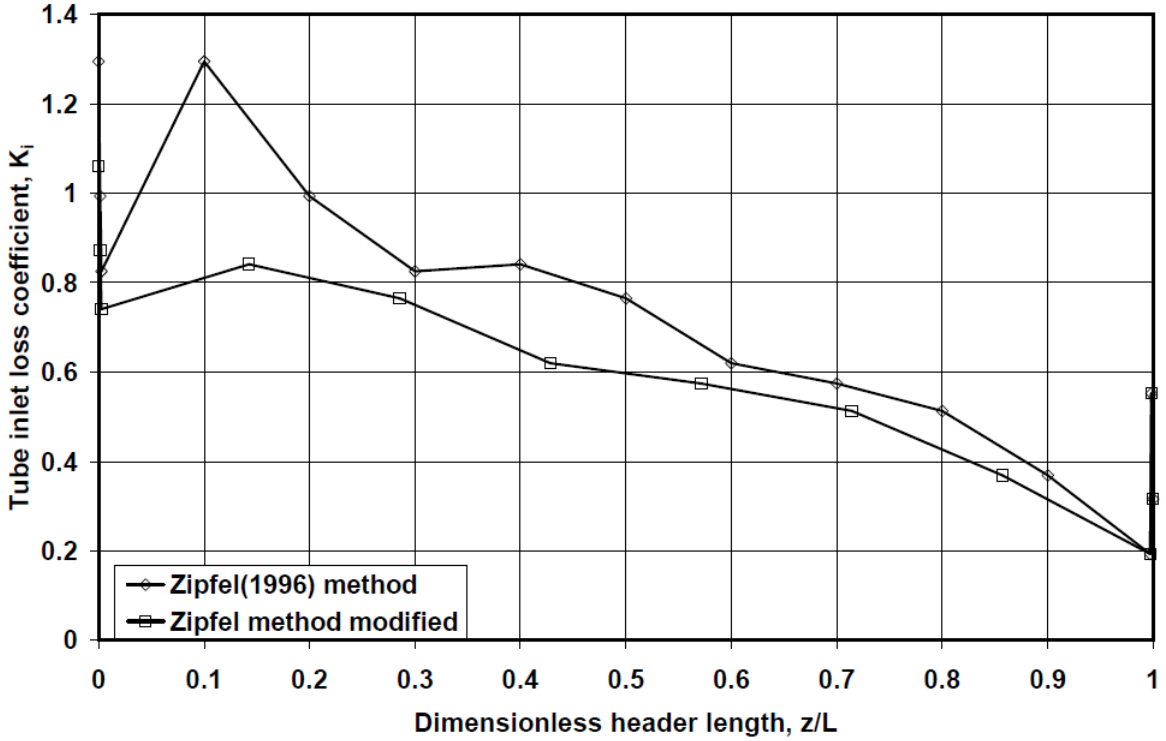

Figure 2.20: Comparison of two different models for the variation in inlet loss coefficients

Zipfel (1996) found that by inserting a backward facing step or a small wedge-like ramp upstream of the tubes, that the inlet loss coefficients of the finned tubes can be reduced. Installing a suitable grid close to the tubes was also seen to reduce the inlet loss coefficients. The grid has the added advantage of reducing erosion at the inlet of the tubes due to water droplets, as these are caught by the grid (Zipfel, 1996). Schematics of each of these configurations are shown in figure 2.21.

A comparison of the experimentally determined inlet loss coefficients for the 10 tubes for the different configurations is shown in figure 2.22 for v_{hi} = 70 m/s and v_{l} = 50 m/s. The loss coefficient for a parallel plate sudden contraction is also included as this method was used by Kröger (2004). The inlet loss coefficient is then

$$K_c = \left(-1/\sigma_c\right)^2 \tag{2.49}$$

and

$$\sigma_c = 0.6144517 + 0.04566493\sigma_{21} - 0.336651\sigma_{21}^2 + 0.4082743\sigma_{21}^3 + 2.672041\sigma_{21}^4 - 5.963169\sigma_{21}^5 + 3.558944\sigma_{21}^6 \tag{2.50}$$

where

$$\sigma_{21} = \frac{A_L}{A_i} \tag{2.51}$$

Table 2.1: Parallel plate inlet loss coefficient comparison

	σ_{21}	K_c (Eq 2.49)
Zipfel (1996)	0.25	0.406
Current	0.34	0.42

The area ratio for the Zipfel geometry and the current geometry and the inlet loss coefficient as given by equation (2.49) is shown in table 2.1. Although the area ratios differ, the inlet loss coefficients are very close for the two geometries. The parallel plate inlet loss coefficients will therefore not influence the inlet loss coefficients for the current geometries.

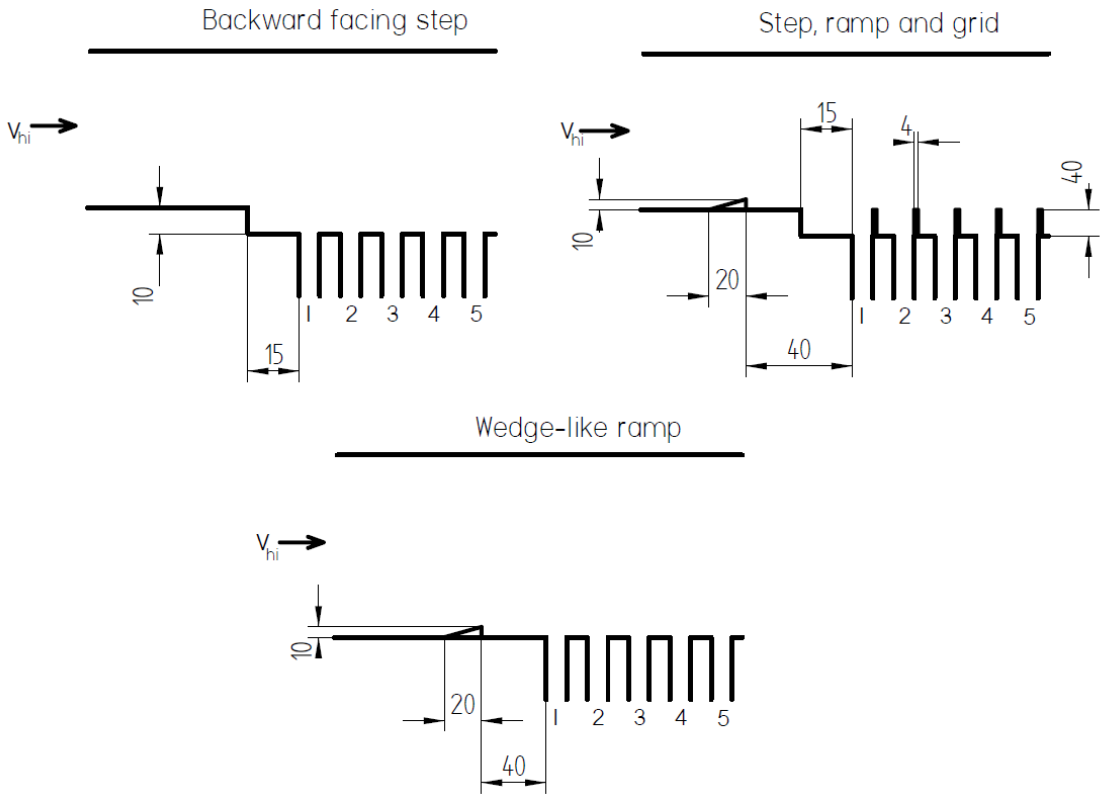

Figure 2.21: Schematic of backward facing step, ramp and grid configurations

Equation (2.49) is rewritten in equation (2.47)'s form with $\alpha_d = 1$. There is a large difference between the corrected equation (2.49)'s inlet loss coefficients and that of Zipfel (1996). This is because for equation (2.49) the flow is assumed to be parallel in the header and the finned tube and not perpendicular as the case with Zipfel (1996).

The combination of the backward facing step, wedge-like ramp and grid has the lowest inlet loss coefficients for results obtained by Zipfel (1996). After the fourth tube the difference in inlet loss coefficient is small for the straight inlet, the backward facing step and the wedge-like ramp. The combination of the step, ramp

and grid follows a more erratic trend, but the inlet loss coefficients are smaller than for the other configurations.

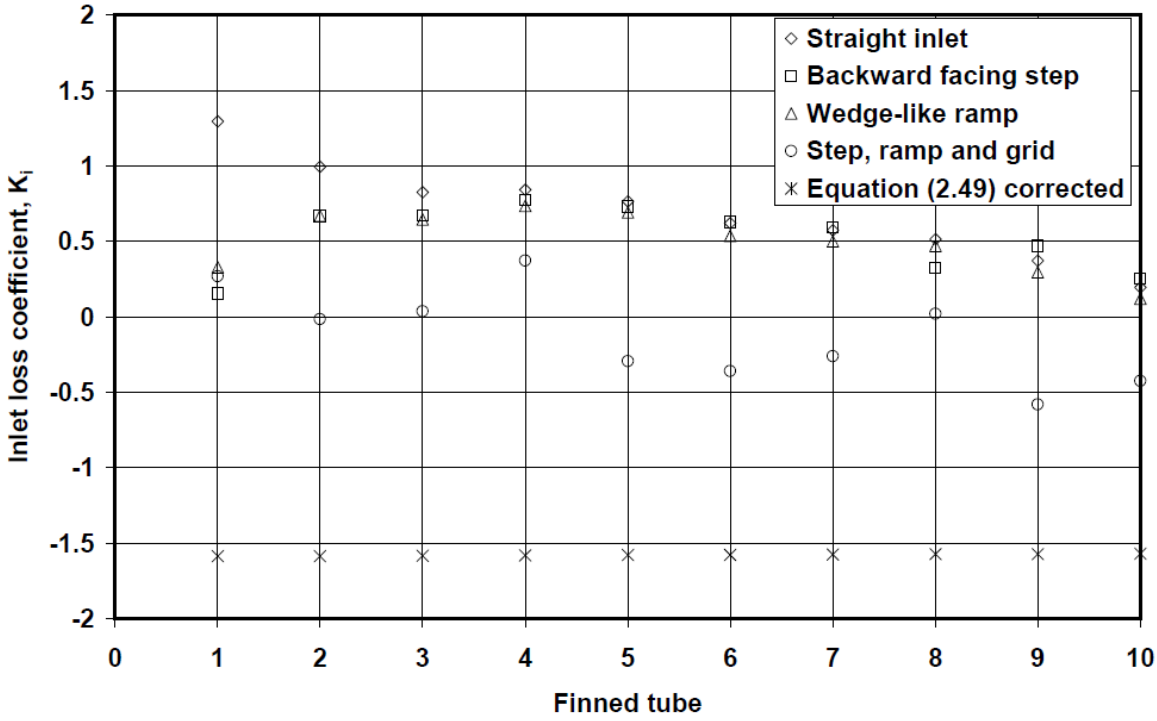

Figure 2.22: Comparison of the inlet loss coefficients with $v_{hi}/v_l = 1.4$

2.6.3 Derivation of pressure equations for a finned condenser tube

The pressure in the finned tube will not be constant due to the condensation process and other factors like friction, momentum and elevation changes. The changing pressure also means that the steam temperature will change along the length of the finned tube and this will influence the heat transfer as given by equation (2.34).

Kröger (2004) derived equations for the pressure differential in a condenser tube between two headers as shown in figure 2.23. It was assumed that all the steam condenses in the tube and no steam left the tube at the combining header side. In the present derivation the analysis will be extended and it will not be assumed that all the steam condenses and the effect of the steam leaving the bottom of the tube will be taken into account.

The incremental pressure change in the finned tube is given by

$$dp_v = dp_{vf} + dp_{vs} + dp_{vm} \qquad (2.52)$$

where dp_{vf} , dp_{vg} and dp_{vm} are the pressure changes due to friction, gravity and momentum respectively.

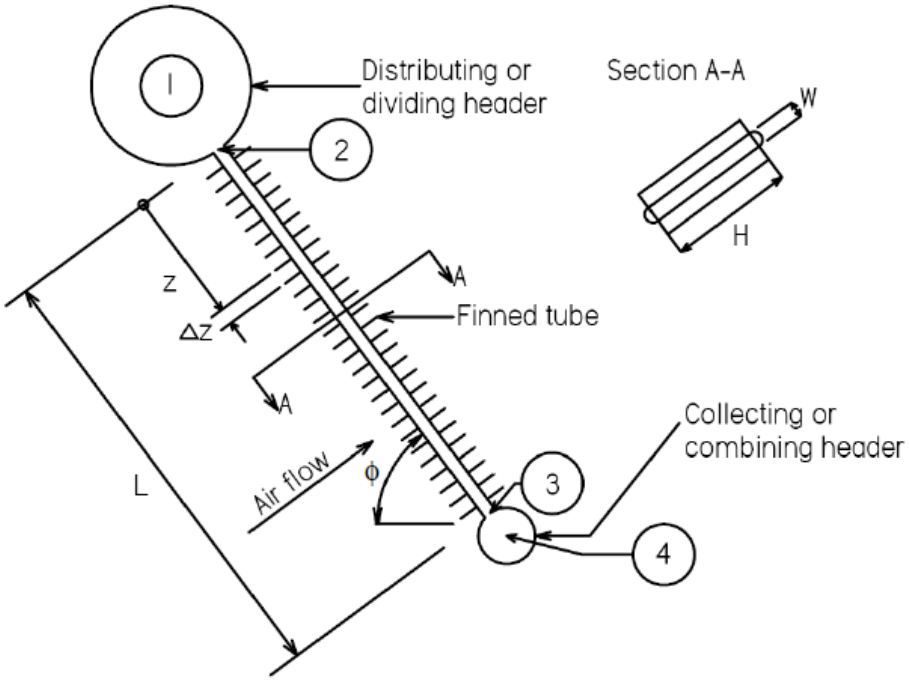

Figure 2.23: Schematic drawing of the headers and finned tube for the pressure equations derivation

An effective friction factor, f_{De}, that takes into consideration the formation of waves and the distorted velocity profile as steam flows towards the condensing surface, is presented by Kröger (2004). The differential friction pressure change is then

$$dp_{vf} = -f_{De}\rho_v v_v^2\, dz/\ 2d_e \tag{2.53}$$

where d_e is the hydraulic diameter of the duct.
Further for a flattened finned tube

$$f_{De} = f_D\left(1 + a_2/Re_v\right) \tag{2.54}$$

where

$$a_1 = 1.0649 + 1.0411\times10^{-3}\,Re_{vn} - 2.011\times10^{-7}\,Re_{vn}^3 \tag{2.55}$$

$$a_2 = 290.1479 + 59.3153\,Re_{vn} + 1.5995\times10^{-2}\,Re_{vn}^3 \tag{2.56}$$

and the Reynolds number is

$$Re_v = \rho_{v2} v_v\, d_e/\mu_{v2} \tag{2.57}$$

if changes in density are assumed to be negligible.

The Darcy friction factor is approximated as $f_D = 0.3164\,Re_v^{-0.25}$ in the range $2300 \le Re_v \le 10^5$. In equations (2.55) and (2.56) the Reynolds number of the vapor normal to the condensing surface is in the range of $0 \le Re_{vn} \le 40$.

An expression for Re_{vn} is obtained by assuming that the rate of condensation along the tube is essentially uniform. Because there is vapor leaving the bottom of the condenser tube and the condensation rate is uniform the steam speed will decrease linearly along the tube. The local vapor speed therefore is given by

$$v_v = \frac{(v_{v3} - v_{v2})}{L} z + v_{v2} \tag{2.58}$$

The local Reynolds number can now be expressed as

$$Re_v = \rho_{v2}\left[v_{v2}\ (1 - z/L) + v_{v3} z/L \right] d_e/\mu_{v2} = Re_{v2}\ (1 - z/L) + Re_{v3}\ z/L \tag{2.59}$$

where $Re_{v2} = \rho_{v2} v_{v2} d_e/\mu_{v2}$ and $Re_{v3} = \rho_{v2} v_{v3} d_e/\mu_{v2}$.

The mass flow rate of vapor per unit length of duct normal to the condensing surface is approximately

$$m_{vn} \approx 2\rho_{v2} v_{vn} H = \rho_v WH(-dv_v/dz) = -\rho_{v2} WH\left(\frac{v_{v3} - v_{v2}}{L} \right) = \rho_{v2} WH\left(\frac{v_{v2} - v_{v3}}{L} \right) \tag{2.60}$$

or

$$v_{vn} = \frac{W(v_{v2} - v_{v3})}{2L} \tag{2.61}$$

The Reynolds number normal to the surface that corresponds to this speed is defined as

$$Re_{vn} = 2\rho_{v2} v_{vn}\ W/\mu_{v2} = \frac{\rho_{v2} W^2\ (v_{v2} - v_{v3})}{L\mu_{v2}} = Re_{v2} \frac{W}{2L} - Re_{v3} \frac{W}{2L} \tag{2.62}$$

Groenewald and Kröger (1995) show that for a practical air-cooled steam condenser the change in pressure for the laminar region is negligible compared to that in the turbulent section. For this analysis it is also possible that the laminar region is never reached. This is due to the fact the that not all the steam condenses in the tube. Upon substituting equation (2.54) into (2.53), the pressure change across the tube can be approximated as follows

$$\begin{aligned}
p_{v3} - p_{v2\ f} &\approx -\int_0^L f_{De} \left(\frac{\rho_{v2} v_v^2}{2} \right) \frac{dz}{d_e} \\
&= -\int_0^L f_D\ (a_1 + a_2/Re_v) \left(\frac{\rho_{v2} v_v^2}{2} \right) \frac{dz}{d_e} \\
&= -\int_0^L 0.3164\, Re_v^{-0.25}\ (a_1 + a_2/Re_v) \left(\frac{\rho_{v2} v_v^2}{2} \right) \frac{dz}{d_e} \\
&= -\int_0^L \frac{0.1582\, Re_v^{-0.25} \mu_{v2}^2}{\rho_{v2} d_e^3}\ (a_1 + a_2/Re_v) \left(\frac{\rho_{v2}^2 v_v^2 d_e^2}{\mu_{v2}^2} \right) dz
\end{aligned} \tag{2.63}$$

By differentiating equation (2.57) and rearranging dz can be written in terms of dRe_v

$$dz = \frac{d\,Re_v\,L}{\left(Re_{v3} - Re_{v2}\right)} \tag{2.64}$$

Substitute equation (2.64) into equation (2.63) to find

$$p_{v3} - p_{v2\ f} = -\int_{Re_{v2}}^{Re_{v3}} \frac{0.1582\,Re_v^{-0.25}\,\mu_{v2}^2 L}{\rho_{v2} d_e^3\ \left(Re_{v3} - Re_{v2}\right)}\ \left(a_1 Re_v^2 + a_2\,Re_v\right)\ dRe_v$$

$$= -\frac{0.1582\mu_{v2}^2 L}{\rho_{v2} d_e^3\ \left(Re_{v3} - Re_{v2}\right)} \int_{Re_{v2}}^{Re_{v3}} \left(a_1 Re_v^{1.75} + a_2\,Re_v^{0.75}\right)\ dRe_v$$

$$= -\frac{0.1582\mu_{v2}^2 L}{\rho_{v2} d_e^3\ \left(Re_{v3} - Re_{v2}\right)} \left[\frac{a_1}{2.75}\left(Re_{v3}^{2.75} - Re_{v2}^{2.75}\right) + \frac{a_2}{1.75}\left(Re_{v3}^{1.75} - Re_{v2}^{1.75}\right)\right] \tag{2.65}$$

The static pressure change due to gravity is given by

$$p_{v3} - p_{v2\ s} = \rho_{v2} g\ \left(z_3 - z_2\right)\ \sin\phi = \rho_{v2} g L \sin\phi \tag{2.66}$$

where ϕ is the angle of the tube with respect to the horizontal.

The change in pressure due to momentum effects is

$$p_{v3} - p_{v2\ m} = -\rho_{v2}\ \left(v_{v3}^2 - v_{v2}^2\right) \tag{2.67}$$

In addition to these pressure changes in the duct there are also those due to the inlet contraction and outlet expansion. The pressure change from the header, at 1, to inside the condenser tube, at 2, assuming density changes are small, is calculated with equation (2.48).

The pressure change at the outlet of the tube, from 3 to 4, can be calculated by using $\sigma_{34} = \sigma_{21}$. The outlet pressure change is then

$$p_{v4} - p_{v3} = -\frac{\rho_{v3} v_{v3}^2}{2}\left[K_e - 1 + \alpha_c \frac{v_{v4}^2}{v_{v3}^2}\right] \tag{2.68}$$

where

$$K_e = \left(1 - \sigma_{34}^2\right) \tag{2.69}$$

The pressure change between the dividing header and the combining header can be calculated, assuming that, $\rho_{v3} \approx \rho_{v2}$ by adding equations (2.65) to (2.67), (2.48) and (2.67) i.e.

$$p_{v4} - p_{v1} = \left(p_{v2} - p_{v1}\right) + \left(p_{v3} - p_{v2\ f}\right) + \left(p_{v3} - p_{v2\ s}\right) + \left(p_{v3} - p_{v2\ m}\right) + \left(p_{v4} - p_{v3}\right)$$

$$= -\frac{\rho_{v1} v_{v2}^2}{2}\left(K_i + 1\right) - \frac{0.1582\mu_{v2}^2 L}{\rho_{v2} d_e^3\ \left(Re_{v3} - Re_{v2}\right)}\left[\begin{array}{l}\frac{a_1}{2.75}\left(Re_{v3}^{2.75} - Re_{v2}^{2.75}\right) \\ + \frac{a_2}{1.75}\left(Re_{v3}^{1.75} - Re_{v2}^{1.75}\right)\end{array}\right]$$

$$+\rho_{v2} g L \sin\phi - \rho_{v2}\left(v_{v3}^2 - v_{v2}^2\right) - \frac{\rho_{v2} v_{v3}^2}{2}\left[K_e - 1 + \alpha_c \frac{v_{v4}^2}{v_{v3}^2}\right] \tag{2.70}$$

Figure 2.24 shows the pressure and temperature difference between the dividing and combining headers. The pressure and temperature change from the dividing header to the combining header was calculated for steam temperatures from 40°C to 80°C. The inlet mass flow rate to the 9.5m finned tube is 0.0195 kg/s and the outlet mass flow rate is 0.0021 kg/s. The steam has a quality of 1. The dividing header has a mass flow rate of 46.4346 kg/s and the combining header of 0 kg/s. The mass flow rates were calculated for an ideal condenser unit with an ambient ground level temperature of 15.6°C. It can be seen that as the steam temperature increases the pressure loss decreases, the temperature shows the same trend. As the steam temperature increases the steam density increases and the pressure change between the dividing and combining headers decrease. A sample calculation for a particular tube is included in the appendix D.

To determine the steam and condensate properties in the condenser tube it is necessary to calculate an average steam pressure and temperature. An equation to calculate the average pressure in the condenser tube is derived below.

The frictional pressure change between the inlet to the finned tube and any other section of the duct is given by

$$\begin{aligned} p_v - p_{v2\ f} &\approx -\int_0^z f_{De}\left(\frac{\rho_{v2} v_v^2}{2}\right)\frac{dz}{d_e} = -\frac{0.1582\mu_{v2}^2 L}{\rho_{v2} d_e^3\ \mathrm{Re}_{v3} - \mathrm{Re}_{v2}} \int_{\mathrm{Re}_{v2}}^{\mathrm{Re}_v} a_1 \mathrm{Re}_v^{1.75} + a_2 \mathrm{Re}_v^{0.75}\ d\mathrm{Re}_v \\ &= -\frac{0.1582\mu_{v2}^2 L}{\rho_{v2} d_e^3\ \mathrm{Re}_{v3} - \mathrm{Re}_{v2}}\left[\frac{a_1}{2.75}\ \mathrm{Re}_v^{2.75} - \mathrm{Re}_{v2}^{2.75}\ + \frac{a_2}{1.75}\ \mathrm{Re}_v^{1.75} - \mathrm{Re}_{v2}^{1.75}\ \right] \end{aligned} \tag{2.71}$$

The gravitational pressure change is

$$p_v - p_{v2\ s} = \rho_{v2} g\ (z - z_2)\ \sin\phi \tag{2.72}$$

and the corresponding differential due to momentum effects is

$$p_v - p_{v2\ m} = -\rho_{v2}\left(v_v^2 - v_{v2}^2\right) \tag{2.73}$$

The pressure at any section of the condenser tube can now be calculated by adding equations (2.70), (2.71) and (2.72) and adding to the inlet pressure, p_{v2},

$$\begin{aligned} p_{vz} &= p_{v2} + (p_v - p_{v2\ f}) + (p_v - p_{v2\ s}) + (p_v - p_{v2\ m}) \\ &= p_{v2} - \frac{0.1582\mu_{v2}^2 L}{\rho_{v2} d_e^3\ \mathrm{Re}_{v3} - \mathrm{Re}_{v2}}\left[\frac{a_1}{2.75}\ \mathrm{Re}_v^{2.75} - \mathrm{Re}_{v2}^{2.75}\ + \frac{a_2}{1.75}\ \mathrm{Re}_v^{1.75} - \mathrm{Re}_{v2}^{1.75}\ \right] \\ &\quad - \rho_{v2}\left(v_v^2 - v_{v2}^2\right) + \rho_{v2} g \sin\phi\ (z - z_2) \end{aligned} \tag{2.74}$$

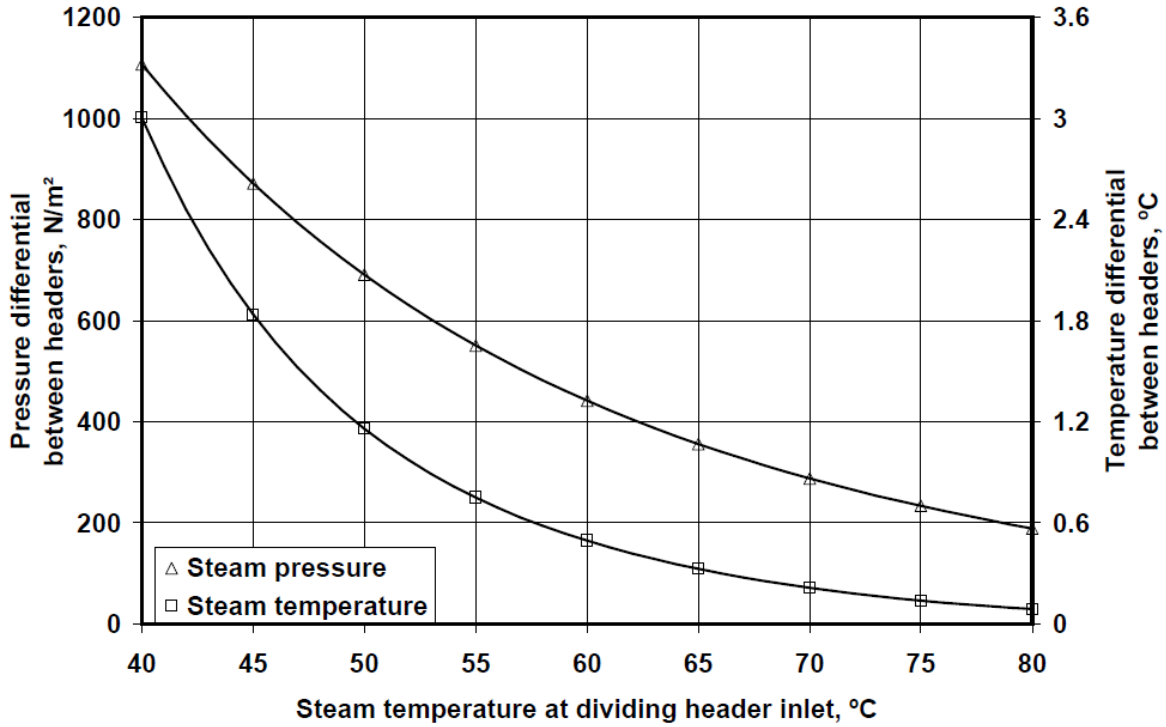

Figure 2.24: Pressure and temperature difference between the dividing and combining headers

The average vapor pressure can now be obtained by integrating equation (2.74) and dividing by the length of the tube. The average pressure is then

$$p_{vm} = \int_0^L \left[\begin{array}{l} p_{v2} - \dfrac{0.1582\mu_{v2}^2 L}{\rho_{v2} d_e^3 \ Re_{v3} - Re_{v2}} \left\{ \dfrac{a_1}{2.75} \ Re_v^{2.75} - Re_{v2}^{2.75} \ + \dfrac{a_2}{1.75} \ Re_v^{1.75} - Re_{v2}^{1.75} \right\} \\ -\rho_{v2} \ v_v^2 - v_{v2}^2 \ + \rho_{v2} g \sin\phi \ z - z_2 \end{array} \right] \frac{dz}{L} \qquad (2.75)$$

The integral will be evaluated by dividing it into smaller integrals as follows, except for p_{v2} which will stay a constant,

$$p_{vm} = p_{v2} - \frac{1}{L} \int_0^L \frac{0.1582\mu_{v2}^2 L}{\rho_{v2} d_e^3 \ Re_{v3} - Re_{v2}} \left\{ \frac{a_1}{2.75} \ Re_v^{2.75} - Re_{v2}^{2.75} \ + \frac{a_2}{1.75} \ Re_v^{1.75} - Re_{v2}^{1.75} \right\} dz$$

$$- \frac{1}{L} \int_0^L \rho_{v2} \ v_v^2 - v_{v2}^2 \ dz + \frac{1}{L} \int_0^L \rho_{v2} g \sin\phi \ z - z_2 \ dz$$

and each term will be evaluated separately. L is defined as $L = z_3 - z_2$.

The frictional pressure change in the duct is given by

$$\frac{1}{L} \int_0^L \ p_v - p_{v2} \ _f dz$$

$$= \frac{1}{L} \int_0^L \left[- \frac{0.1582\mu_{v2}^2 L}{\rho_{v2} d_e^3 \ Re_{v3} - Re_{v2}} \left(\frac{a_1}{2.75} \ Re_v^{2.75} - Re_{v2}^{2.75} \ + \frac{a_2}{1.75} \ Re_v^{1.75} - Re_{v2}^{1.75} \right) \right] dz$$

Set C = $-\dfrac{0.1582\mu_{v2}^2 L}{\rho_{v2} d_e^3 \ \mathrm{Re}_{v3} - \mathrm{Re}_{v2}}$ and substituting $\mathrm{Re}_v = \mathrm{Re}_{v2}\left(-z/L\right) + \mathrm{Re}_{v3}\left(z/L\right)$ to find

$$\frac{1}{L}\int_0^L \left(p_v - p_{v2}\right)_f dz$$

$$= \frac{C}{L}\int_0^L \left[\begin{array}{l} \dfrac{a_1}{2.75}\left(\left(\mathrm{Re}_{v2}\left(1-\dfrac{z}{L}\right)+\mathrm{Re}_{v3}\dfrac{z}{L}\right)^{2.75} - \mathrm{Re}_{v2}^{2.75}\right) \\ + \dfrac{a_2}{1.75}\left(\left(\mathrm{Re}_{v2}\left(1-\dfrac{z}{L}\right)+\mathrm{Re}_{v3}\dfrac{z}{L}\right)^{1.75} - \mathrm{Re}_{v2}^{1.75}\right) \end{array}\right] dz$$

To simplify the integral further it is split into two again. The two integrals are very similar and only one will be done step wise.

$$\int_0^L \left(\left(\mathrm{Re}_{v2}\left(1-\frac{z}{L}\right)+\mathrm{Re}_{v3}\frac{z}{L}\right)^{2.75} - \mathrm{Re}_{v2}^{2.75}\right) dz$$

$$= \frac{1}{3.75}\left(\mathrm{Re}_{v2}\left(1-\frac{z}{L}\right)+\mathrm{Re}_{v3}\frac{z}{L}\right)^{3.75} \Bigg/ \left(\frac{-\mathrm{Re}_{v2}}{L}+\frac{\mathrm{Re}_{v3}}{L}\right) - \mathrm{Re}_{v2}^{2.75} z \Bigg|_0^L$$

$$= \frac{1}{3.75}\left(\mathrm{Re}_{v2}\left(1-\frac{L}{L}\right)+\mathrm{Re}_{v3}\frac{L}{L}\right)^{3.75} \Bigg/ \left(\frac{-\mathrm{Re}_{v2}}{L}+\frac{\mathrm{Re}_{v3}}{L}\right) - \mathrm{Re}_{v2}^{2.75} L$$

$$-\frac{1}{3.75}\left(\mathrm{Re}_{v2}^{3.75} \Bigg/ \left(\frac{-\mathrm{Re}_{v2}}{L}+\frac{\mathrm{Re}_{v3}}{L}\right)\right)$$

$$= \frac{1}{3.75}\left(\mathrm{Re}_{v3}^{3.75} - \mathrm{Re}_{v2}^{3.75}\right) \Bigg/ \left(\frac{\mathrm{Re}_{v3}}{L}-\frac{\mathrm{Re}_{v2}}{L}\right) - \mathrm{Re}_{v2}^{2.75} L$$

Similarly

$$\int_0^L \left(\left(\mathrm{Re}_{v2}\left(1-\frac{z}{L}\right)+\mathrm{Re}_{v3}\frac{z}{L}\right)^{1.75} - \mathrm{Re}_{v2}^{1.75}\right) dz$$

$$= \frac{1}{2.75}\left(\mathrm{Re}_{v3}^{2.75} - \mathrm{Re}_{v2}^{2.75}\right) \Bigg/ \left(\frac{\mathrm{Re}_{v3}}{L}-\frac{\mathrm{Re}_{v2}}{L}\right) - \mathrm{Re}_{v2}^{1.75} L$$

The integral for the frictional pressure change in the duct is then

$$\frac{1}{L}\int_0^L \left(p_v - p_{v2}\right)_f dz$$

$$= C\left[\frac{a_1\left(\mathrm{Re}_{v3}^{3.75} - \mathrm{Re}_{v2}^{3.75}\right)}{10.3125\left(\mathrm{Re}_{v3} - \mathrm{Re}_{v2}\right)} - \frac{a_1 \mathrm{Re}_{v2}^{2.75}}{2.75} + \frac{a_2\left(\mathrm{Re}_{v3}^{2.75} - \mathrm{Re}_{v2}^{2.75}\right)}{4.8125\left(\mathrm{Re}_{v3} - \mathrm{Re}_{v2}\right)} - \frac{a_2 \mathrm{Re}_{v2}^{1.75}}{1.75}\right] \qquad (2.76)$$

The integral for the momentum pressure change in the duct is

$$\frac{1}{L}\int_0^L -\left[p_v - p_{v2}\right]_m dz$$
$$= \frac{1}{L}\int_0^L -\rho_{v2}\left[v_v^2 - v_{v2}^2\right] dz$$

where

$$v_v^2 = \left(\frac{(v_{v3} - v_{v2})z}{L} + v_{v2}\right)^2$$
$$= \frac{(v_{v3} - v_{v2})^2 z^2}{L^2} + \frac{2(v_{v3} - v_{v2})v_{v2}z}{L} + v_{v2}^2$$

thus

$$\frac{1}{L}\int_0^L -\rho_{v2}\left[v_v^2 - v_{v2}^2\right] dz$$
$$= -\frac{\rho_{v2}}{L}\int_0^L \left[\frac{(v_{v3} - v_{v2})^2 z^2}{L^2} + \frac{2(v_{v3} - v_{v2})v_{v2}z}{L} + v_{v2}^2 - v_{v2}^2\right] dz$$
$$= -\frac{\rho_{v2}}{L}\left[\frac{(v_{v3} - v_{v2})^2 z^3}{3L^2} + \frac{(v_{v3} - v_{v2})v_{v2}z^2}{L}\right]_0^L$$
$$= -\rho_{v2}\left[\frac{(v_{v3} - v_{v2})^2}{3} + (v_{v3} - v_{v2})v_{v2}\right]$$
$$= -\frac{\rho_{v2}}{3}\left[v_{v3}^2 + v_{v3}v_{v2} - 2v_{v2}^2\right] \qquad (2.77)$$

Finally the integral for gravitational pressure change is

$$\frac{1}{L}\int_0^L \rho_{v2} g \sin\phi z dz = \frac{\rho_{v2} g \sin\phi}{L}\int_0^L z dz$$
$$= \frac{\rho_{v2} g \sin\phi}{L}\left(\frac{L^2}{2} - 0\right) = \frac{\rho_{v2} g L \sin\phi}{2} \qquad (2.78)$$

The average pressure change in the duct can now be written as the sum of all the different average pressure changes. The average pressure in the duct is then

$$p_{vm} = p_{v2} - \frac{0.1582\mu_{v2}^2 L}{\rho_{v2} d_e^3 (Re_{v3} - Re_{v2})}\left[\frac{a_1 (Re_{v3}^{3.75} - Re_{v2}^{3.75})}{10.3125 (Re_{v3} - Re_{v2})} - \frac{a_1 Re_{v2}^{2.75}}{2.75} + \frac{a_2 (Re_{v3}^{2.75} - Re_{v2}^{2.75})}{4.8125 (Re_{v3} - Re_{v2})} - \frac{a_2 Re_{v2}^{1.75}}{1.75}\right] \qquad (2.79)$$
$$- \frac{\rho_{v2}}{3}\left[v_{v3}^2 + v_{v3}v_{v2} - 2v_{v2}^2\right] + \frac{\rho_{v2} g L \sin\phi}{2}$$

2.7 Dephlegmator

2.7.1 Prevention of non-condensable gas build-up and backflow

In a two-row condenser the upstream row has a greater potential to condense steam because it receives colder ambient air than the second row which receives pre-heated air. The first row therefore has a greater steam side pressure drop over the condenser tube than the second row. Steam from row two is then sucked back into row one at the outlet of row one. The pressure change between the two headers will be equal to the pressure drop over the second row (Kröger 2004). A schematic of a two-row condenser is shown in figure 2.25 with backflow occurring. Non-condensable gasses can then accumulate in row one and block the flow out of the tube and thereby reduce the performance of the condenser.

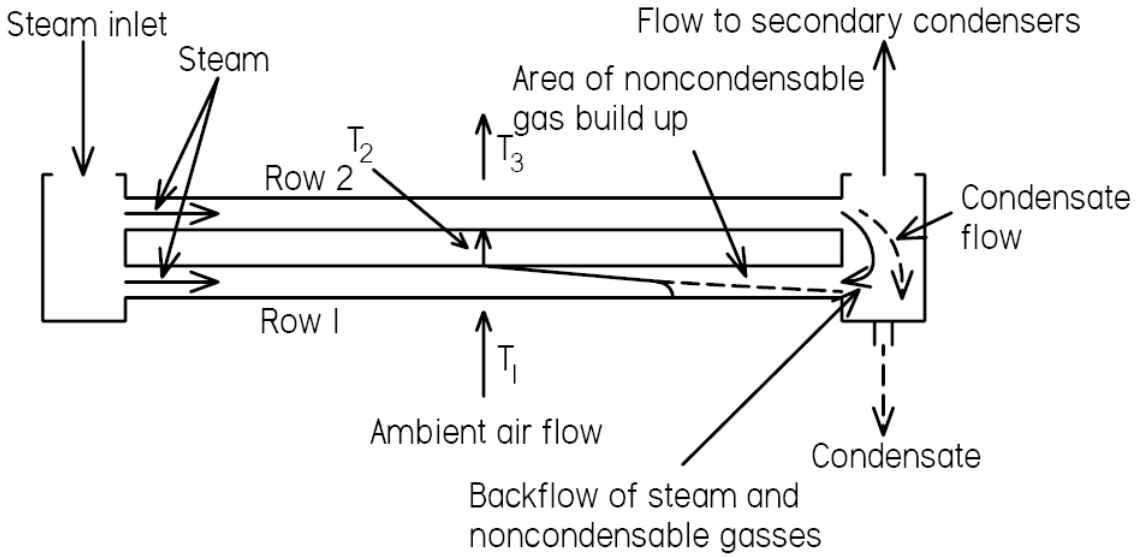

Figure 2.25: Schematic of a two-row condenser with backflow occurring

To solve the problem of backflow and non-condensable gas build-up a dephlegmator was added in series. A schematic of a dephlegmator fan unit(D-type condenser fan unit) is shown in figure 2.26. The dephlegmator is positioned below the reducer in the dividing header as seen in figure 2.10. This was done so that there will be steam flow out of both tube rows in the condenser. The steam is then condensed in the dephlegmator and the non-condensable gasses are extracted by a vacuum pump at the top. It is important that the suction pump is sized correctly so that all the non-condensable gasses are removed.

2.7.2 Governing equations

The governing equations for a dephlegmator fan unit are the same as for a normal condenser fan unit. When disturbances like backflow and flooding occur, then the average pressure in the condenser tube will differ from equation 2.79.

2.7.3 Flooding

Flooding is defined as the condition that exists when there is a sharp increase in the pressure drop across the dephlegmator tube. This is due to the condensate being accumulated in the tube due to the steam entering the bottom of the tube. The governing equations that are used to calculate the heat transfer to the air can not be used when this situation arises.

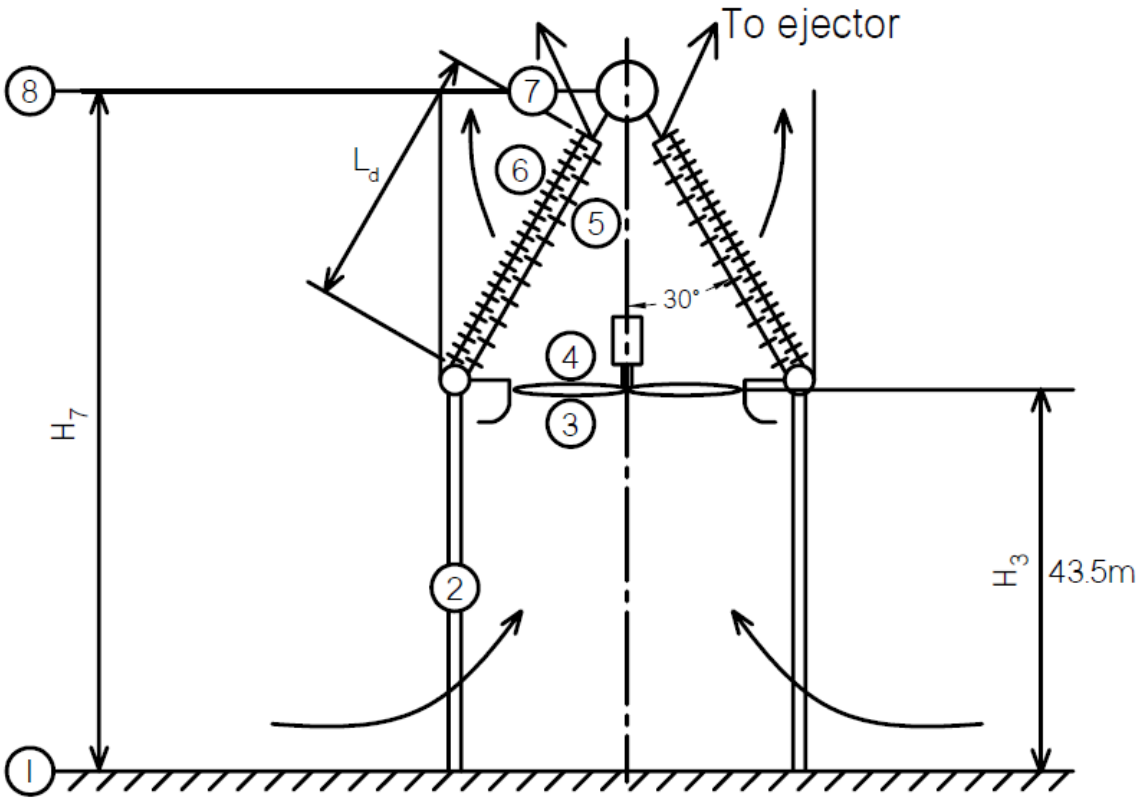

Figure 2.26: Schematic of D-type condenser fan unit

Zapke (1994) found that there is a wide range of scatter in predicted flooding velocities. This is due to different geometries of the test tubes used and also the definition that was used.

The following correlation was developed by Zapke et al (2000) to calculate the flooding speed

$$Fr_{Dg} = a_3 \exp\left(-a_4 Fr_{Dl}^{0.6} / Oh^{-0.2}\right) \tag{2.80}$$

where

$$a_3 = 7.9143\times10^{-2} + 4.9705\times10^{-3}\phi + 1.5183\times10^{-4}\phi^2 - 1.9852\times10^{-6}\phi^3 \tag{2.81}$$

$$a_4 = 18.149 - 1.9471\phi + 6.7058\times10^{-2}\phi^2 - 5.3227\times10^{-4}\phi^3 \tag{2.82}$$

and ϕ is the inclination angle of the finned tube in degrees.

Kröger(2004) suggests that because $a_4 Fr_{Dl}^{0.6} / Oh^{-0.2} << 1$ for most cases in air-cooled reflux steam condensers that equation (2.80) can be simplified by expressing the exponential function in terms of a power series and ignoring the higher order terms. Equation (2.80) simplifies to

$$Fr_{Dg} \approx a_3 \left(1 - a_4 Fr_{Dl}^{0.6} / Oh^{-0.2}\right) \approx a_3 \tag{2.83}$$

The flooding speed can then be expressed as

$$v_{gs} \approx \left[a_3 (\rho_l - \rho_g) g H / \rho_g\right]^{0.5} \tag{2.84}$$

where H is the inside height of the tube.

In very cold weather, with temperatures under zero, the condensate can freeze in the tube if flooding should occur. This can cause the tubes to burst.

Table 2.2: Dephlegmator flooding speeds for different steam temperatures

Single tube row condenser			Two tube row condenser		
T_v, °C	v_{gs}, m/s	v_{in}, m/s	v_{gs}, m/s	v_{in1}, m/s	v_{in2}, m/s
40	108.787	99.155	75.761	113.935	108.7273
50	85.221	62.642	59.350	73.310	68.5856
60	67.867	40.213	47.264	47.567	43.4804
70	54.859	26.442	38.205	31.556	27.7342
80	44.948	17.828	31.303	21.456	17.3201

Table 2.2 shows the flooding steam speed, v_{gs}, and inlet steam speed, v_{in}, for different inlet steam temperatures. The flooding and inlet steam speed for both the single and two-row condensers are included. The dephlegmator tube length is 9m. No flooding will take place in the single-row condenser due to the higher tube height and corresponding lower inlet steam speeds. The flooding steam speed for the two-row condenser is lower than for the single-row due to the lower tube height. The inlet steam speeds are also higher due to the smaller cross sectional area of the two-row tubes. Flooding is present in both the tube rows from 40ºC to 50ºC and in the first row for 60ºC. From table 2.2 it is clear that flooding is less likely to occur at higher steam temperatures than at low steam temperatures.

In the next chapter the different air side disturbances that can be present during the operation of an air-cooled condenser are discussed.

Chapter 3: Effect of ambient conditions on air-cooled steam condenser

Ambient conditions like wind and temperature distributions have an effect on the operation of the condenser and reducing the cooling capacity in most cases. Duvenhage and Kröger (1996) state that fan performance reduction and recirculation of the hot air plume are the main reasons for the reduction of the performance of the condenser, but neglect the effect of temperature distributions. Different temperature distributions cause different inlet conditions for the condenser fans causing different heat transfer rates within the condenser. In this chapter the different disturbances and the corresponding effects will be investigated.

3.1 Temperature distributions and fan inlet conditions

An air temperature distribution describes the air temperature change with elevation. Shown in figure 3.1 are the air temperature distributions for a 24 hour period. The temperatures were recorded on a 96m high weather mast (Kröger 2004). The temperature distributions are seen to change during the day.

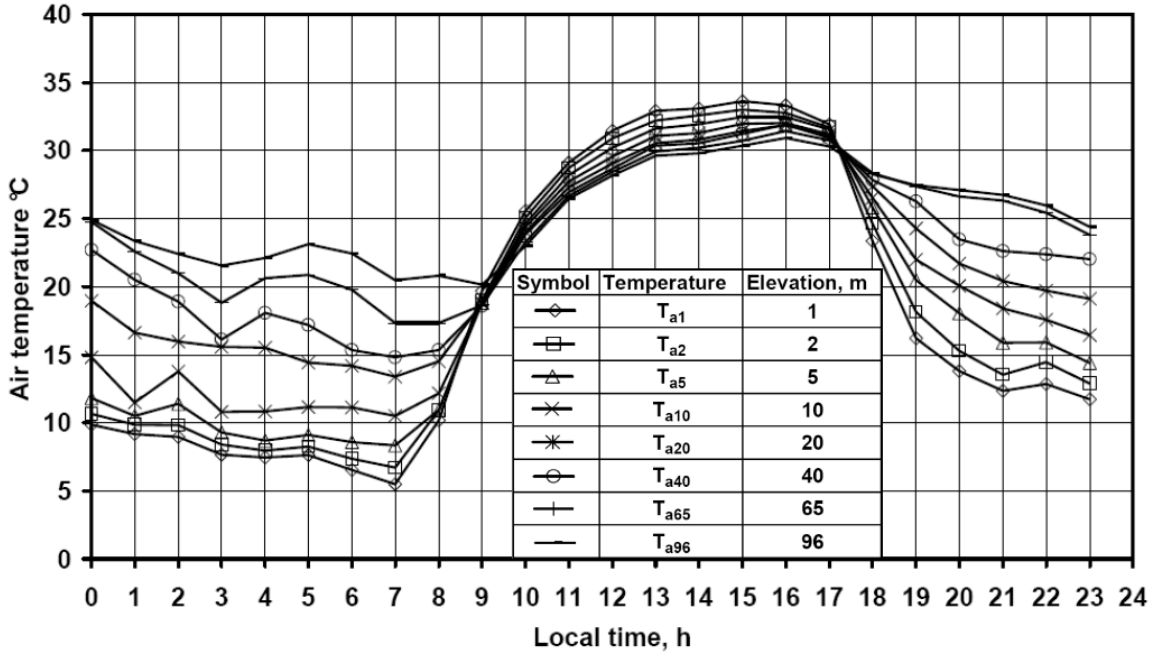

Figure 3.1: Temperature distributions for a 24 hour period

Shown in figure 3.2 are the individual air temperature distributions for every hour. At 00:00 hours the air temperature increases with an increase in elevation. This is a night time temperature distribution and is also called a temperature inversion. This distribution is seen till 09:00 hours when the ground level temperature starts to increase. This is due to the sun rising and heating the ground. The air temperature distribution is now a day time distribution. The temperature distribution is closer to constant during the day in comparison to the night time when larger changes in the temperature are present. The distribution starts to

change again at about 17:00 hours. When the sun sets the ground looses heat faster, due to radiation to the sky, than the air. This causes the temperature inversions that are present during the night.

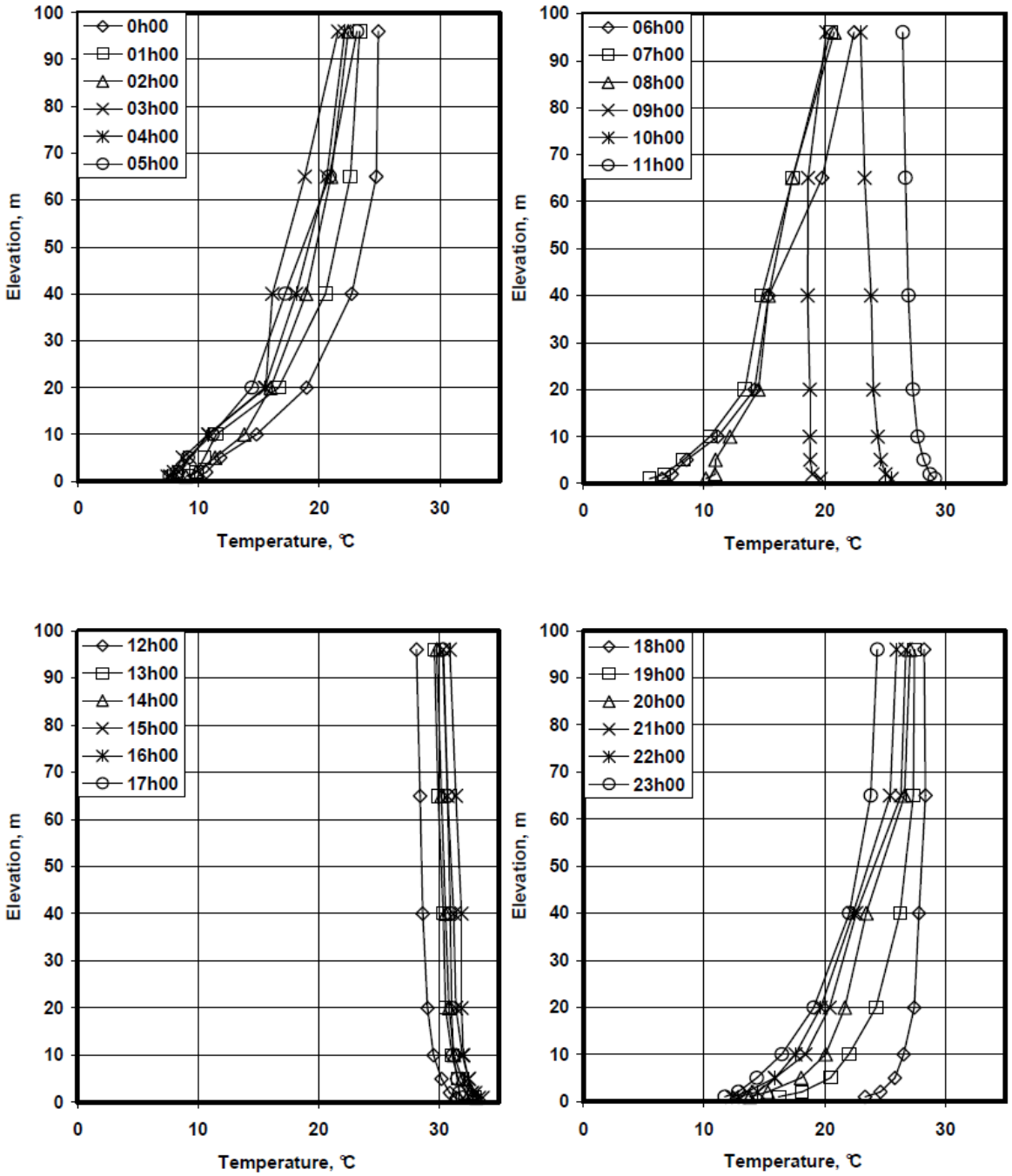

Figure 3.2: Individual air temperature distributions for 24 hour period

A schematic side view of a section of an essentially two-dimensional air-cooled condenser is shown in the figure 3.3. The temperature distribution is also included as well as approximate flow paths of the ambient air as it is sucked into the fans.

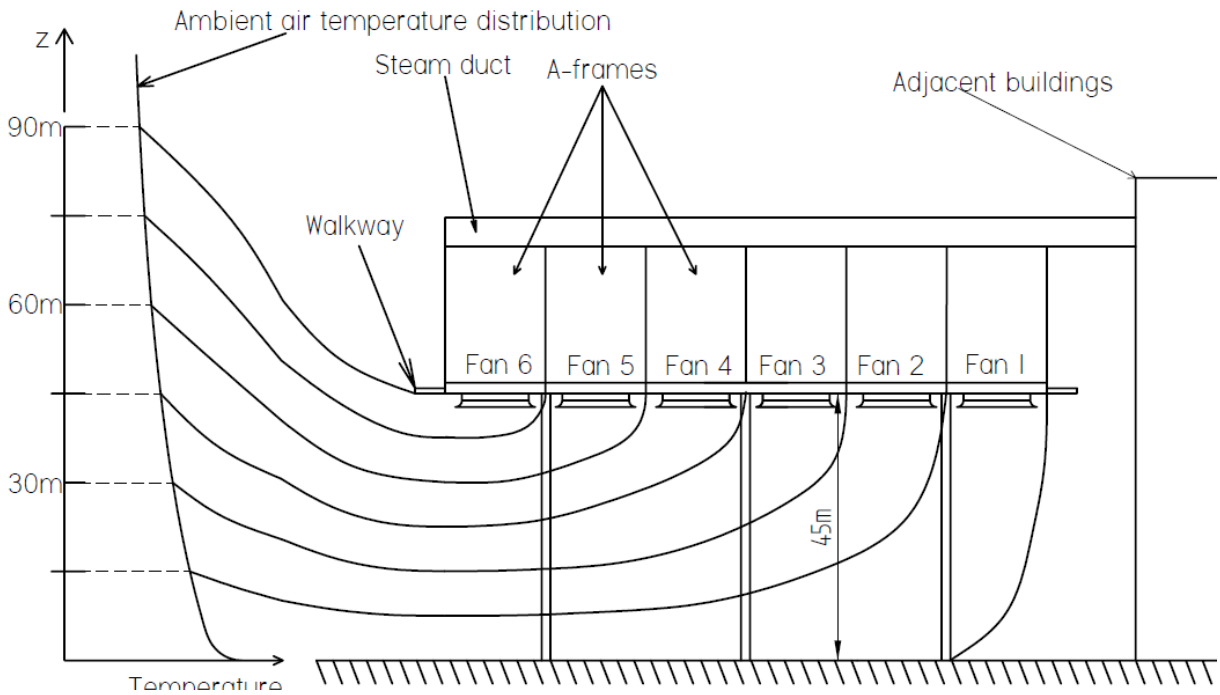

Figure 3.3: Schematic side view of a two-dimensional air-cooled condenser with temperature distribution and approximate flow paths

Ambient air is drawn in from approximately twice the fan platform height. Because of this, there are inlet air temperature differences between the different fans, as the air temperature changes with elevation. Small air temperature changes are experienced as the air is drawn into the fan inlets. This is due to pressure changes that take place as the elevation of the approaching air changes and the air accelerates into the fan. For the essentially two-dimensional air-cooled condenser shown in figure 3.3, fan 1 receives air from ground level to about 15m and fan 6 receives air from about 75m to 90m.The other fans receive air from in between fan 1 and 6. Each of these sections will be referred to as the intake elevation of each fan.

3.1.1 Fan inlet conditions

To determine the inlet temperature and pressure for each fan in the condenser, the ambient conditions for the intake elevation of each fan must be known. If the pressure at ground level and the temperature distribution is known, this information can be used to calculate the pressure at the different elevations. Klopper and Kröger (2005) give a simple equation to calculate the temperature distribution of a temperature inversion. It was found that this equation could also be used for normal day time temperature distribution. The equation requires only two temperatures at different elevations,

$$T_z = T_1 + 273.15\left(\frac{z}{z_r}\right)^{b_T} - 0.00975z \qquad (3.1a)$$

$$\approx T_1 + 273.15\left(\frac{z}{z_r}\right)^{b_T} \qquad (3.1b)$$

where T_1 is in °C and measured close to ground level (typically 1 to 2 meters above ground) and z_1 is the elevation corresponding to T_1. The temperature distribution is known and therefore b_T can be solved for by an optimizing algorithm. The pressure distribution for a certain temperature distribution is

$$p_z = p_0 \exp\left[\frac{-g \left(z^{1-b_T} - z_r^{1-b_T} \right)}{T_1 + 273.15 \; R \; 1 - b_T \; z_r^{-b_T}} \right] \tag{3.2}$$

where p_0 is the ground level pressure. The derivation of equation (3.2) is given in appendix G.

The average temperature for each intake elevation is derived in appendix G and is

$$T_{iamb} = \frac{T_1 + 273.15 \left(z_{(i+1)a}^{b_T+1} - z_{ia}^{b_T+1} \right)}{z_{(i+1)a} - z_{ia} \; z_1^{b_T} \; b_T + 1} \tag{3.3}$$

where T_{iamb} is the average temperature the between $z_{(i+1)}$ and z_i, z_1 is the elevation of T_1,the ground level temperature, which is at 1m. The average pressure is calculated from

$$p_{amb} = \frac{\sum_{j=1}^{n} p \; j \times \Delta z}{\left| z_{i+1} - z_i \right|} \tag{3.4}$$

where $\Delta z = |z_{(i+1)} - z_i|/n$ and n is the number of points taken between $z_{(i+1)}$ and z_i. The derivation of equations (3.3) and (3.4) is included in appendix G. Since the changes in temperature and pressure are small from the ambient conditions, as described by equations (3.3) and (3.4), to the fan inlets, it was decided to use the ambient conditions as the inlet conditions to each fan since the uncertainty in equation (3.1) is larger than the temperature change to the fan inlet.

The temperature distribution shown in figure 3.4 below is a distribution normally found during the day time when the sun heats up the ground up and the air temperature decreases as the elevation increases. The distribution was recorded by Kröger (2004) at 12:00 local time. Both the measured temperature distribution and the distribution generated by equation (3.1b) are shown. Equation (3.1b) describes the measured data very accurately.

Figure 3.5 shows a typical night time temperature distribution (inversion) measured by Kröger (2004) at 00:00 local time. The fit in figure 3.5 is not as accurate as in figure 3.4. The opposite trend can be seen in figure 3.5 to figure 3.4. In figure 3.5 a temperature inversion is present, the ground is losing heat through radiation to the sky, but the air takes longer to cool and so the temperature rises as the elevation increases.

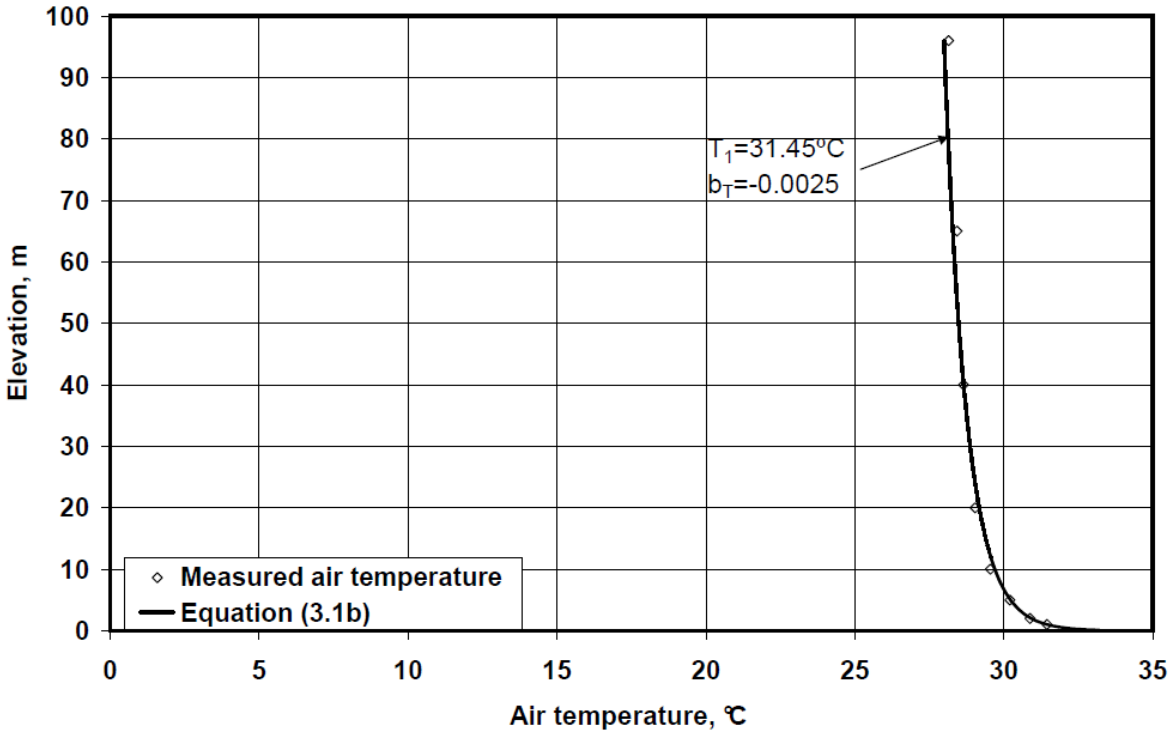

Figure 3.4: Day time temperature distribution at 12:00 local time

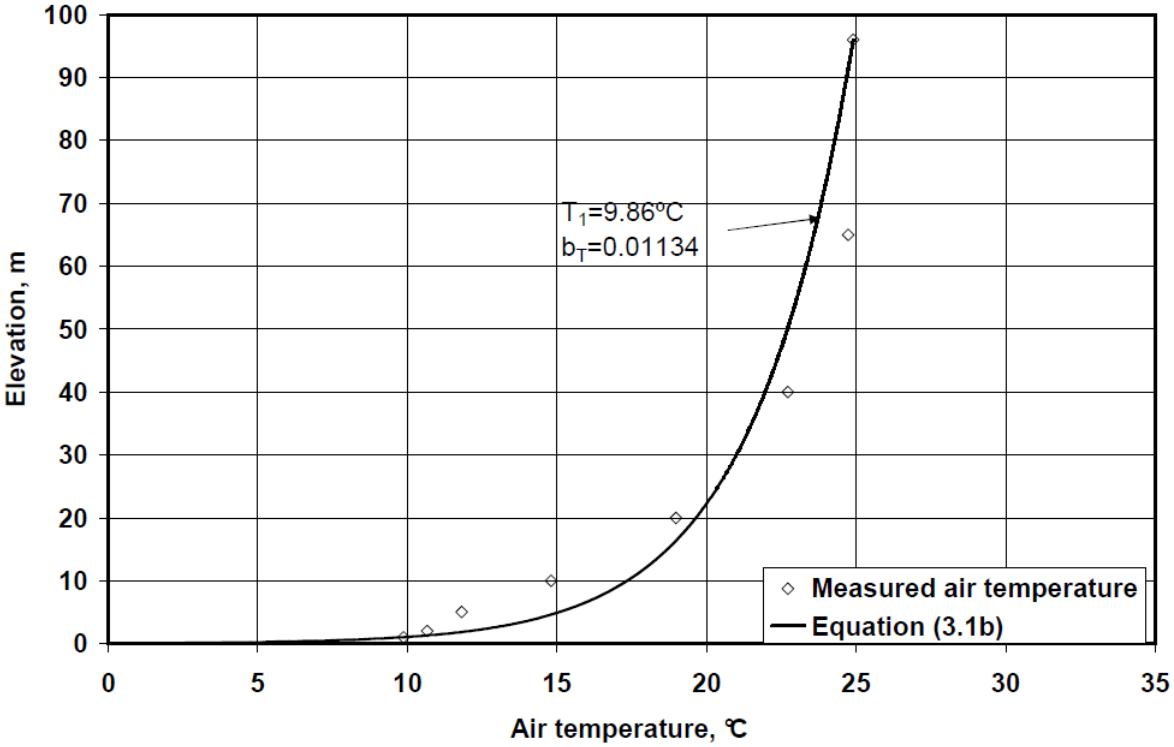

Figure 3.5: Night time temperature distribution at 00:00 local time

3.2 Extreme ambient temperature effects

Extreme hot and cold ambient conditions can have a negative effect on the operation of the air-cooled condenser. Under extreme cold the turbine exhaust temperature can be low because of the low ambient temperature. Figure 2.9 shows that as the steam temperature decreases the pressure change in the duct system increases. The steam temperature that enters the condenser is therefore

significantly lower than the turbine exhaust temperature. The condensate can freeze in the tubes if the ambient conditions are cold enough and this can cause the condenser tubes to burst. The steam speeds in the condenser increase with decreasing steam temperature and erosion of tube entrances increase (Badr et al. 2006). Extreme hot conditions can cause the turbine to trip as the exhaust temperature increase to achieve the required cooling needed. Varying the mass flow rate of the air through the fans can be used to control the exhaust steam temperature to keep the turbine exhaust temperature in the operating range.

3.3 Fan performance reduction

It is of utmost importance that the fans of an air-cooled condenser deliver sufficient air to the finned tube bundles so that the heat from the condensing steam can be effectively rejected. If the performance of the fans should decrease, then the system is under pressure and in extreme cases turbine tripping can occur. Two factors are identified as important for fan performance, the fan platform height must be of sufficient height and secondly the wind affects the performance of the fans.

3.3.1 Wind effect on fan performance

Wind has in most cases a negative effect on the performance of an air-cooled condenser. Duvenhage and Kröger (1996) did a numerical investigation into effect of cross winds on the performance of an air-cooled heat exchanger bank and found that the wind reduced the mean performance of the fans, although some fans downwind performed better than in an ideal no wind situation. It was found that wind had a similar effect on the fan performance as reducing the platform height.

Duvenhage and Kröger (1996) numerically modeled the air flow patterns about and through an air-cooled heat exchanger under windy conditions. A schematic of the system is shown in figure 3.6. Both recirculation and fan performance reduction was taken into consideration. When the wind blows in the longitudinal direction of the heat exchanger bank it was seen that the reduction in performance of the air-cooled heat exchanger is mainly due to the recirculation of the hot plume air. Under cross wind conditions it was seen that the reduction in heat exchanger performance was mainly due to fan performance reduction. The geometry of the air-cooled heat exchanger is different from that used in this investigation, but it is assumed that the same trends will be visible. These results were obtained for a free-standing air-cooled heat exchanger.

Gu et al. (2005) used micro-fans in a scaled model of a condenser bank with surrounding buildings to determine the amount of plume recirculation that takes place. The proximity of surrounding buildings was seen to influence the recirculation of the condenser bank. Bredell et al. (2006) found that different fans have different sensitivities to wind effects. It is therefore questionable if the micro-fans will exhibit the same performance characteristics as the full-scale condenser fans. The rotational speed was varied to give a constant exhaust air speed to counter the performance effect of the cross-flow on the fan performance, but it is still questionable if the detrimental effect of the wind on fan performance could be removed completely.

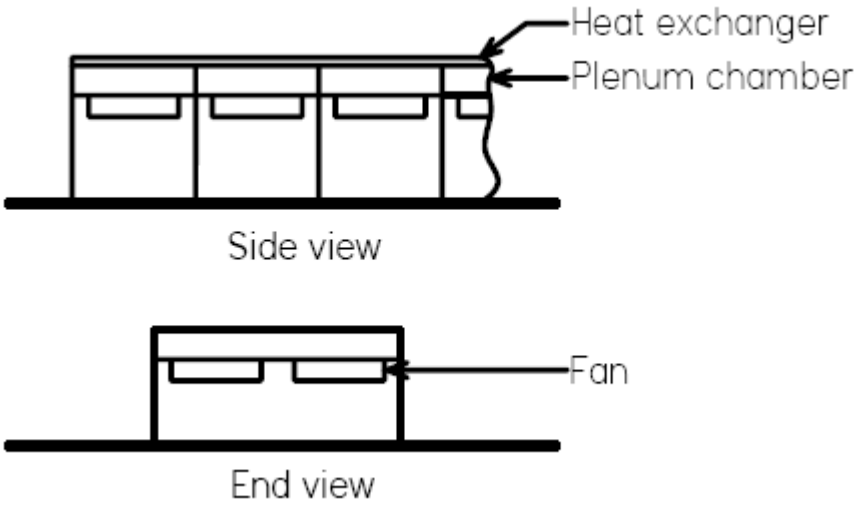

Figure 3.6: Schematic of air-cooled heat exchanger numerically analyzed by Duvenhage and Kröger (1996)

Gu et al. (2005) did wind tunnel tests to study the effect of wind direction on recirculation of an air-cooled condenser. The model used included the boiler house and turbine halls. The highest recirculation was found when the wind blows from the direction of the boiler house and turbine hall. A secondary peak in recirculation was found when the wind blows in the longitudinal direction of the condenser. Under cross winds conditions coming from the opposite side of the turbine halls nearly no recirculation was seen. This agrees with the results given by Duvenhage and Kröger (1996). Recirculation contour lines are also given, but as the origin of the recirculated gas is not given, these can't be used to determine the inlet temperatures to the fans unless it is assumed that all exhaust temperatures are equal.

Van Rooyen (2007) numerically modeled the effect of different wind speeds on an air-cooled steam condenser. The results are given as a ratio of actual to ideal mass flow rates, V/V_{id} . Two wind directions were modeled, one where the wind blows perpendicular to the long axis of the condenser and one where the wind is blowing at 45° to the long axis. The condenser that was modeled was a free standing unit with no other structures modeled that could influence the air flow patterns. It was found if the wind blows perpendicular to the long axis of the condenser that the edge fans experience a large reduction in performance. The addition of a walkway around the edge of the condenser was seen to increase the performance of the edge fans considerably.

Van Rooyen (2007) also found that the wind profile has a small effect on the performance of the fans. Both uniform and non-uniform wind distributions were tested with the platform height wind speed being the same. The wind speed and direction at the platform height is therefore important when designing a new air-cooled steam condenser.

Chapter 4: Computational model of air-cooled steam condenser

In this chapter the method that was used to calculate the steam distribution in the condenser is described. The model that was developed is a combination of analytical derivations and empirical equations.

The condenser is made up of four parts, the dividing header, the condenser tubes(K-type condenser), the combining header and the dephlegmator tubes(D-type condenser). The pressure change equations given in chapter 2 for duct flow are used to calculate the pressure change in the steam duct. The condenser solution is more complicated and will be discussed below.

4.1 Solution of distributions in condenser

In the condenser the steam mass flow rate and pressure distributions must be continuous without discontinuities between control volumes. The distributions in the condenser must be solved iteratively to satisfy these criteria. Shown in figure 4.1 is a schematic of a section in a single-row condenser. The different headers are divided into control volumes and each finned tube is seen as one control volume.

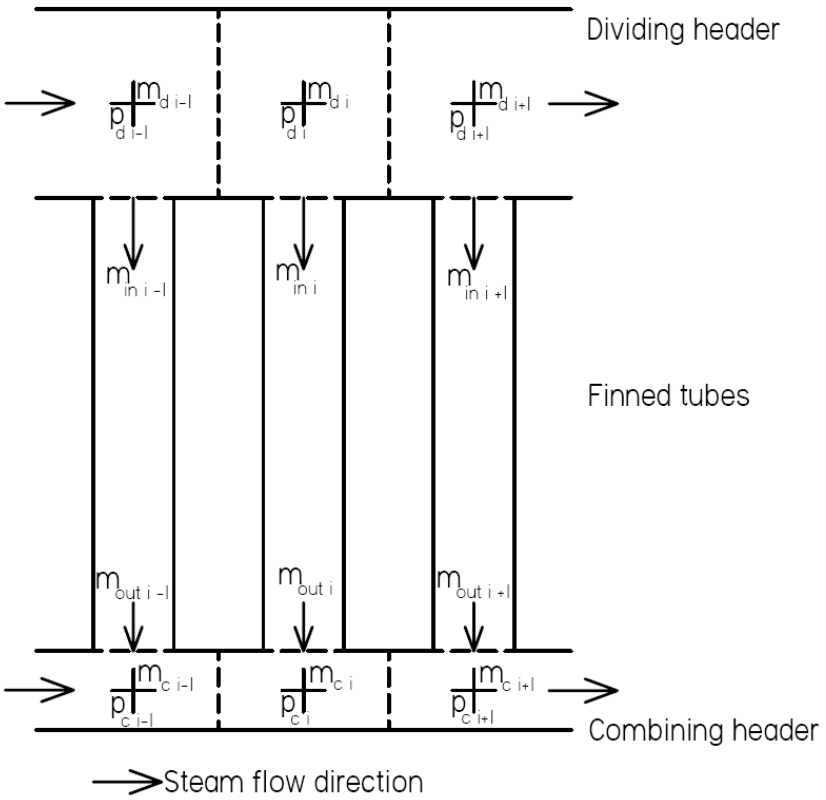

Figure 4.1: Schematic of division of two-row condenser

Steam enters the dividing header from the left with a mass flow rate of $m_{d\,i-1}$ and a steam pressure of $p_{d\,i-1}$. Steam flows into the finned tubes from the dividing header and the dividing header steam mass flow rate is reduced to $m_{d\,i}$. The

steam pressure also changes and the new pressure is $p_{d\ i}$. The mass flow continuity equation for the dividing header section is then

$$m_{d\ i} = m_{d\ i-1} - m_{in\ i-1} \tag{4.1}$$

The steam pressure changes in the dividing header is

$$p_{d\ i} = p_{d\ i-1} + \left(p_{d\ i} - p_{d\ i-1}\right)_m + \left(p_{d\ i} - p_{d\ i-1}\right)_f \tag{4.2}$$

Part of the steam that flows into the finned tube condenses and the excess steam flows into the combining header. The outlet steam pressure of the finned tubes must be equal to the steam pressure in the combining header at that location to stop backflow from occurring. The outlet pressure of the finned tube is calculated with equation (2.70). The mass flow continuity equation for the finned tube control volume is

$$m_{in\ i} = m_{con\ i} + m_{out\ i} \tag{4.3}$$

An initial outlet mass flow rate, $m_{out\ I}$, is assumed and is then adjusted based on the pressure difference between the pressure just outside of the finned tube and the combining header pressure. The pressure difference is calculated as follows

$$\Delta p_i = \frac{p_{c\ i} - p_{out\ i}}{p_{c\ i}} \tag{4.4}$$

and the new outlet mass flow rate is

$$m_{out\ i} = m_{out\ i} \times \left(1 + a \times \Delta p_i\right) \tag{4.5}$$

where a is a relaxation factor.

It can be seen in figure 2.10 that the combining header has two parts with opposing flow directions. On the left hand side of the dephlegmator the flow is co-current with the dividing header while on the right hand side it is counter-current. The mass flow rate continuity equation for the left hand side of the condenser is

$$m_{c\ i} = m_{c\ i-1} + m_{out\ i-1} \tag{4.6}$$

and on the right hand side

$$m_{c\ i} = m_{c\ i-1} - m_{out\ i-1} \tag{4.7}$$

The difference in sign is due to the direction of the flow. It is assumed that the flow on the left is in the positive direction and on the right in the negative direction.

The pressure change in the combining header is calculated as

$$p_{c\ i} = p_{c\ i-1} + \left(p_{c\ i} - p_{c\ i-1}\right)_m + \left(p_{c\ i} - p_{c\ i-1}\right)_f \tag{4.8}$$

4.2 Prediction of backflow into finned tubes

If it is predicted by equation (4.5) that the outlet mass flow rate must be negative, then backflow will occur in that control volume. To save computational time it was decided that a lower mass flow rate limit for the outflow of the finned tubes will be

set. If the outlet mass flow rate becomes lower than the limit then backflow is predicted in that control volume. The limit that was set is

$$m_{out\ i} < 1 \times 10^{-15}\ kg/s \tag{4.9}$$

The model used in this study can only predict backflow, but does not take the effect that backflow has on the combining header into account. If backflow occurs flow is sucked out of the combining header into the outlet of the finned tube and therefore the mass flow rate in the combining header decreases.

The backflow from 9 to 11 and from 12 to 15, in figure 2.10, is calculated. The outlet mass flow rates of the first and the last tube in the condenser is then adjusted according to the number of tubes with backflow in that section of the condenser. The outlet mass flow rates are increased to increase the total pressure change between the dividing and combining headers. This will cause steam to be sucked out of the tubes where backflow is predicted. The outflow for the first tube is adjusted as follows

$$m_{out\ 1,1} = m_{out\ 1,1} \times \left(1 + a \frac{n_{back9-11}}{n_{total}} \right) \tag{4.10}$$

and for the last tube in the condenser street

$$m_{out\ 1,1} = m_{out\ 1,1} \times \left(1 + a \frac{n_{back12-15}}{n_{total}} \right) \tag{4.14}$$

where a is a relaxation factor, $n_{back9\text{-}11}$ is the number of tubes where back flow is predicted from 9 to 11, $n_{back12\text{-}15}$ is the number of tubes where back flow is predicted from 12 to 15 and n_{total} is the total number of tubes in the condenser.

4.3 Calculation of critical dephlegmator tube length

The model is solved in three parts. Firstly fan units 1 to 3 are solved, then an initial guess of the dividing header for fan units 4 to 6 is calculated and lastly fan units 4 to 6 is solved in reverse order with the combining header.

The inlet steam temperature is constant along with the ambient conditions. An initial inlet steam mass flow rate is assumed and changed after each global iteration to the amount of steam that is condensed, so that

$$m_{d,1} = m_{c\ total} \tag{4.15}$$

where $m_{d,1}$ is the inlet mass flow rate to the header and $m_{c\ total}$ is the total amount of steam that is condensed. After solving the condenser from the first to the last finned tube equation (4.15) is used to redefine the inlet mass flow rate to the dividing header.

The dephlegmator tube length is adjusted by comparing the amount of steam that is calculated at 12 for the left, under the dephlegmator, and from the right in the combining header. This can be seen in figure 4.2. The difference is calculated as follows

$$e_{mass} = \frac{m_{c,12^+} - m_{c,12^-}}{m_{c,11} - m_{c,12^+}} \tag{4.16}$$

The new dephlegmator tube length is then

$$L_{d\ new} = L_{d\ old} \times\ 1 + e_{mass} \tag{4.17}$$

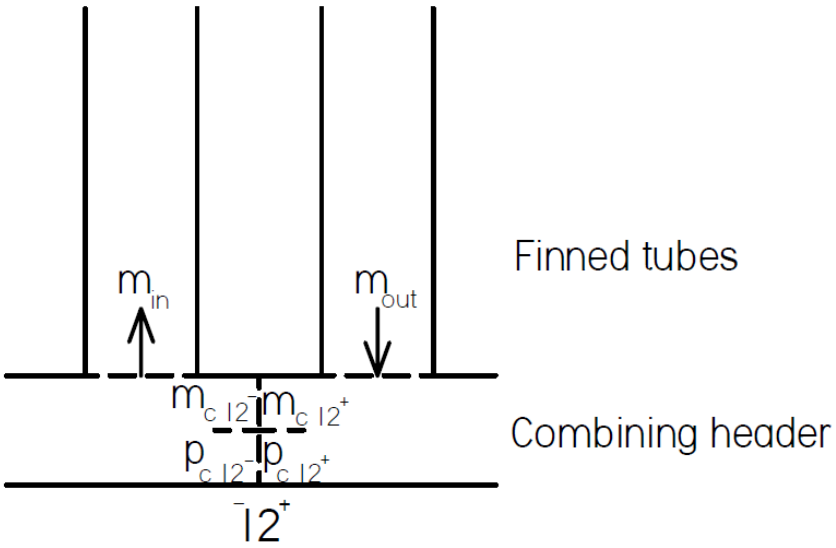

Figure 4.2: Schematic of node point 12 in combining header

Due to space restrictions the upper limit for the dephlegmator tube length is

$$L_d \leq 9m \tag{4.18}$$

Should equation (4.17) calculate a tube length longer than 9m then $L_d = 9m$ and the calculation is continued with a constant dephlegmator tube length so that the areas where backflow will occur can be identified.

4.4 Solving condenser with ambient disturbances

The condenser is forced to condense the same amount of steam when disturbances are present as for the ideal case. The solution method differs from the ideal case because the steam inlet temperature is changed until the same amount of steam is condensed.

The difference in the steam condensed and the ideal case inlet mass flow rate is calculated by

$$e_{T_v} = \frac{m_{con} - m_{ideal}}{m_{ideal}} \tag{4.19}$$

The new inlet steam temperature is then calculated as

$$T_{v1} = T_{v1} \times\ 1 - a \times e_{T_v} \tag{4.20}$$

This is repeated until equation (4.19) reaches the convergence criteria.

4.5 Solving a two-row condenser

Figure 4.3 shows the division of control volumes for a two-row condenser. The second row of tubes has one more tube per bundle and therefore the first control volume has three tubes. Since the two rows don't have the same number of tubes the discritization of figure 4.1 can't be used. The solution is generated for the first tube in each row and then it is assumed that the second tube in the second row has the same performance as the first. The first control volume of each bundle is calculated in this way. The other control volumes have two tubes, one from each tube row.

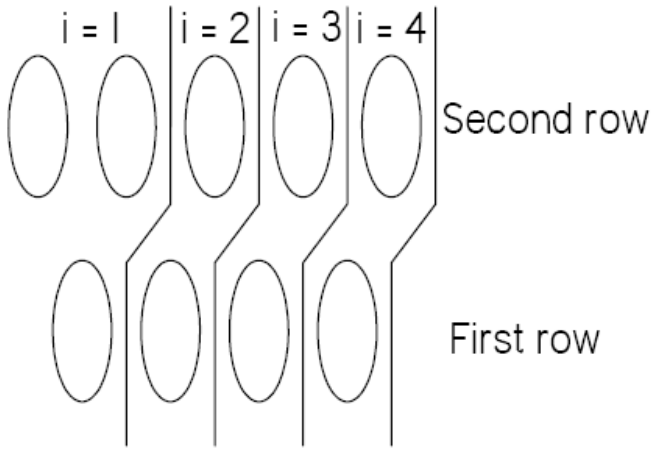

Figure 4.3: Division of condenser tubes for modeling of condenser

It is important that the outlet pressure of each tube in a control volume is equal to each other to stop steam from flowing back into the outlet of the other tube as can be seen in figure 2.24. This is done by calculating the outlet pressures of the tubes in each row and adjusting the outlet mass flow rate until the outlet steam pressures are the same. If tube row two has a lower steam pressure change between the headers then the outlet mass flow rate must be adjusted as follows

$$m_{out\ 2,i} = m_{out\ 2,i} \times 1 + a \times \Delta p_{out\ i} \qquad (4.22)$$

or if the steam pressure change is lower over the first tube row then

$$m_{out\ 1,i} = m_{out\ 1,i} \times 1 + a \times \Delta p_{out\ i} \qquad (4.23)$$

where

$$\Delta p_{out\ i} = \frac{p_{out\ 2,i} - p_{out\ 1,i}}{p_{out\ 1,i}} \qquad (4.24)$$

and a is a relaxation factor.

Once the outlet steam pressures are the same equation (4.4) is used to calculate the pressure difference between the tube outlet pressure and the combining header pressure.

Chapter 5: Steam side effects on the critical dephlegmator tube length of a single-row air-cooled condenser

In this chapter the influence of variations in inlet loss coefficient, momentum correction factor, and position of the dephlegmator fan unit in the condenser street will be investigated.

5.1 Effect of variation in the inlet loss coefficient on the critical dephlegmator tube length

In chapter 2 different inlet configurations for the dividing header was given. In this section the effect of the different configurations on the critical dephlegmator tube lengths will be investigated.

Table 5.1: Critical dephlegmator tube lengths for the different inlet loss coefficient models for a single-row condenser

	Equation (2.49)	Straight entry	Backward facing step	Wedge-like ramp	Step, ramp and grid
Ld	1.0506m	>9m	4.374m	6.3325m	>9m

The critical dephlegmator tube lengths for the different inlet loss coefficient models are shown in table 5.1. When equation (2.49) is used the critical dephlegmator tube length is the shortest, but it was shown in figure 2.21 that the experimental inlet loss coefficients differ significantly from that of the corrected equation (2.49). For the straight entry inlet loss coefficient the critical dephlegmator tube length is longer than 9m and backflow will occur in the condenser. The backward facing step and the wedge-like ramp both show improvements over the straight entry and the backward facing step has the lowest predicted critical dephlegmator tube length. The critical areas in the condenser for backflow are the first few tubes at the inlet to the condenser and to the right of the dephlegmator.

The combination of the backward facing step, the wedge-like ramp and the grids at the inlet of the tubes has a critical dephlegmator tube length of longer than 9m. This is due to the variation in the inlet loss coefficients as can be seen in figure 5.1. The corresponding outlet mass flow rate is shown in figure 5.2. The effect of the variation in the inlet loss coefficient is clear in figure 5.2. When the inlet loss coefficient decreases, the outlet mass flow rate is seen to increase. This is so that the pressure change across the tube is large enough to ensure that no backflow occurs. The opposite is seen when the inlet loss coefficient increases as the outlet mass flow rate decreases. Significant variation in the inlet loss coefficients increases the critical dephlegmator tube length.

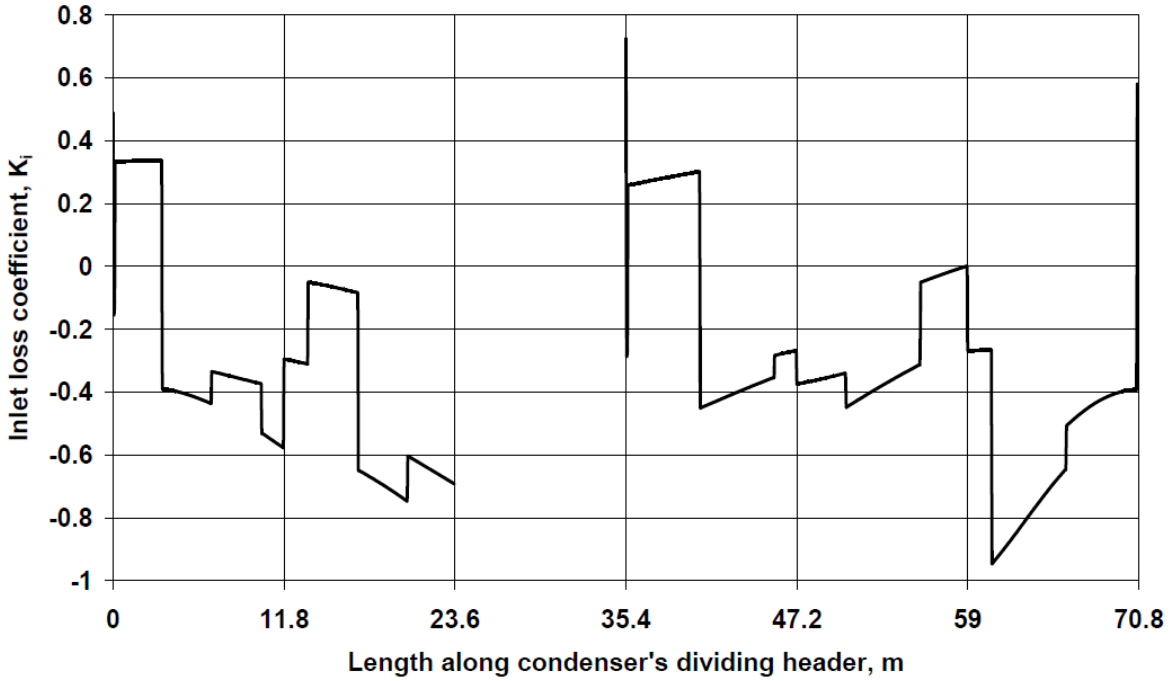

Figure 5.1: Inlet loss coefficients for the backward facing step, wedge-like ramp and grid combination geometry

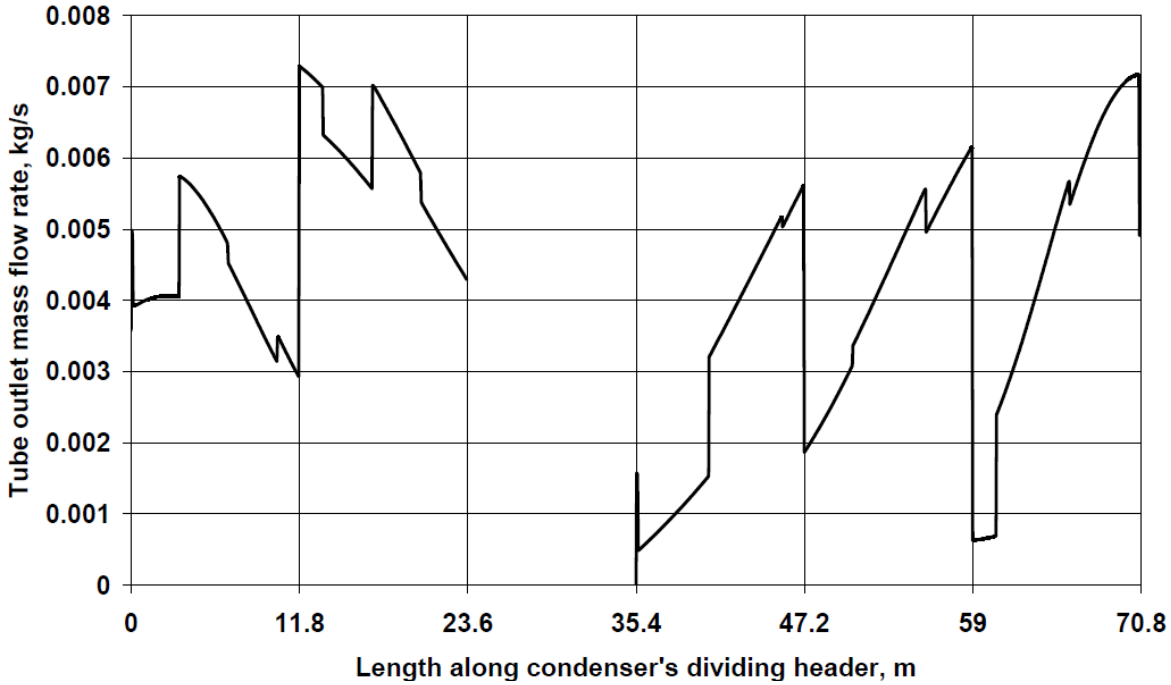

Figure 5.2: Tube outlet mass flow rate for the backward facing step, wedge-like ramp and grid combination geometry

It was shown that the backward facing step has the shortest critical dephlegmator tube length. The outlet mass flow rate of the finned tubes is shown in figure 5.3. The regions where backflow is likely to occur can be seen to the right of 9 and 12. The area where backflow could occur is larger at 9 than at 12 and therefore if the dephlegmator tubes are shorter than the critical tube length more backflow will occur at 9 than 12. There is less steam coming out of the first tube at 9 than at 12, so the first tube at 9 will experience backflow before the tube at 12 if the

dephlegmator tubes are too short. The effect of the two header configurations can also be seen in the outlet mass flow rates. Between 9 and 11 there is a Z-type configuration and between 12 and 15 is a U-type header arrangement. Less steam is seen to exit the tubes for the U-type than the Z-type.

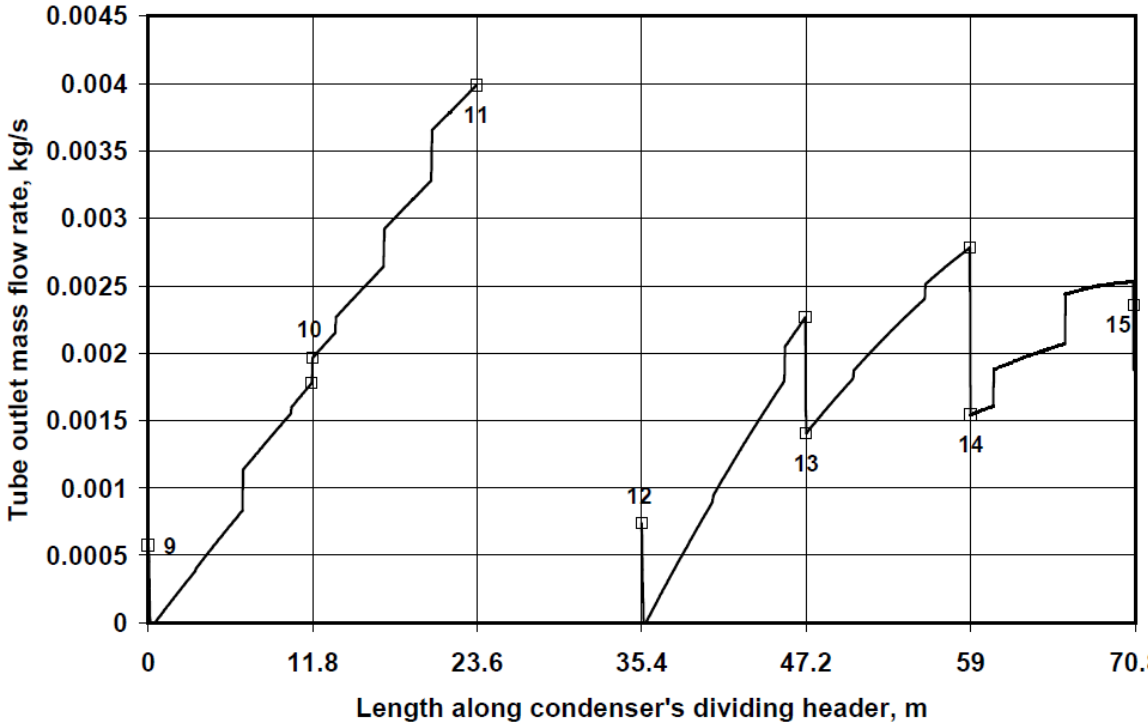

Figure 5.3: Outlet mass flow rate of the finned tubes in a single-row condenser street with a backward facing step dividing header inlet geometry

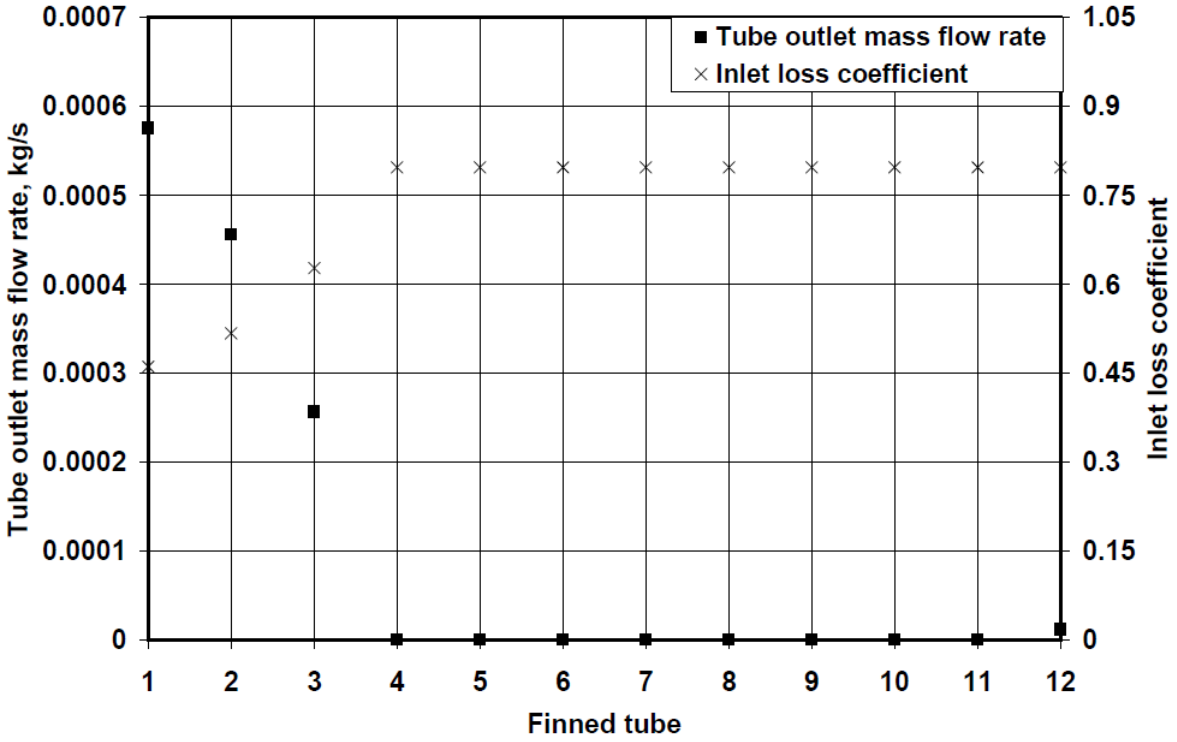

Figure 5.4: Inlet loss coefficients for first 12 tubes to the right 9

The inlet loss coefficients and outlet mass flow rates for the first 12 tubes to the right of 9 are shown in figure 5.4. It can be seen that the inlet loss coefficients for the first 3 tubes are lower than for the rest. The outlet mass flow rates are seen to be very close to zero from 4 to 1 after which it starts to increase again. Tubes 4 to 11 are therefore the critical tubes at 9 for backflow.

The backward facing step has the shortest critical dephlegmator length and therefore by increasing the dephlegmator tube length the occurrence of backflow in the condenser street can be eliminated. This backward facing step configuration will therefore be used to calculate the effect of the ambient conditions on the air-cooled condenser.

5.2 Effect of the overall momentum correction factor on the critical dephlegmator tube length

It can be seen from equations (2.27), (2.48) and (2.68) that the overall momentum correction factors affect the pressure change in the condenser. Bajura (1971) states that for the dividing header the overall momentum correction factor is very close to unity while for the combining header it is approximately 2.6. The effect of the combining header correction factor on the critical dephlegmator tube length will be investigated below for a condenser street with the backward facing step discussed above.

Figure 5.5 shows the outlet pressure change of the finned tubes for an inlet steam temperature of 60ºC. The effect of the larger correction value is clearly visible as the pressure change for $\alpha_c = 2.6$ is much greater than for $\alpha_c = 1$. The pressure change is also negative except for a few tubes at the start and end of the header since the steam speed in the combining header is higher than at the outlet of the finned tube. When α_c is larger than 1 this effect is increased as is evident from figure 5.5. It is interesting to note that the outlet pressure changes at the header ends at 9 and 15 are close to each other due to no steam or a very small amount being present in the header and therefore the effect of the momentum correction factor is negligible at the edges of the headers.

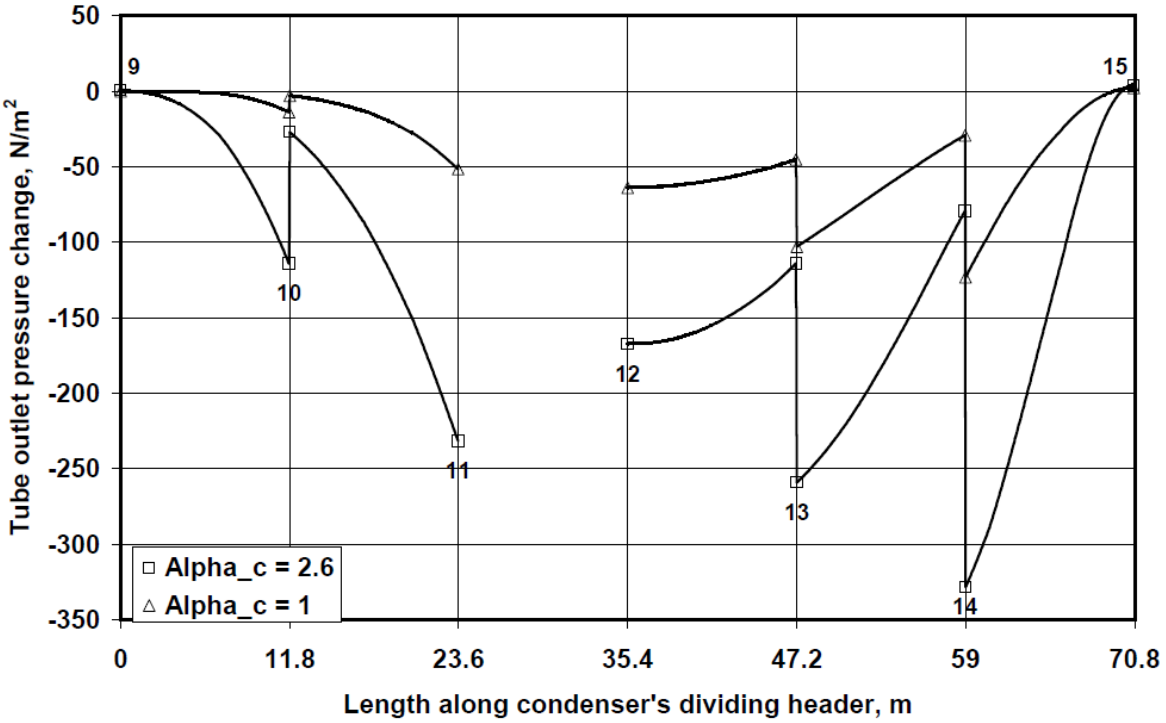

Figure 5.5: Outlet pressure change of the finned tubes for different α_c values

Shown in table 5.2 is the critical dephlegmator tube lengths needed for the two values of the momentum correction factor for different steam and corresponding air temperatures. The critical dephlegmator tube length is shorter in all cases for α_c = 2.6. The difference in critical dephlegmator tube length is about 1m in all cases, but does decrease slightly with an increase in steam temperature. The difference in length is not significant enough and it should just be noted that the critical tube length needed could be slightly longer if the momentum correction factor decreases. For all cases considered the critical dephlegmator tube length is shorter than the 9m maximum and therefore the effect of the momentum correction factor is small compared to the inlet loss coefficient. It can also be seen that a 10ºC change in steam temperature corresponds to change of about 10ºC in air temperature.

Table 5.2: Critical dephlegmator tube lengths for different momentum correction factors and steam temperatures

T_v	T_a	α_c	L_d
50ºC	5.64ºC	2.6	4.7525 m
		1	5.6758 m
60ºC	15.6ºC	2.6	4.374 m
		1	5.3846 m
70ºC	25.94ºC	2.6	4.8142 m
		1	5.2896 m

5.3 *Effect of the position of the dephlegmator on the critical dephlegmator tube length*

In this section the effect of moving the dephlegmator to the two positions shown in figure 5.6 is compared with the present configuration shown in figure 2.10. Figure 2.10 shows that the condenser street headers is in a combined configuration, with both co-current (U-type configuration) and counter-current flow (Z-type configuration) being present as shown in figure 2.11. When the dephlegmator is the first fan unit in the condenser street, a Z-type configuration is used. When the dephlegmator is the last fan unit in the condenser street a U-type configuration is used. There is no reducer in the dividing header and the duct diameter is the same as the inlet diameter in figure 2.10. A backward facing step geometry is used at the inlet to the dividing header.

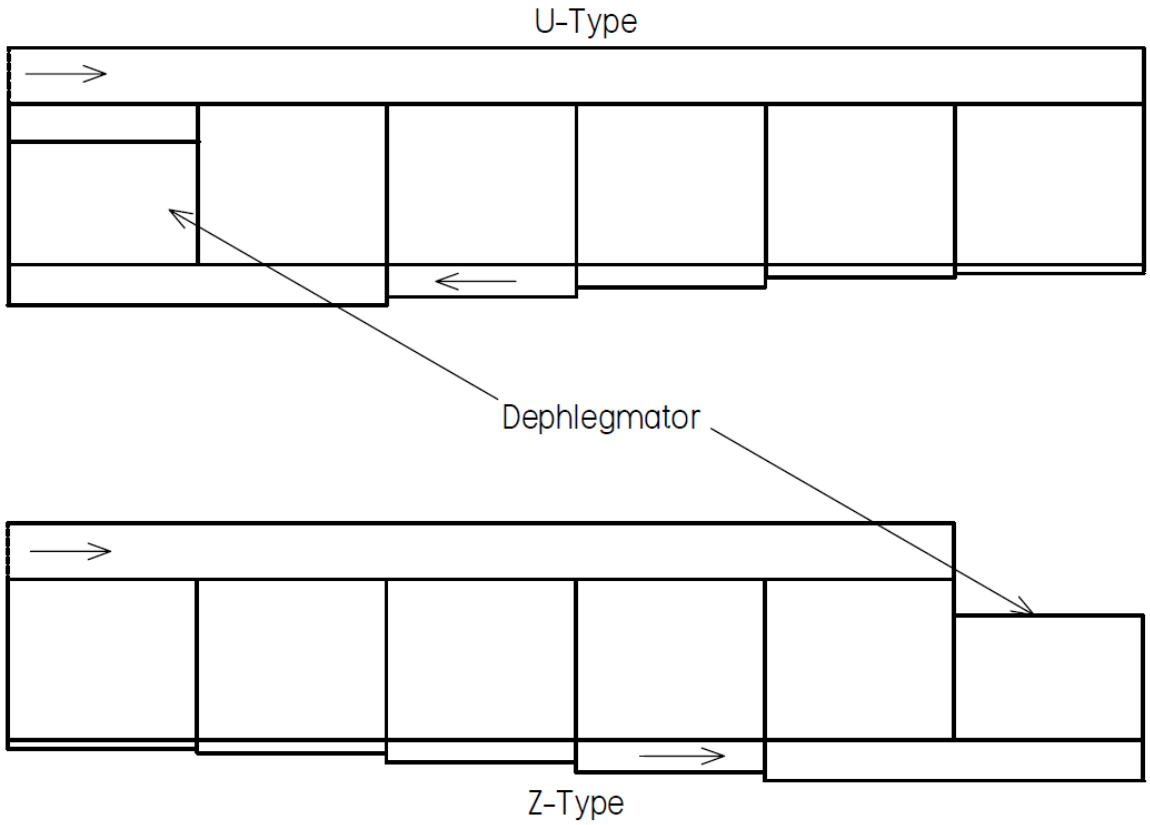

Figure 5.6: Different condenser street configurations

Table 5.3 shows the resulting critical dephlegmator tube lengths. The U-type configuration has the shortest critical length, and the Z-type has the longest critical length. The area where backflow may occur for the two configurations shown above is the first few tubes at the inlet to the condenser street. This differs from the present case where two areas of concern were identified, at the inlet to the condenser street and to the right of the dephlegmator fan unit.

Table 5.3: Comparison of critical dephlegmator tube length for different condenser street configuration

Configuration	L_d
Present	4.374 m
U-type	3.3751 m
Z-type	> 9 m

Figure 5.7 shows the total to total pressure change between the dividing and combining headers. The total to total pressure difference for the Z-type configuration is seen to increase down the condenser. This corresponds well with the critical dephlegmator length of over 9m. The U-type configuration has a high starting total to total pressure change which decrease along the length of the condenser. The U-type configuration has the lowest critical dephlegmator tube length. The present configuration is a combination of the other two configurations and for the first two condenser fan units the total to total pressure change follows the same trend as for the Z-type, while after the dephlegmator the U-type trend is followed. The present configuration has a higher critical dephlegmator length due to the inlet loss coefficient that is used. The present case is modeled as two headers, while the other two configurations can be modeled as one header. This results in a different inlet loss coefficient distribution in the condenser.

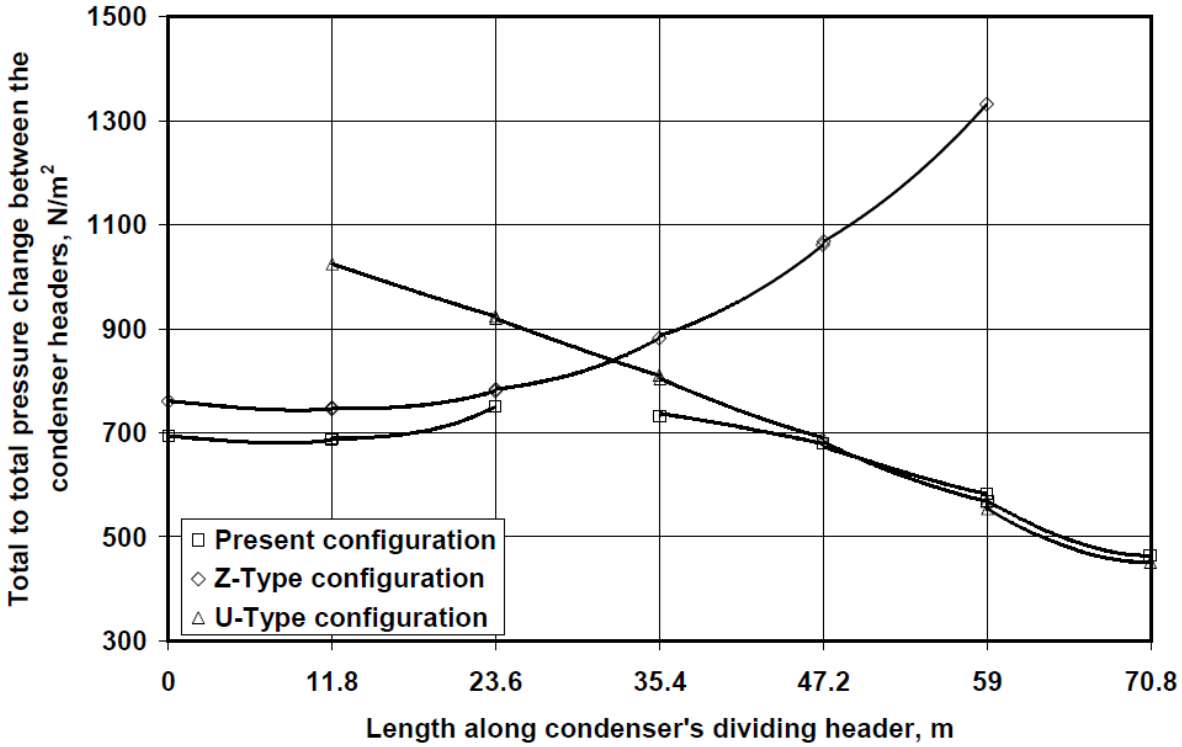

Figure 5.7: Total to total pressure change for different condenser street configurations

Chapter 6: Effect of ambient conditions on a single-row air-cooled condenser

In this chapter the effect of different ambient conditions on a condenser will be investigated. The effect of a night-time air temperature distribution (inversion) and a 6 m/s wind on the condenser will be investigated. The effect of the different ambient conditions on the critical dephlegmator tube length, the tube outlet mass flow rate distribution and the heat rejection distribution will be investigated. Shown in figure 6.1 is a schematic of an air-cooled power station showing all the buildings and the wind direction that will be investigated. In this chapter the ideal condition is defined as a condenser where all the fans receive air at 15.6ºC, as was the case in the previous chapter.

6.1 Effect of night-time air temperature distribution on air-cooled condenser

A night-time air temperature distribution is shown in figure 6.2. The ground level temperature is the same as for the ideal condition in the previous chapter so that the effect of the temperature distribution can be compared to that of the ideal case. Equation (3.1b) was used to describe the temperature distribution and is also included in figure 6.2.

The average inlet air temperatures, calculated with equation (3.3), for a condenser street situated in the middle of unit 1, are shown in table 6.1. Fan 1 receives the lowest inlet air temperature with the inlet air temperature rising to fan 6. The higher inlet temperatures will have the effect that the inlet steam temperature to the condenser street must increase to ensure that the required heat can be rejected.

Table 6.1: Average inlet air temperature for the fan units for night-time air temperature distribution (inversion)

Fan	1	2	3	4	5	6
Inlet temperature, ºC	18.9883	21.7674	22.8554	23.5867	24.1086	24.5251

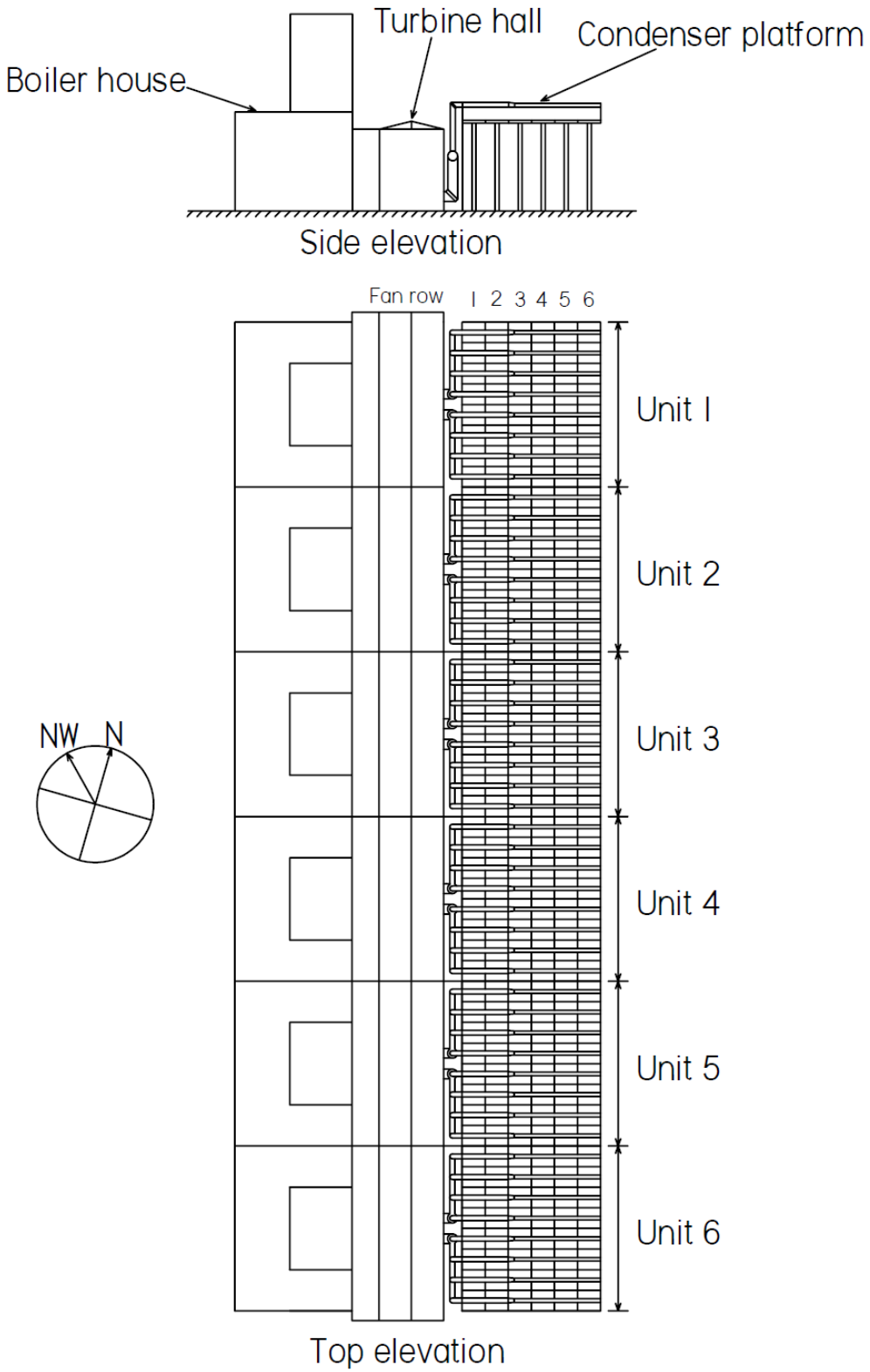

Figure 6.1: Schematic of air-cooled power station showing buildings and wind directions

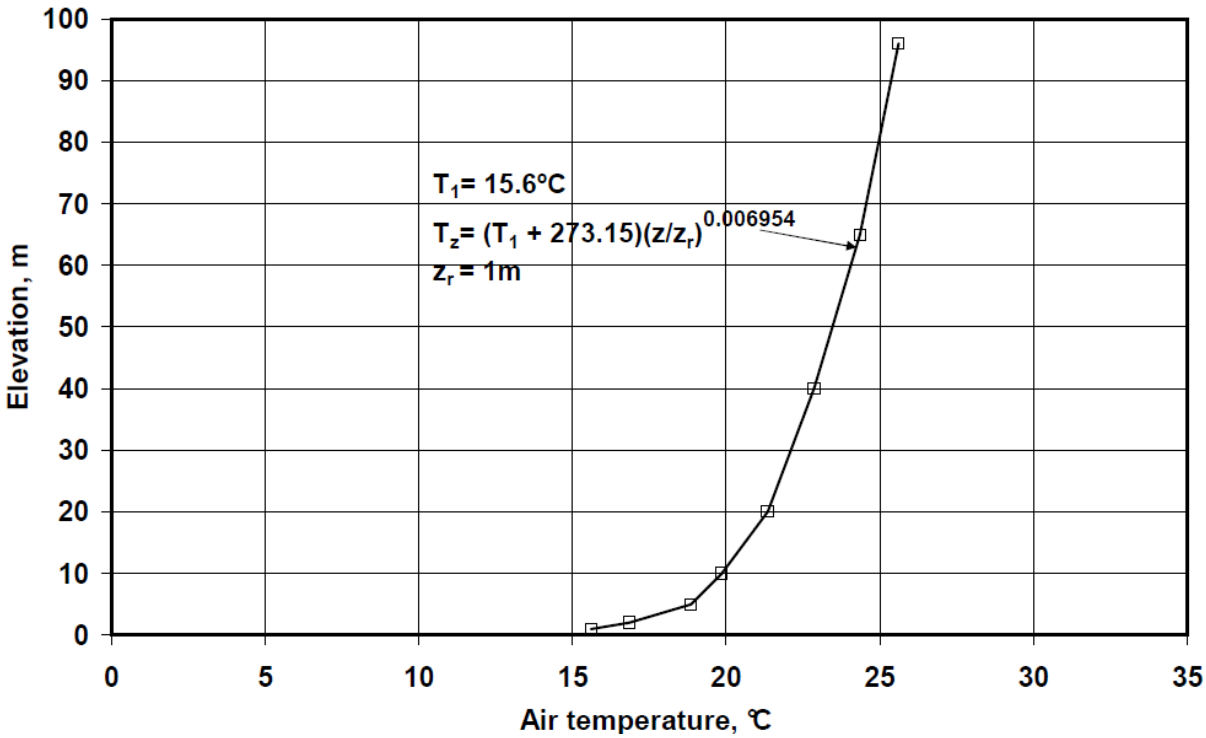

Figure 6.2: Night-time air temperature distribution

Table 6.2 shows the inlet steam temperature and the critical dephlegmator tube length for ideal conditions and the night-time air temperature distribution. The inlet steam temperature is seen to increase due to the higher inlet air temperatures. The average fan inlet temperature is 22.64ºC. This is about 7ºC higher than for ideal conditions. It was seen in section 5.2 that under ideal conditions there is a fairly linear correlation between the average fan inlet temperature and the inlet steam temperature. The inlet steam temperature in this case is about 5.6ºC higher which is less than the 7ºC increase in average fan inlet air temperature. This is due to the critical dephlegmator length being longer than for the ideal case. The heat transfer area is therefore increased and the inlet steam temperature does not have to increase as much to reject the prescribed amount of heat.

Table 6.2: Inlet steam temperature and critical dephlegmator comparison for night-time air temperature distribution

Ambient condition	L_d	T_v
Ideal	4.3740 m	60.00 °C
Night-time temperature distribution(Inversion)	6.1034 m	65.644 °C

The tube outlet mass flow rates are shown in figure 6.3. The critical dephlegmator tube must be longer for the night-time distribution since more steam is leaving the finned tubes. As shown before fan 1 receives air at the lowest temperature and because of the higher temperature difference between the air and the steam will reject the most heat. This causes the pressure change across the finned tubes to be higher due to more steam being drawn into the finned tubes because of the higher condensation rates. Fan 2 receives air with a slightly higher temperature

and therefore condenses less steam and more steam must flow out to ensure that the pressure changes across the tubes are adequate.

The larger amount of steam at 11 compared to the ideal case means that more steam is needed at 12 to ensure that pressure change from 15 to 12 is large enough so that pressure continuity is kept at 12. The higher fan inlet air temperatures for fans 4 to 6 also increase the amount of steam flowing into the combining header because of lower condensation rates. This is to ensure an adequate pressure change over the finned tube so that no backflow occurs. No potential backflow is present at 12 as was seen for ideal conditions and the only area of concern is at the inlet to the condenser street at 9.

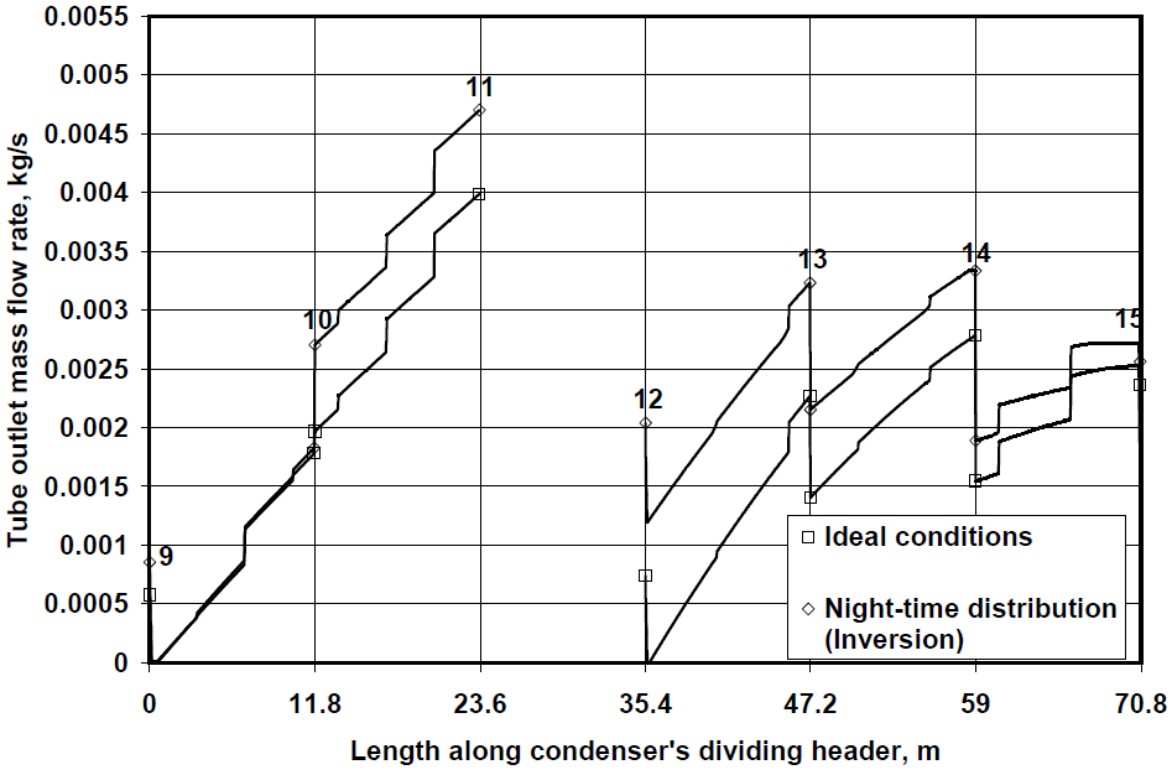

Figure 6.3: Finned tube outlet mass flow rate for ideal conditions and night-time distribution (Inversion)

The heat rejected by each of the condenser fan units for ideal conditions and for the night-time air temperature distribution (inversion) is shown in figure 6.4. For ideal conditions the heat rejected by the fans increase from fan 1 to 6, except for the dephlegmator which has a shorter tube length. The heat rejection distribution for the night-time air temperature distribution follows the same trend seen in table 6.1. Fan 1 receives air at the lowest temperature and rejects the most heat, while fan 6 has the highest fan inlet air temperature and rejects the least amount of heat.

The larger changes in air temperature close to the ground compared to higher elevations can be seen by the difference in heat rejected by the different condenser fan units. There is a much larger difference between fans 1 and 2 than between fans 4, 5 and 6.

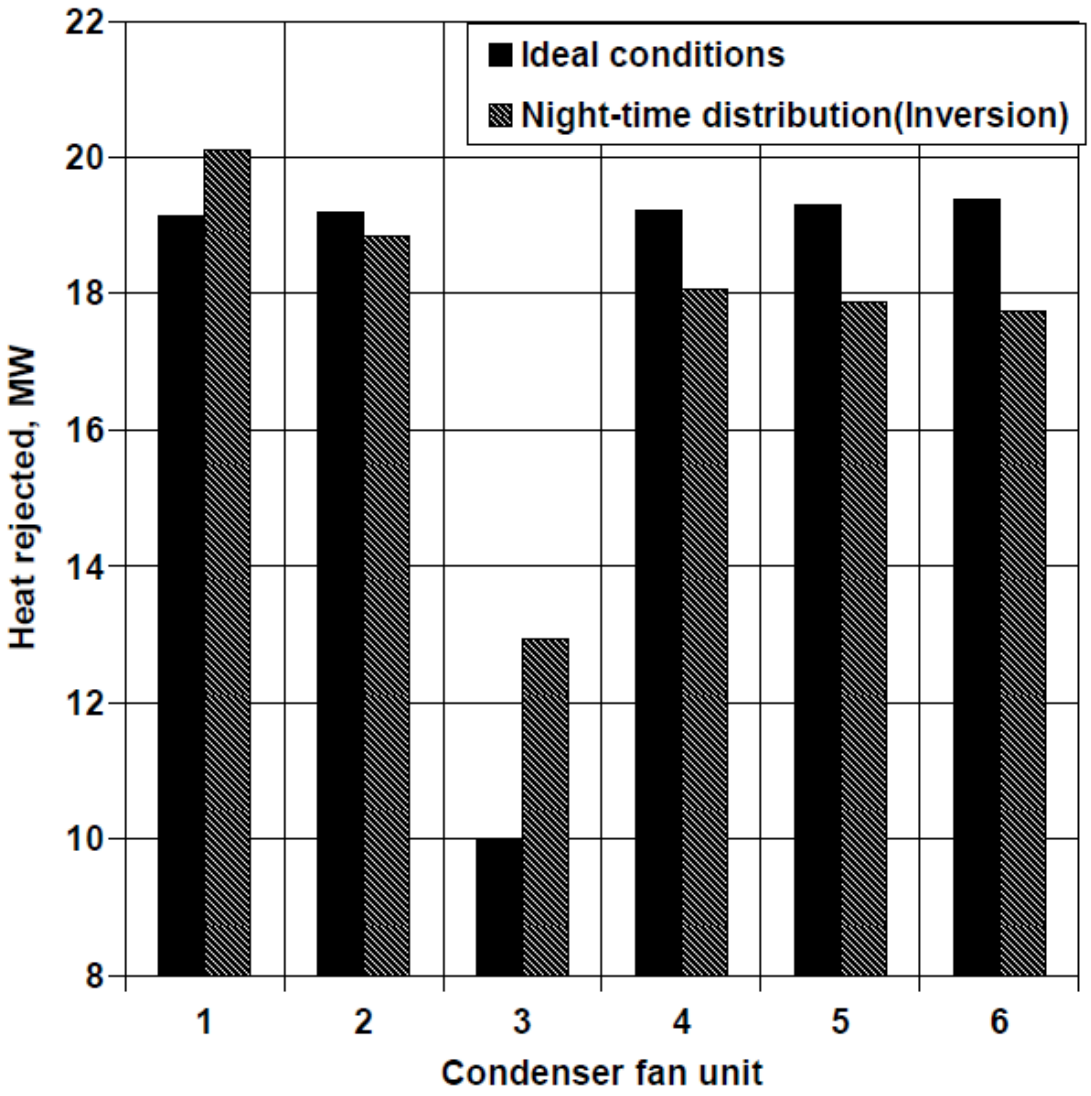

Figure 6.4: Heat rejected by each of the condenser fans under ideal conditions and night-time air temperature distribution

The dephlegmator fan unit rejects more heat than for ideal conditions due to the longer dephlegmator tube length. Due to the higher inlet steam temperature the steam pressure changes in the condenser are smaller and the temperature change between the inlet steam temperature and the steam temperature at the dephlegmator fan unit are smaller. This also results in a higher heat transfer rate for the dephlegmator fan unit because of higher steam temperatures in the tubes.

The night-time air temperature distribution alters the tube outlet mass flow rate distribution and the heat rejection distribution. The area where backflow could occur differs from that of the ideal conditions. For the night-time distribution only the area at 9 is important for backflow. The heat rejected follows the trend of the inlet air temperature and decreases from fan 1 to 6 with the exception of the dephlegmator.

6.2 *Effect of wind on air-cooled condenser*

In this section the effect of a 6 m/s north-westerly wind, at platform height, on a condenser will be investigated. In figure 6.1 the direction from which the wind blows can be seen. The wind blows over the boiler houses and turbine halls and then across the condenser platform.

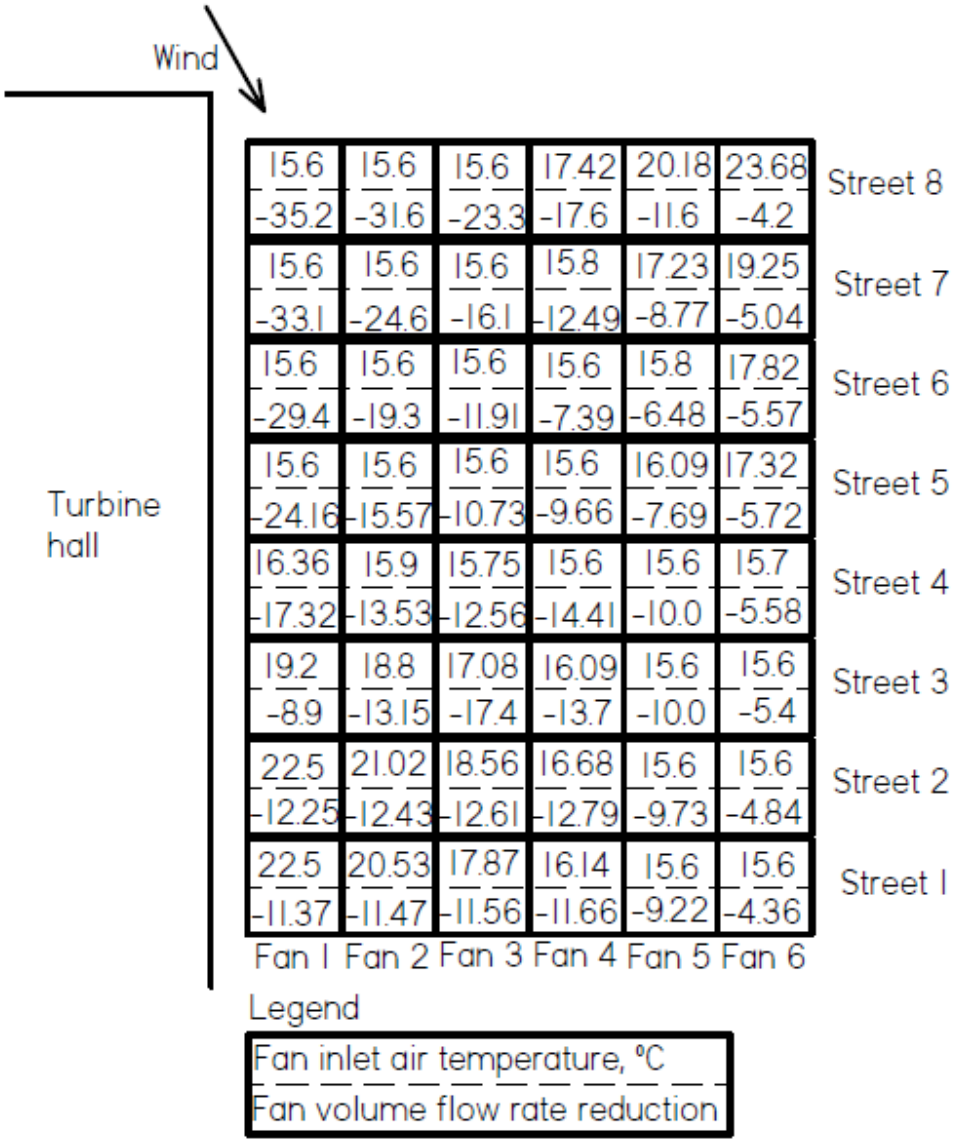

Figure 6.5: Schematic showing numbering scheme

Figure 6.5 is a schematic of condenser unit 1 showing the fan inlet air temperatures and reduction in fan volumetric performance. For a north-westerly wind large portions of the condenser platform will be in the wake created by the boiler houses. Some of the edge fans at the top of figure 6.5 will be hit directly by the wind. This will affect how the fans perform and could lead to changes in fan inlet temperatures.

The ambient temperature for the condition described in figure 6.5 is 15.6ºC. The higher fan inlet temperatures are due to hot exhaust plume air being drawn in back under the condenser platform, thereby raising the fan inlet temperatures. This is known as plume recirculation. Two areas of high recirculation can be seen,

the first is around fan 1, condenser street 1 and the other is around fan 6, condenser street 8. The fan with the highest inlet air temperature is fan 6 in condenser street 8.

All the fans are adversely affected by the wind as seen in figure 6.5. Condenser street 8 shows the highest average reduction in fan performance with the largest being fan 1. Looking at figure 6.5, it can be seen that condenser street 8 is directly in the line of the wind. There are strong cross flow conditions under the platform which cause the large fan performance reductions. It was decided to investigate condenser street 8 as it experiences the largest ambient disturbances.

The combined effect of the recirculation and the fan performance reduction on the inlet steam temperature and critical dephlegmator tube length is shown in table 6.5. The individual effects of the recirculation and fan performance reduction is also included. The inlet steam temperature is higher due to the ambient disturbances and the dephlegmator tubes must be longer to ensure that no backflow occurs.

The individual effect of the reduction in fan performance has a much larger impact on the performance of the condenser than the recirculation, as the increase in inlet steam temperature is higher. The critical dephlegmator tube is longer for the fan performance reduction than for the ideal case.

Table 6.5: Comparison of the effect of recirculation, fan performance reduction and the combination of the effects for condenser street 8

	T_v	L_d
Ideal conditions	60.00 °C	4.374 m
Fan performance reduction	66.569 °C	4.7112 m
Recirculation	62.169 °C	5.1321 m
Combined	69.598 °C	4.7779 m

The average fan inlet temperature for the recirculation is 18.0133ºC, or 2.41ºC higher than that of the ideal condition. From table 6.5 it can be seen that the change in inlet steam temperature is 2.169ºC and the close correlation between the change in average fan inlet temperature and change in the inlet steam temperature is confirmed again. The increase in steam temperature is lower due to the longer dephlegmator tube and the corresponding larger heat transfer area.

The tube outlet mass flow rates are shown in figure 6.6 for ideal conditions and for the 6 m/s north-westerly wind. The outlet mass flow rates between 9 and 11 are higher than for the ideal conditions. This can be explained by looking at figure 6.5. The K-type condenser fan unit with the largest fan performance reduction will reject the least amount of heat and will therefore have a smaller pressure change between the headers. Fan 1 in the condenser street has the biggest reduction in fan performance and therefore more steam must flow through the first tube so that there is an adequate pressure change between the headers so that pressure continuity will be met at 12. There are small changes between the outlet mass flow

rates from 12 to 15 with the wind case having larger outlet mass flow rates. The area where backflow will commence first is to the right of 12 and not at 9 and 12 as for ideal conditions.

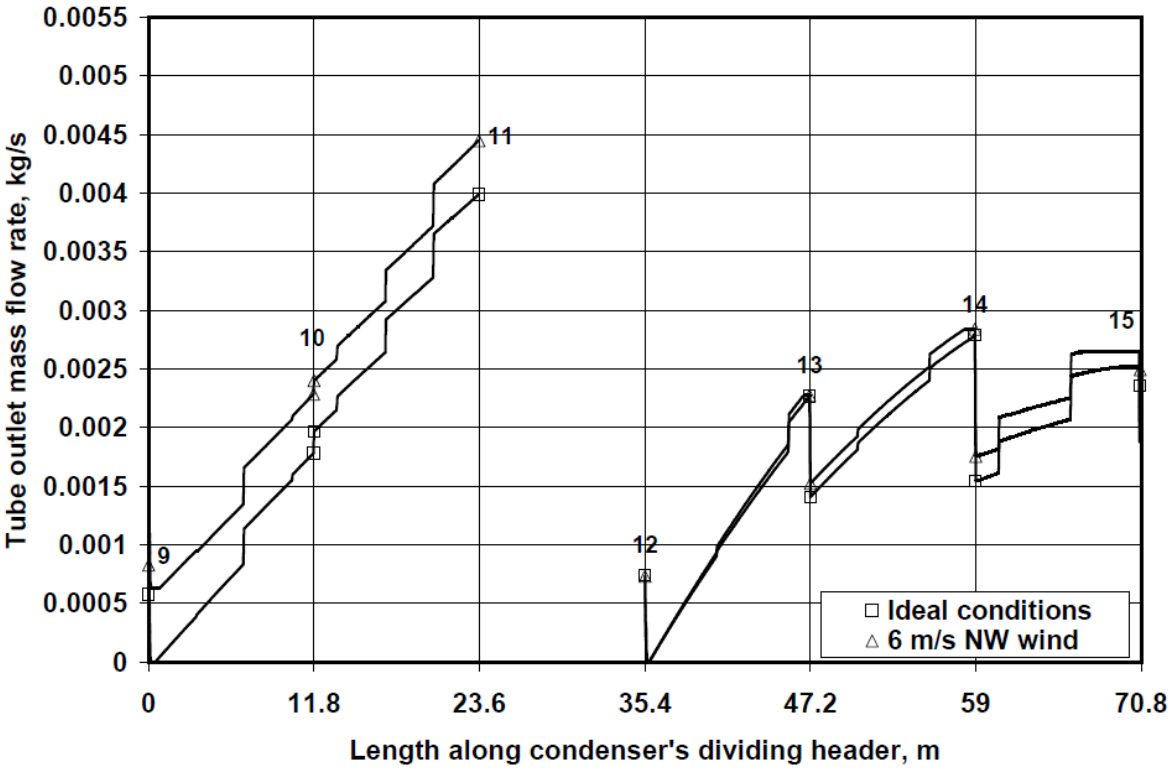

Figure 6.6: Tube outlet mass flow rates for 6 m/s north-westerly wind

The heat rejection distribution for ideal conditions and for the wind condition is shown in figure 6.7. Fan 1 rejects the least amount of heat for the wind condition as was expected due to the large reduction in fan performance. Fan 4 rejects the most heat due to the relatively small increase in inlet temperature and a mild decrease in fan performance. The fan performance increases from fan 4 to 6, but the increase in inlet air temperature offsets this gain in performance and the heat rejected decreases from fan 4 to 6. The dephlegmator is seen to reject more heat than for ideal conditions. This is due to the longer dephlegmator tube length, lower inlet air temperature and because the reduction in fan performance is smaller than for fans 1 and 2.

The wind increases the inlet steam temperature and critical dephlegmator tube length. This is due to the reduction in fan performance and recirculation. The ambient disturbances for the wind are large, but the critical dephlegmator tube does not increase significantly over the critical length for ideal conditions. The inlet steam temperature does however increase significantly. This shows that the ambient conditions described in this section do not have a significant effect on the critical dephlegmator tube length, but the effect on the inlet steam temperature is significant.

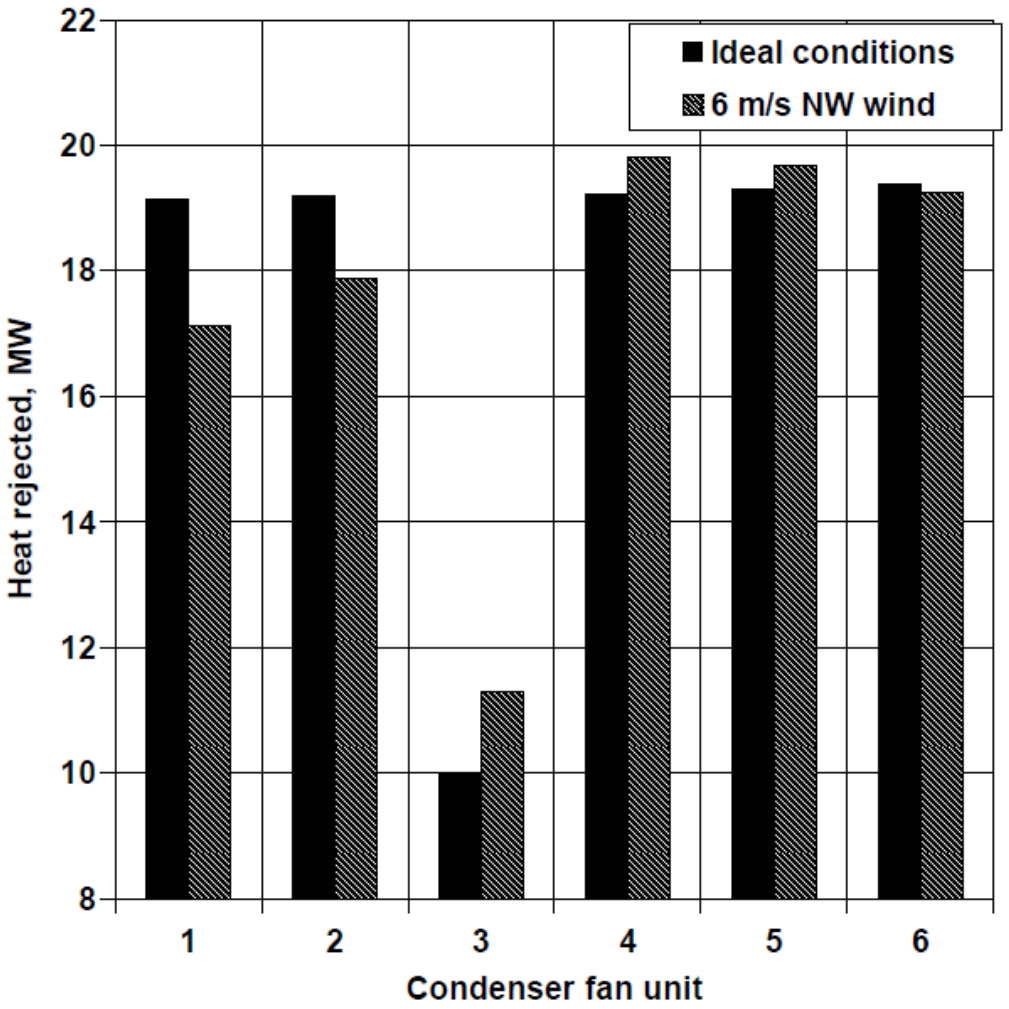

Figure 6.7: Heat rejected by each of the condenser fans under ideal conditions and for 6 m/s NW wind

From the two cases that were investigated above a prediction can be made for where backflow will occur in a system. Backflow will potentially occur on the side where the fan is situated that rejects the most heat. When the night-time air temperature distribution is present, fan 1 rejects the most heat and potential backflow is predicted at 9, while for the wind case fan 4 rejects the most heat and potential backflow is predicted at 12. For the ideal case the heat rejected by each fan units are close to constant and backflow is predicted at both 9 and 12. Therefore if the heat rejected by each fan unit is known, it would be possible to predict where areas of potential backflow are located in a single-row condenser street.

Chapter 7: Effect of ambient conditions on a two-row air-cooled condenser

In this chapter the effect of different ambient conditions on a two-row steam condenser will be investigated. The same ideal conditions, night-time air temperature distribution and wind that were used for the single-row condenser will be used again.

In a two-row condenser backflow can occur where steam flows from the second tube row back into the first tube row, as shown in figure 2.24. The iteration described in section 4.5 is used to eliminate the potential occurrence of backflow between the tube rows. The same inlet loss coefficient model that was decided upon in chapter 5 is used for the two-row condenser. The operation of the two-row condenser will first be analyzed for ideal conditions, then for the night-time air temperature distribution and lastly for the 6 m/s north-westerly wind.

7.1 Two-row air-cooled condenser operating under ideal conditions

The critical dephlegmator tube length for ideal conditions for a two-row condenser is shown in table 7.1. The critical dephlegmator tube length for the ideal case for a single-row condenser is also included for comparison. The increase in critical dephlegmator tube length is just less than double that of the single-row condenser for ideal conditions. Therefore the effect of the second tube row is less than that of the tube inlet loss coefficients for ideal conditions.

Table 7.1: Critical dephlegmator tube length for two-row condenser for ideal conditions

	L_d
Single-row condenser	4.374 m
Two-row condenser	8.0397 m

The outlet mass flow rates of the two tube rows are shown in figure 7.1. More steam flows out of the second row's tubes than for the first. This is so that there is an adequate pressure change across the second tube row to stop backflow to occur as shown in figure 2.24 due to lower condensation rates for the second tube row.

Comparing the outlet mass flow rates for the two-row condenser with that of the single-row condenser, refer to figure 5.3, the trend between 9 and 11 is similar, however the opposite is true from 12 to 15. The two-row condenser has increasing outlet mass flow rates while the single-row condenser has a decreasing trend. This is due to more steam entering the combining header from 9 to 11 and the corresponding longer critical dephlegmator tube which cause a lower steam pressure at 12 than was the case for the single-row condenser. A larger pressure change is needed from 15 to 12 so that the pressure distribution is continuous, with the result that more steam is present in the combining header at 12 than for

the single-row condenser. The increasing trend in tube outlet mass flow rate is the result of the higher pressure change that is needed in the combining header.

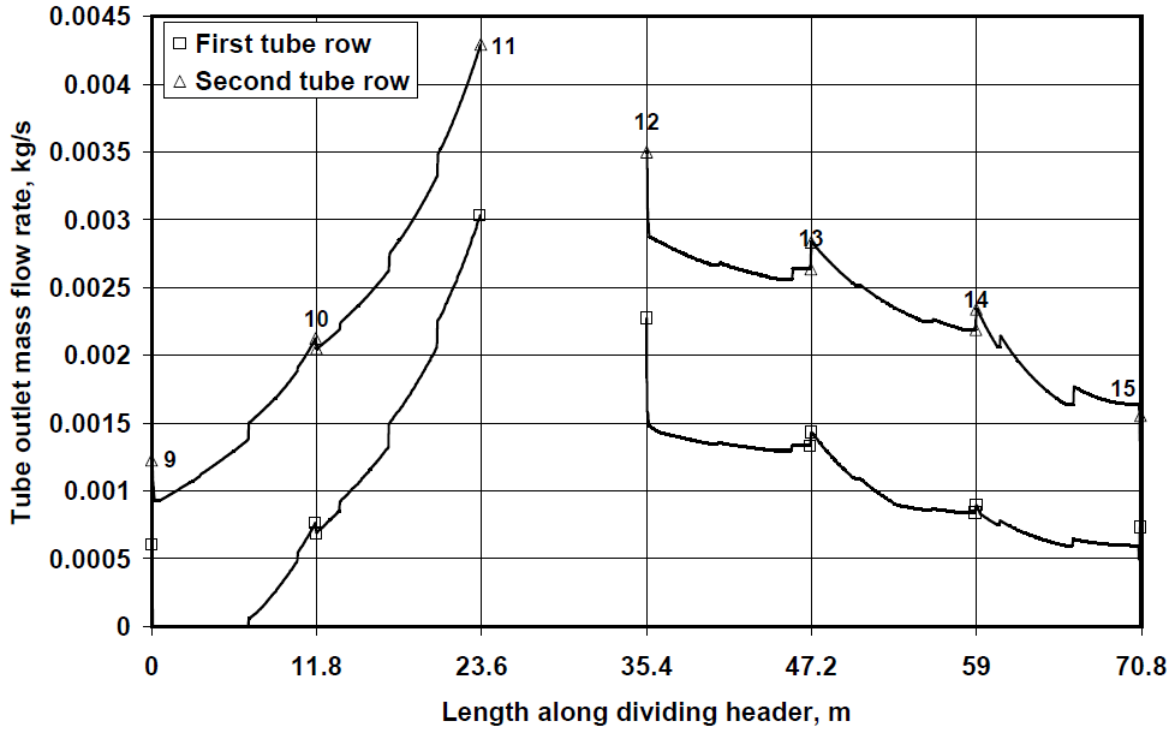

Figure 7.1: Outlet mass flow rates of the finned tube rows in a two-row condenser street for ideal conditions

There is only one area of potential backflow for the two-row condenser and this is to the right of 9. More than half of the first row tubes in the first condenser fan unit have almost no flow exiting the tubes. This area is larger than that of the single-row condenser. Due to the different trend in the outlet mass flow rate from 15 to 12, no area of backflow is present at 12.

The heat rejected by each of the tube rows and the total heat rejected by each condenser fan unit, is shown in figure 7.2. The heat rejected by the single-row condenser is also included for comparison. Row 1 rejects more heat than row 2 for all the condenser fan units. This corresponds well with the higher tube outlet mass flow rates as seen in figure 7.1.

The difference in heat rejected between the single-row and two-row condensers is small. This is because the heat transfer characteristic of the single-row bundle is very close to that of the two-row bundle. The extra row does not have a significant effect on the heat transferred as long as the heat transfer characteristics of the bundles are similar.

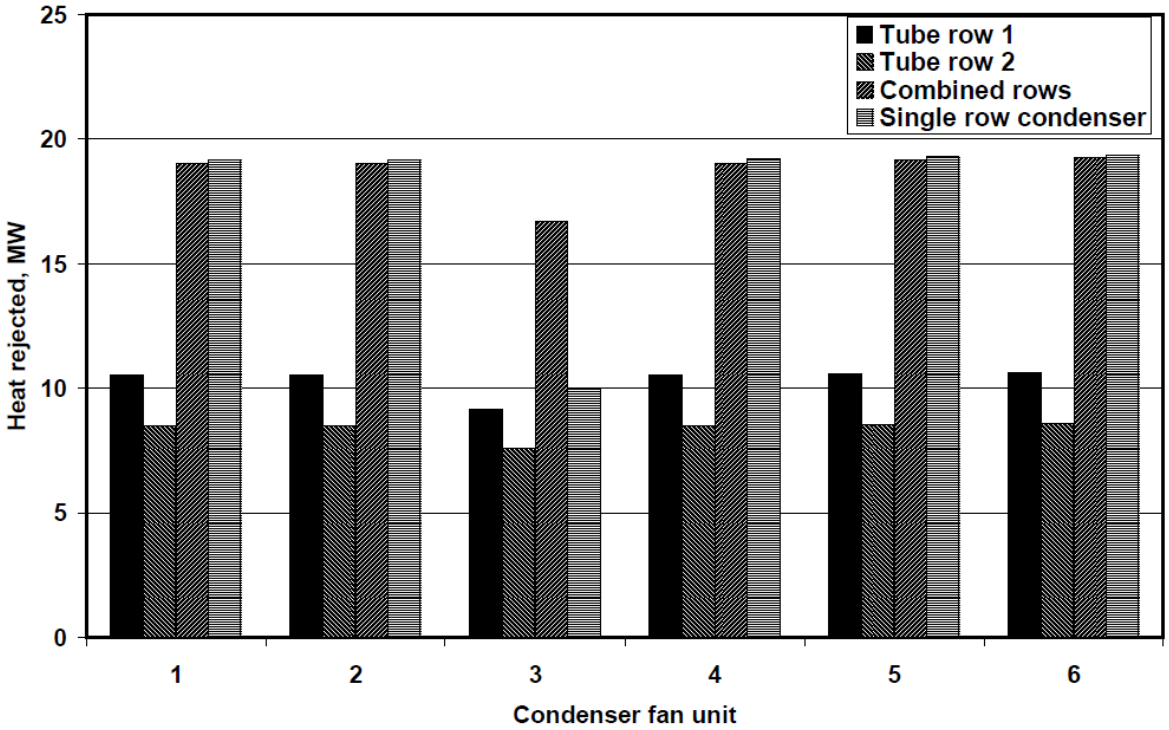

Figure 7.2: Heat rejected by each tube row, total heat rejected and heat rejected by single-row condenser for ideal conditions

7.2 Effect of night-time air temperature distribution on two-row air-cooled steam condenser

The effect of the night-time air temperature distribution shown in figure 6.2, on the two-row condenser is investigated. The fan inlet air temperatures are the same as given in table 6.1. The effect on the inlet steam temperature, critical dephlegmator tube length, the mass flow distribution and the heat rejection distribution will be discussed.

The inlet steam temperature and critical dephlegmator tube lengths for ideal conditions and the night-time air temperature distribution are shown in table 7.2. There is an increase in the inlet steam temperature because of the higher fan inlet air temperatures. The critical dephlegmator tube length is slightly shorter than for ideal conditions.

Table 7.2: Inlet steam temperature and critical dephlegmator tube length for ideal conditions and night-time air temperature distribution

	T_v	L_d
Ideal conditions	60.00°C	8.0397 m
Night-time air temperature distribution	67.5317°C	7.9053 m

The correlation between the average fan inlet temperature and the steam inlet temperature is evident again. There is roughly a 7°C increase in the average fan

inlet temperature and there is a 7.53ºC steam temperature increase. The steam temperature is higher due to the shorter dephlegmator tube length.

The tube outlet mass flow rates of the two tube rows for the night-time air temperature distribution, are shown in figure 7.3. The same trends that were seen for ideal conditions are present again. The area of potential backflow is larger than for ideal conditions with practically no flow coming out of the first row for the first K-type condenser fan unit. More steam is present at 11 and 12 in the combining header even though the critical dephlegmator tube is shorter. The pressure changes in the condenser are smaller due to higher steam temperature and therefore the dephlegmator receives steam with a higher temperature. More steam can therefore be condensed and shorter tubes result.

Since fan 1 receives the coldest ambient air it will reject the most heat. This will result in more steam being drawn into the finned tubes and larger pressure changes will result than for the other fan units. The combining header pressure at 9 will therefore be lower. This will result in a lower steam pressure at 11. Therefore more steam is needed from 15 to 12 so that there is an adequate pressure change that pressure continuity is satisfied at 12.

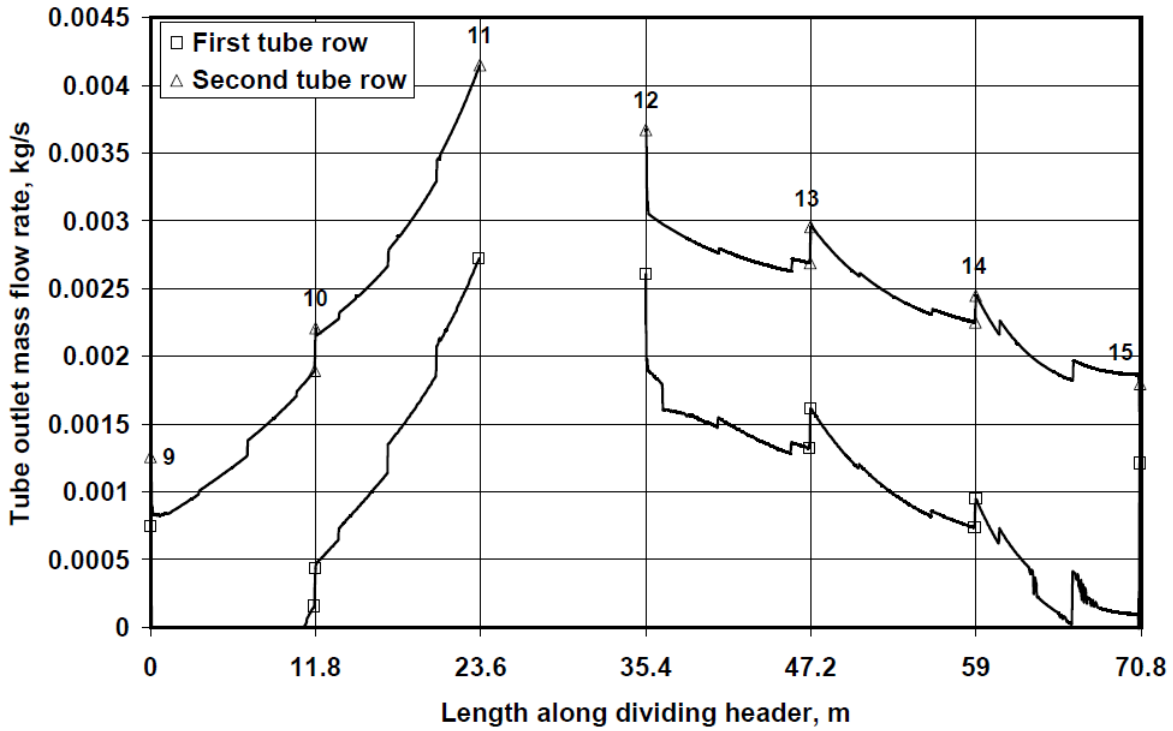

Figure 7.3: Outlet mass flow rates of the finned tube rows in a two-row condenser street for a night-time air temperature distribution

The heat rejected by each of the condenser fan units is shown in figure 7.4. As was the case for the single-row condenser the heat rejected follows the same trend as the fan inlet air temperature, except for the dephlegmator fan unit which has shorter tubes. Fans 1 and 2 reject more heat than for ideal conditions. Fans 3 to 6 reject less heat than for ideal conditions. Since fans 4 to 6 reject less heat more steam must flow through the tubes to generate a large enough pressure

change between the headers so that pressure continuity is met at 12. The larger outlet mass flow rates are shown in figure 7.3.

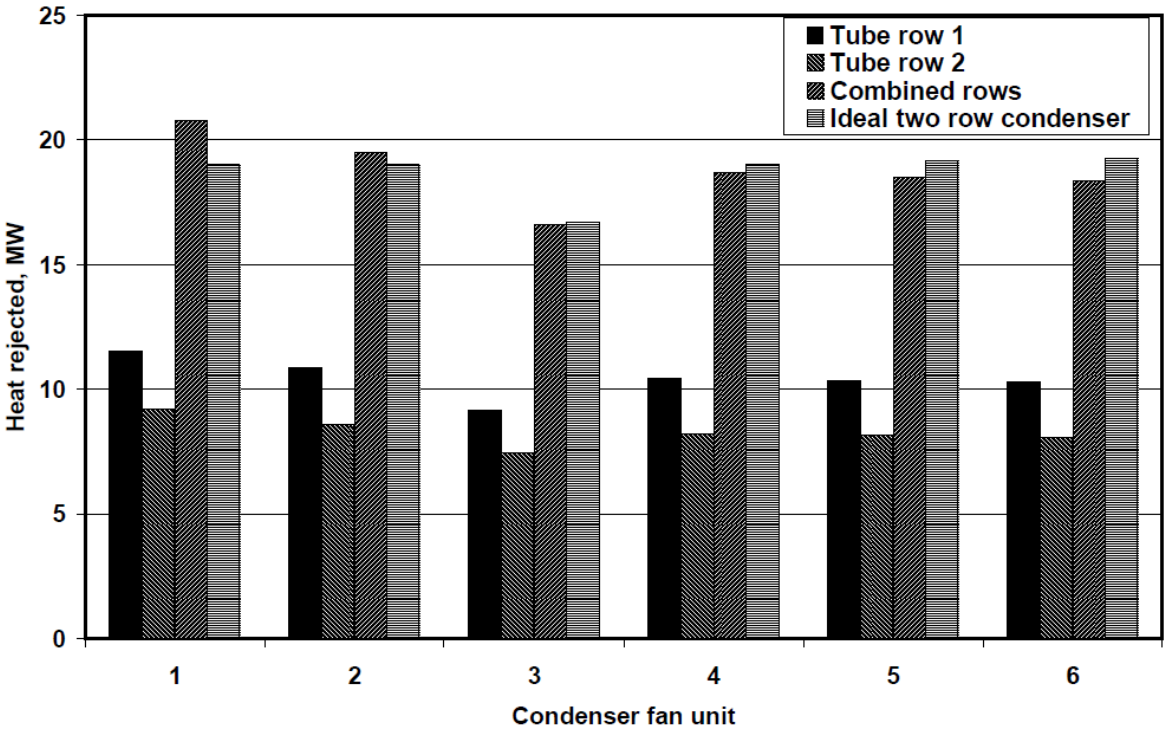

Figure 7.4: Heat rejected by each tube row and total heat rejected for night-time air temperature distribution and heat rejected by two-row condenser for a night-time air temperature distribution

7.3 Effect of wind on two-row air-cooled condenser

The disturbances as described in figure 6.5, will be used to investigate the effect of a 6 m/s north-westerly wind on a two-row condenser. Condenser street 8 will be under investigation again. The inlet steam temperature, critical dephlegmator tube length, mass flow distribution and the heat rejected by each of the condenser fan units will be discussed.

Table 7.3: Inlet steam temperature and critical dephlegmator tube length for ideal conditions and 6 m/s north-westerly wind

	T_v	L_d
Ideal conditions	60.00°C	8.0397 m
6 m/s north-westerly wind	73.10°C	5.1543 m

The inlet steam temperature and critical dephlegmator tube length is compared with the ideal two-row condenser in table 7.3. There is a large increase in the inlet steam temperature due to the ambient disturbances. There is also a decrease in the critical dephlegmator tube length. Less steam is therefore present in the combining header for the wind conditions than for the ideal conditions. The shorter dephlegmator tube will decrease the heat transfer area and this will have the effect of raising the inlet steam temperature further.

The tube outlet mass flow rates of the two tube rows are shown in figure 7.5. Comparing with figure 7.1, it can be seen that the trend from 9 to 11 is the same. The area of potential backflow in the first fan unit is larger than for the ideal case. The outlet mass flow rate trend between 12 and 15 is different from that of the previous two cases. The increase in the outlet mass flow rates for both tube rows is only present for fan 6. Between 13 and 14 there is an increase in the direction of the steam flow for the second row while the first row experience a decrease and increase. The first row between 12 and 13 has basically no outflow while the second row outlet mass flow rate decreases in the flow direction. This results in a smaller mass flow rate at 12.

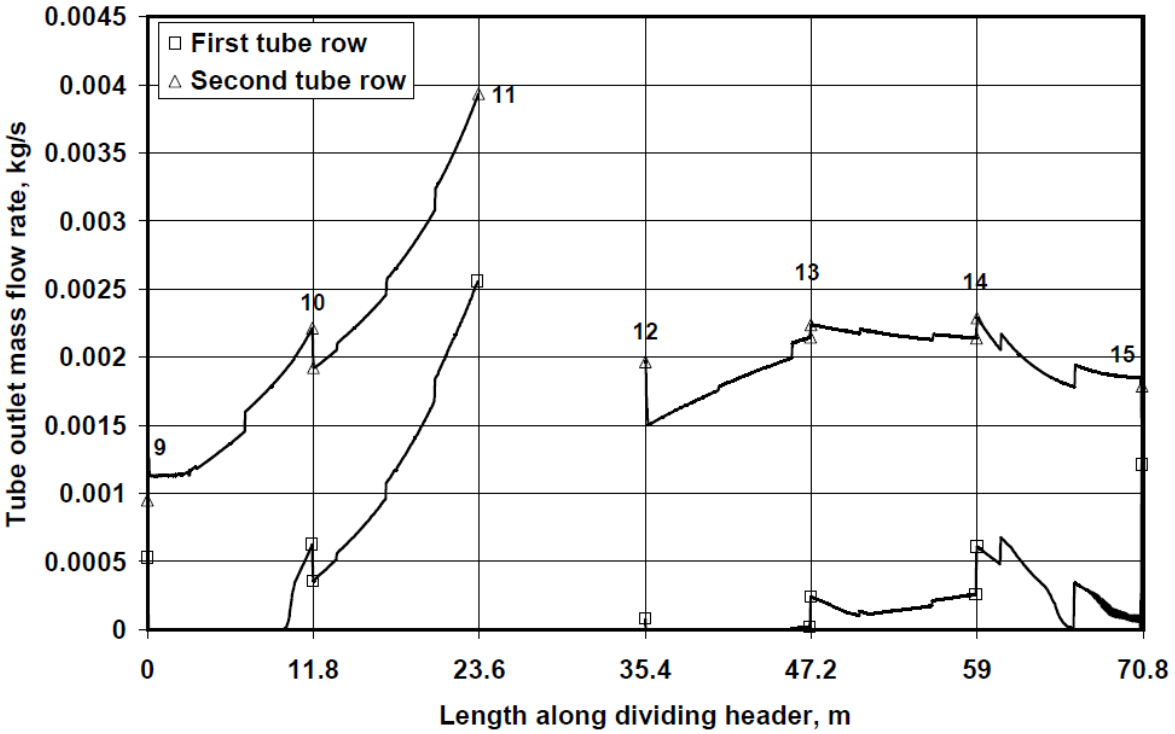

Figure 7.5: Outlet mass flow rates of the finned tube rows in a two-row condenser street for a 6 m/s north-westerly wind

In figure 7.6 it is shown that fan 4 rejects the most heat. Fan 4 also experiences higher tube inlet loss coefficients than fans 5 and 6, due to it position in the dividing header. This results in a large pressure change between the dividing and combining headers which cause the area where potential backflow can occur between 12 and 13.

Because similar amounts of heat is rejected by fans 4 to 6, the amount of steam drawn into the tubes should be similar. The tube inlet loss coefficients will therefore have the largest effect on the pressure changes for individual tubes. The inlet loss coefficients decrease from 12 to 15 and results in the tube outlet mass flow rate distribution between 12 and 15.

From the heat rejection distribution in figure 7.6 it can be seen that fans 1 and 2 reject less heat than for the ideal case. This is due to the large fan performance reduction. The dephlegmator rejects less heat than for the ideal case, because of the shorter dephlegmator tubes. There is a 36% reduction in dephlegmator length,

but only a 23% reduction in heat rejected. This is due to the lower fan performance reduction and no recirculation being present.

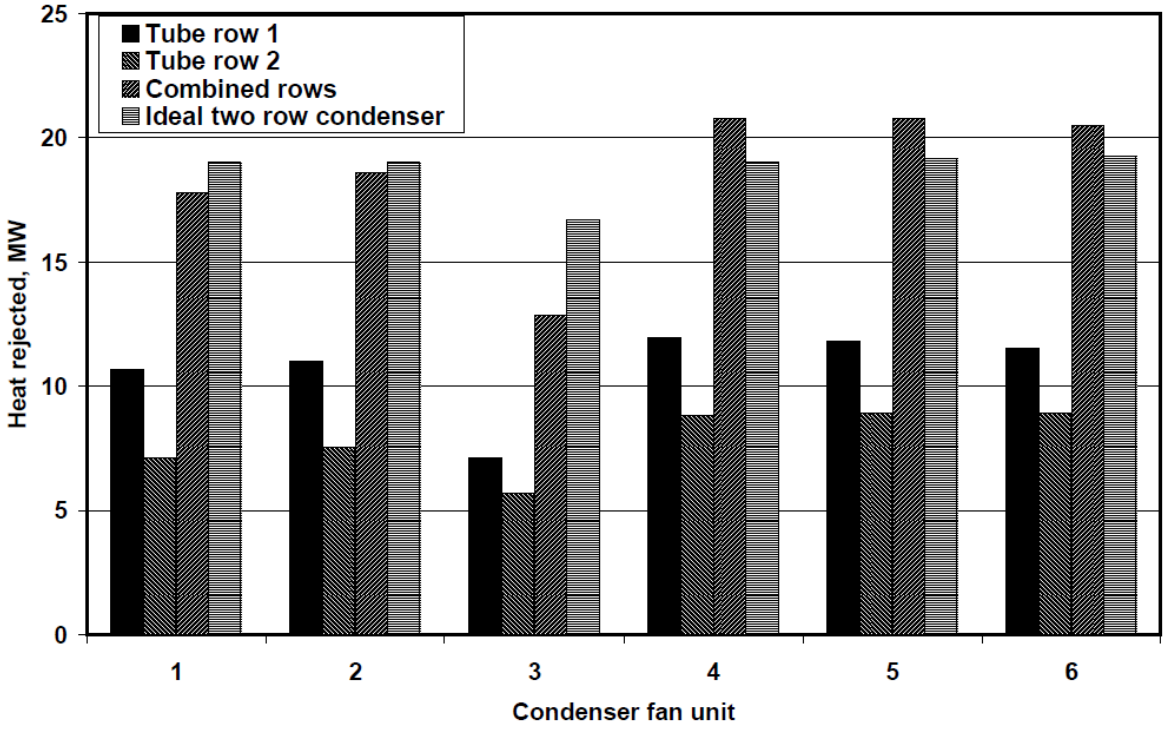

Figure 7.6: Heat rejected by each tube row and total heat rejected for a 6 m/s north-westerly wind and heat rejected by two-row condenser for ideal conditions

Chapter 8: Conclusions

8.1 Single-row condenser

The tube inlet loss coefficients have a large effect on the critical dephlegmator tube length. Four different dividing header inlet geometries were investigated, the straight inlet, a step at the inlet, a wedge-like ramp at the inlet and a combination of a step, ramp and a grid at the inlet to the tubes. The step provided the shortest critical dephlegmator tube length. The combination of the step, ramp and grid had the lowest inlet loss coefficients, but it was seen that the inlet loss coefficient distribution was important for the critical dephlegmator tube length and not the physical inlet loss coefficient value.

The effect of the combining header momentum correction factor on the critical dephlegmator tube length is smaller to that of the inlet loss coefficients for 50ºC, 60ºC and 70ºC.

Under ideal conditions the areas where backflow could potentially occur is at 9 and 12 as shown in figure 5.3 should the dephlegmator tube be shorter than the critical length.

The condenser street configuration that will result in the shortest critical dephlegmator tube length is a U-type condenser with a backward facing step just before the first tube in the dividing header.

When a night-time air temperature distribution is present the inlet steam temperature rises and the critical dephlegmator tube length increases. There is only one area of potential backflow at 9 and not at 9 and 12 as for the ideal conditions. The heat rejection distribution is not constant due to the varying inlet air temperatures that the air temperature distribution creates.

When wind is present the fan performance is affected. Recirculation of the plume also takes place, increasing the fan inlet air temperature. Both these effects decrease the performance of the condenser as seen in table 6.5. Wind has a much larger effect on the performance of the condenser than recirculation.

The outlet mass flow rate distribution is affected by the wind and the area where potential backflow can occur is at 12. As was seen for the night-time air temperature distribution there is only one area and not two as for ideal conditions.

It is concluded that for a single-row condenser areas of potential backflow are located on the side of the dephlegmator where the fan unit that rejects the most heat is located. For the night-time air temperature distribution the first condenser fan unit rejects the most heat while for the wind case the fourth condenser fan unit rejects the most heat. This corresponds to a higher pressure change between the headers.

8.2 Two-row condenser

The same ambient conditions that were investigated for the single-row condenser were investigated for a two-row condenser with a step at the inlet to the dividing header. It was found that the effect of the second tube row on the critical length of the dephlegmator is secondary to that of the tube inlet loss coefficients.

There will also always be an area of potential backflow for the first tube row in the first condenser fan unit. This differs from the single tube row condenser where the area of potential backflow is dependant on the ambient conditions. When ideal ambient conditions are present there is an area of potential backflow at 9 and not at 12 as well as was the case for the single-row condenser.

The outlet mass flow distribution differs from that of the single tube condenser for the same ambient disturbances. Between 9 and 11 the trends are the same, but between 12 and 15 the trends differ and are dependant on the ambient conditions present. For the wind case the tube outlet mass flow distribution between 12 and 15 differs from that of the other two cases for the two-row condenser because of the position of the condenser fan unit that rejects the most heat.

The heat rejection distribution is similar for the single and two-row condensers and is a function of the ambient conditions. If the condenser fan unit that rejects the most heat is situated to the right of the dephlegmator fan unit then an area of backflow will be present between 12 and 13, otherwise only in the first condenser fan unit for the first tube row.

The night-time air temperature distribution increases the inlet steam temperature in the condenser. The critical dephlegmator tube length is reduced slightly even though there is more steam present in the combining header. This is due to a higher steam temperature at the dephlegmator fan unit as pressure changes are smaller due to the higher inlet steam temperature.

The effect of the wind on the two-row condenser is larger than for the single-row condenser. The increase in inlet steam temperature is further increased by the reduction in the critical dephlegmator tube length. The reduction in the dephlegmator tube length is caused by fan 4 that rejects the most heat and therefore has the highest pressure change between the headers.

8.3 Recommendations

It was seen in this thesis that the inlet loss coefficient distribution in the dividing header has the largest impact on the length of the critical dephlegmator tube length. It is therefore recommended that an air-cooled condenser steam flow be solved numerically so that a more accurate solution can be found. The inlet loss coefficient distribution in the dividing header can then be determined and a more accurate model of the variation of the inlet loss coefficients can be created. The effect of the second tube row on the inlet loss coefficient distribution can also be determined. Uncertainties in the momentum correction factors for the combining and dividing headers can then also be excluded. A numerical model will also better predict where potential backflow will occur, as well as the severity of the

backflow. The air-side disturbances' effect on the condenser can also be better modeled.

Chapter 9: References

Badr, H.M., Habib, M.A., Ben-Mansour, R., Said, S.A.M. and Al-Anizi, S.S., Erosion in the Tube Entrance Region of an Air-Cooled Heat Exchanger, International Journal of Impact Engineering, Volume 32, pp. 1440-1463, 2006

Bajura, R.A., A Model for Flow Distribution Manifolds, Trans. ASME, J., Engineering for Power, Paper No. 70-Pwr-3, pp. 7 – 14, 1971

Beattie, D.R.H. and Whalley, P.B., A Simple Two-Phase Frictional Pressure Drop Calculation Method, International Journal of Multiphase Flow, Volume 8, pp. 83-87, 1981

Bredell, J.R., Thiart, G.D. and Kröger, D.G., Numerical Investigation of Fan Performance in a Forced Draft Air-Cooled Steam Condenser, Applied Thermal Engineering, Volume 26, pp.846-852, 2006

Carey, V.P., Liquid-Vapor Phase-Change Phenomena, Hemisphere Publ. Co., Washington, 1992

Çengel, Y.A. and Boles, M.A., Thermodynamics: An Engineering Approach, Fourth Edition McGraw-Hill, New York, USA, 2002

Dukler, A.E., Wicks, M. and Cleveland, R.G. , Frictional pressure drops in two-phase flow, AIChE J 10, p. 44, 1964

Duvenhage, K. and Kröger, D.G., The Influence of Wind on the Performance of Forced Draught Air-cooled Heat Exchangers, Journal of Wind Engineering and Industrial Aerodynamics, Volume 62, pp. 259-277, 1996

Duvenhage, K., Vermeulen, J.A., Meyer, C.J. and Kröger, D.G., Flow Distortions at the Fan Inlet of Forced-draught Air-cooled Heat Exchangers, Applied Thermal Engineering, Volume 16, No. 8/9, pp. 741-752, 1996

Du Toit, C.G., Thiart, G.D., Kröger D.G., Matimba ACC: Analysis of Flow Field (Phase 3), Report 92/02/3, Department of Mechanical Engineering, University of Stellenbosch, June 1993

Fried, E., Idelchik, I.E., Flow Resistance: A Design Guide for Engineers, Hemisphere Publ. Co., New York, 1989

Groenewald, W., Heat Transfer and Pressure Change in an Inclined Air-cooled Flattened Tube During Condensation of Steam, M.Eng Thesis, University of Stellenbosch, Stellenbosch, South Africa, 1993

Groenewald, W. and Kröger D.G., Effect of Mass Transfer on Turbulent Friction During Condensation Inside Ducts, Int. J. Heat Mass Transfer, Volume 38, No. 18, pp. 3385 – 3392, 1995

Gu, Z., Hu, L., Zhang, W., Li, Y. and Peng, J., Wind Tunnel Simulation on Re-Circulation of Air-Cooled Condensers of a Power Plant, Journal of Wind Engineering and Industrial Aerodynamics, Volume 93, pp. 509-520, 2005

Haaland, S.E., Simple and Explicit Formulas for the Friction Factor in Turbulent Pipe Flow, Trans ASME J. Fluids Engineering, Volume 105, No. 3, pp. 89-90, March 1983

Jorgenson, R., Fan Engineering, Buffalo Forge Co., N.Y., 1961

Isbin, H.S., Moen, R.H., Wickey, R.O., Mosher, D.R. and Larson, H.C., Two-phase steam-water pressure drops, Nuclear Science and Engineering Conference, Chicago, 1958

Kirschmer O., Kritische Betrachtungen zur Frage der Rohrreibung, Z.VDI 94, 785,1952

Kloppers, J.C., A Critical Evaluation and Refinement of the Performance Prediction of Wet-Cooling Towers, PhD Thesis, University of Stellenbosch, Stellenbosch, South Africa, 2003.

Kröger, D.G., Air-cooled Heat Exchangers and Cooling Towers: Thermal-flow Performance Evaluation and Design, Pennwell Corporation, Tulsa, USA, 2004

Meyer, C.J., Numerical Investigation of the Effect of Inlet Flow Distortions on Forced Draught Air-cooled Heat Exchanger Performance, Applied Thermal Engineering, Volume 25, pp. 1634-1649, 2005

Nosava, M.M. et al., Resistance of Inlet and Exit Orifices in the Presence of a Passing Stream, Promyshlennaya Aerodinamika, No. 15, pp. 20-37, 1959

Salta, C.A. and Kröger, D.G., Effect of Inlet Flow distortions on Fan Performance in Forced Draught Air-cooled Heat Exchangers, Heat Recovery Systems and CHP, Volume 15, No. 6, pp. 555-561, 1996

Smit, L.v.Z., Inlet Manifold Tests and Performance Evaluation of Dephlegmators in Air-Cooled Steam Condensers, M.Sc.Eng Thesis, University of Stellenbosch, Stellenbosch, South Africa, 2000

Van Heerden, E., Steam Flow Distribution in Air-Cooled Condensers, M.Sc.Eng Thesis, University of Stellenbosch, Stellenbosch, South Africa, 1991

Van Rooyen, J.A., Performance Trends of an Air-cooled Steam Condenser Under Windy Conditions, M.Sc.Eng Thesis, University of Stellenbosch, Stellenbosch, South Africa, 2007

Whalley, P.B., Boiling, Condensation and Gas-Lliquid Flow, Clarendon Press, Oxford, 1990

Zapke, A. and Kröger, D.G., Countercurrent Gas-Liquid Flow in Inclined and Vertical Ducts –I: Flow Patterns, Pressure Drop Characteristics and Flooding, International Journal of Multiphase flow, Volume 26, pp. 1439-1455, 2000

Zapke, A., Pressure Gradient and Flooding During Two-Phase Countercurrent Flow in Inclined Tubes, M.Sc.Eng thesis, University of Stellenbosch, Stellenbosch, South Africa, 1994

Zipfel, T., Flow Distribution in Air-Cooled Steam Condensers, M.Sc.Eng thesis, Stellenbosch University, Stellenbosch, 1996

Appendix A: Physical properties

In this appendix correlations for all the physical properties used are given. All the equations are as presented by Kröger(2004) except the enthalpy of saturated liquid water which was generated from steam table data given by Çengel and Boles(2002).

A.1 Air properties

Density:

$$\rho_a = \frac{p_a}{287.08T}, \mathrm{kg/m^3} \tag{A.1.1}$$

Dynamic viscosity:

$$\mu_a = 2.287973\times10^{-6} + 6.259793\times10^{-8} - 3.131956\times10^{-11}T^2 + 8.15038\times10^{-15}T^3, \mathrm{kg/sm} \tag{A.1.2}$$

Specific heat:

$$c_{pa} = 1.045356\times10^{3} - 3.161783\times10^{-1}T + 7.083814\times10^{-4}T^2 - 2.705209\times10^{-7}T^3, \mathrm{J/kgK} \tag{A.1.3}$$

Thermal conductivity:

$$k_a = -4.937787\times10^{-4} + 1.018087\times10^{-4}T - 4.627937\times10^{-8}T^2 + 1.250603\times10^{-11}T^3, \mathrm{W/mK} \tag{A.1.4}$$

A.2 Saturated water vapor properties

Temperature:

$$T_v = 164.630366 + 1.832295\times10^{-3}p_v + 4.27215\times10^{-10}p_v^2 + 3.738954\times10^{3}p_v^{-1} - 7.01204\times10^{5}p_v^{-2} + 16.161488\ln\ p_v\ - 1.437169\times10^{-4}p_v\ln\ p_v \tag{A.2.1}$$

Vapor pressure:

$$p_v = 10^{z}, \mathrm{N/m^2} \tag{A.2.2}$$

$$z = 10.79586\ \left(1 - 273.16/T_v\right) + 5.02808\log_{10}\ 273.16/T_v + 1.50474\times10^{-4}\left[1-10^{-8.29692\ \left(T_v/273.16\ -1\right.}\right] + 4.2873\times10^{-4}\left[10^{4.76955\ 1-273.16/T_v}\ -1\right] + 2.786118312$$

Vapor density:

$$\rho_v = -4.062329056 + 0.10277044T_v - 9.76300388\times10^{-4}T_v^2 + 4.475240795\times10^{-6}T_v^3 - 1.004596894\times10^{-8}T_v^4 + 8.89154895\times10^{-12}T_v^5, \mathrm{kg/m^3} \tag{A.2.3}$$

Dynamic viscosity:

$$\mu_v = 2.562435\times10^{-6} + 1.816683\times10^{-8}T_v + 2.579066\times10^{-11}T_v^2 - 1.067299\times10^{-14}T_v^3, \text{kg/sm} \quad \text{(A.2.4)}$$

Specific heat:

$$c_{pv} = 1.3605\times10^{3} + 2.31334T_v - 2.46784\times10^{-10}T_v^5 + 5.91332\times10^{-13}T_v^6, \text{J/kgK} \quad \text{(A.2.5)}$$

Thermal conductivity:

$$k_v = 1.3046\times10^{-2} - 3.756191\times10^{-5}T_v + 2.217964\times10^{-7}T_v^2 - 1.111562\times10^{-10}T_v^3, \text{W/mK} \quad \text{(A.2.6)}$$

A.3 Saturated liquid water properties

Density:

$$\rho_w = \left(\begin{matrix}1.49343\times10^{-3} - 3.7164\times10^{-6}T + 7.09782\times10^{-9}T^2 \\ -1.90321\times10^{-20}T^6\end{matrix}\right)^{-1}, \text{kg/m}^3 \quad \text{(A.3.1)}$$

Specific heat:

$$c_{pw} = 8.15599\times10^{3} - 2.80627\times10T + 5.11283\times10^{-2}T^2 - 2.17582\times10^{-13}T^6, \text{J/kgK} \quad \text{(A.3.2)}$$

Dynamic viscosity:

$$\mu_w = 2.414\times10^{-5}\times10^{247.8/(T-140)}, \text{kg/sm} \quad \text{(A.3.3)}$$

Thermal conductivity:

$$k_w = -6.14255\times10^{-1} + 6.9962\times10^{-3}T - 1.01075\times10^{-5}T^2 + 4.74767\times10^{-12}T^4, \text{W/mK} \quad \text{(A.3.4)}$$

Enthalpy:

$$i_w = -1251390 + 5237.45T - 3.39252T^2 + 3.61855\times10^{-3}T^3, \text{J/kg} \quad \text{(A.3.5)}$$

Latent heat of vaporization:

$$i_{vw} = 3.4831814\times10^{6} - 5.8627703\times10^{3}T + 12.139568T^2 - 1.40290431\times10^{-2}T^3, \text{J/kg} \quad \text{(A.3.6)}$$

Surface tension:

$$\sigma_w = 5.148103\times10^{-2} + 3.998714\times10^{-4}T - 1.4721869\times10^{-6}T^2 + 1.21405335\times10^{-9}T^3, \text{N/m} \quad \text{(A.3.7)}$$

Appendix B: Sample calculation for the steam pressure and temperature change in a duct

These are the sample calculations to illustrate trends in the pressure and temperature change in the turbine exhaust steam duct to a power station's direct air-cooled condenser. The exhaust steam is fed to a main duct, which branches into four smaller ducts. These four smaller ducts lead to the ACC. A schematic drawing of the duct system is shown in the figure 2.2.

Steam enters the steam duct at a rate of 200 kg/s at 60°C(333.15K) and is 5% wet. The steam saturation pressure according to equation (A.2.2) at this temperature is

$$
\begin{aligned}
z &= 10.79586\ 1-273.16/T_{v1}\ +5.02808\log_{10}\ 273.16/T_{v1} \\
&\quad +1.50474\times10^{-4}\left[1-10^{-8.29692\ \ T_{v1}/273.16\ -1}\right] \\
&\quad +4.2873\times10^{-4}\left[10^{4.76955\ 1-273.16/T_{v1}}-1\right]+2.786118312 \\
&= 10.79586\ 1-273.16/333.15\ +5.02808\log_{10}\ 273.16/333.15 \\
&\quad +1.50474\times10^{-4}\left[1-10^{-8.29692\left(333.15/273.16\right)-1}\right] \\
&\quad +4.2873\times10^{-4}\left[10^{4.76955\left(-273.16/333.15\right)}-1\right]+2.786118312 \\
&= 4.299401 \\
p_1 &= 10^{z} = 10^{4.299401} = 19925.1152\ \mathrm{N/m^2}
\end{aligned}
\qquad \text{(A.2.2)}
$$

The steam enters the steam duct through a rectangular section. This section then is reduced to a circular duct. This section is shown in the schematic of the steam duct between 1 and 2.

According to equation (2.24) the inlet density is,

$$
\rho_{vw1} = \left(\frac{x_1}{\rho_{v1}} + \frac{1-x_1}{\rho_{w1}}\right)^{-1} \qquad \text{(2.20)}
$$

where according to equations (A.2.3) and (A.3.1) the densities are

$$
\begin{aligned}
\rho_{v1} &= -4.062329056 + 0.10277044T_{v1} - 9.76300388\times10^{-4}T_{v1}^2 \\
&\quad + 4.475240795\times10^{-6}T_{v1}^3 - 1.004596894\times10^{-8}T_{v1}^4 + 8.89154895\times10^{-12}T_{v1}^5 \\
&= -4.062329056 + 0.10277044\ 333.15\ -9.76300388\times10^{-4}\ 333.15\ ^2 \\
&\quad + 4.475240795\times10^{-6}\ 333.15\ ^3 - 1.004596894\times10^{-8}\ 333.15\ ^4 \\
&\quad + 8.89154895\times10^{-12}\ 333.15\ ^5 \\
&= 0.1302\ \mathrm{kg/m^3}
\end{aligned}
\qquad \text{(A.2.3)}
$$

and

$$\rho_{w1} = \begin{pmatrix} 1.49343\times10^{-3} - 3.7164\times10^{-6}T_{v1} + 7.09782\times10^{-9}T_{v1}^2 \\ -1.90321\times10^{-20}T_{v1}^6 \end{pmatrix}^{-1} \qquad \text{(A.3.1)}$$

$$= \begin{pmatrix} 1.49343\times10^{-3} - 3.7164\times10^{-6}\ \ 333.15\ \ + 7.09782\times10^{-9}\ \ 333.15\ ^2 \\ -1.90321\times10^{-20}\ \ 333.15\ ^6 \end{pmatrix}^{-1}$$

$$= 983.2168\,\mathrm{kg/m^3}$$

so

$$\rho_{vw1} = \left(\frac{0.95}{0.1302} + \frac{1-0.95}{983.2168} \right)^{-1} = 0.1371\ \ \mathrm{kg/m^3}$$

The inlet void fraction is calculated with equation (2.24)

$$\alpha_1 = \frac{1}{1+\left(\frac{1-x}{x}\frac{\rho_{v1}}{\rho_{w1}} \right)} = \frac{1}{1+\left(\frac{1-0.95}{0.95}\frac{0.1302}{983.2168} \right)} \approx 1 \qquad \text{(2.24)}$$

Since the void fraction is practically 1, the assumption can be made that the dynamic viscosity is that of the vapor and that the effect of the liquid is negligible. Equation (2.22) then reduces to

$$\mu_{vw1} = \mu_{v1}\alpha + \mu_{w1}\ \ 1-\alpha\ \ \ 1+2.5\alpha \qquad \text{(2.22)}$$

$$= \mu_{v1}\times1 + \mu_{w1}\ \ 1-1\ \ \ 1+2.5\times1$$

$$= \mu_{v1}$$

and the dynamic viscosity is then

$$\mu_{v1} = 2.562435\times10^{-6} + 1.816683\times10^{-8}T_{v1} + 2.579066\times10^{-11}T_{v1}^2 \qquad \text{(A.2.4)}$$

$$-1.067299\times10^{-14}T_{v1}^3$$

$$= 2.562435\times10^{-6} + 1.816683\times10^{-8}\ \ 333.15\ \ + 2.579066\times10^{-11}\ \ 333.15\ ^2$$

$$-1.067299\times10^{-14}\ \ 333.15\ ^3$$

$$= 1.1083\times10^{-5}\,\mathrm{kg/ms}$$

The inlet to the steam duct system has a rectangular cross section with dimensions 5.842m by 5.042m. The hydraulic diameter of the rectangular section is

$$d_e = 4A_{rect}/P_{rect} = 4\times\ 5.842\times5.042\ \ /\left[2\times\ 5.842+5.042\ \right] = 5.412\mathrm{m}$$

The steam mass flux at the inlet to the section is

$$G_{vw1} = m_{vw1}/A_1 = 200/\ 5.842\times5.042\ = 6.7899\,\mathrm{kg/m^2s} \qquad \text{(B.1)}$$

The mean hydraulic diameter of the section is

$$d_m = \ d_e + d_2\ \ /2 = \ 5.412+4.988\ \ /2 = 5.2\mathrm{m}$$

The steam mass flux at the exit of the section is then

$$G_{vw2} = m_{vw2}/A_2 = 200/\ \pi\ 4.988^{\ 2}/4\ = 10.235\,\mathrm{kg/m^2 s}$$

The average steam mass flux for this section is then

$$G_{vwm12} = \frac{G_{vw1} + G_{vw2}}{2} = \frac{6.7899 + 10.235}{2} = 8.51245\,\mathrm{kg/m^2 s}$$

The Reynolds number for this section is

$$\mathrm{Re} = G_{vwm12} d_m / \mu_{v1} = 8.51245 \times 5.2 / 1.1083 \times 10^{-5} = 3.99 \times 10^6 \qquad \text{(B.2)}$$

The friction factor is required to determine the friction pressure loss in the duct. The relative roughness of welded steel is approximately $\varepsilon = 10^{-4}$ m (Kirschmer 2002). To account for the water film that forms on the inside of the steam duct and some oxidation that may form on the inside of the duct, the roughness is assumed to be to $\varepsilon \approx 1\text{x}10^{-3}$ m. This is a conservative value, but it has a very small impact on the pressure drop in the duct. The flow inside the steam duct is not fully developed and therefore secondary flows may be present that will influence the friction factor and momentum changes of the steam. These effects will however be ignored in this analysis, but the calculated pressure changes in the steam duct are therefore only approximations. The friction factor is determined using equation (2.9) since

$$\varepsilon/d_m = 1 \times 10^{-3}/5.2 = 1.923 \times 10^{-4} > 1 \times 10^{-4}$$

therefore

$$f_D = \frac{0.30864}{\left[\log\left\{\left(\frac{6.9}{\mathrm{Re}}\right) + \left(\frac{\varepsilon/d_m}{3.7}\right)^{1.11}\right\}\right]^2} \qquad \text{(2.9)}$$

$$= \frac{0.30864}{\left[\log\left\{\left(\frac{6.9}{3.99 \times 10^6}\right) + \left(\frac{1.923 \times 10^{-4}}{3.7}\right)^{1.11}\right\}\right]^2}$$

$$f_D = 0.01388$$

Equation (2.7) is used to determine the frictional pressure change in the first section of the steam duct,

$$p_2 - p_{1\ f} = -\frac{1}{2}\frac{f_D G_{vwm12}^2 L_{1-2}}{\rho_{vw1} d_m} = -\frac{0.01388 \times 8.51245^2 \times 4.7}{2\ \ 0.1371 \times 5.2} = -3.3153\,\mathrm{N/m^2}$$

There is also a pressure change due to gravity and using the second term of equation (2.5),

$$p_2 - p_{1\ s} = \rho_{vw1} g L_{1-2} = 0.1371 \times 9.8 \times 4.7 = 6.3148\ \mathrm{N/m^2}$$

Due to the geometry of the inlet section there is also a reducer pressure change. To simplify the inlet it is assumed that the inlet is round with the hydraulic diameter as inlet diameter. Equation (2.18) is used to calculate the pressure change over the inlet section due to the geometry of the inlet,

$$p_2 - p_{1\ r} = \rho_{vw1}\left(\frac{v_{vw1}^2}{2} - \frac{v_{vw2}^2}{2}\right) - \frac{K_{red}\rho_{vw1}v_{vw2}^2}{2} \qquad (2.14)$$

The reducer loss coefficient is given by equation (2.13)

$$K_{red} = \frac{-0.0125\sigma_{21}^4 + 0.0224\sigma_{21}^3 - 0.00723\sigma_{21}^2 + 0.00444\sigma_{21} - 0.00745}{8\theta^3 - 8\pi\theta^2 - 20\theta} \qquad (2.13)$$

where the area ratio is

$$\sigma_{21} = \frac{A_2}{A_1} = \frac{\pi\ 4.988^2\ /4}{\pi\ 5.412^2\ /4} = 0.8494$$

and the reducer half angle is

$$\theta = \frac{\tan^{-1}\left[\ d_1 - d_2\ /L_{1-2}\right]}{2} = \frac{\tan^{-1}\left[\ 5.412 - 4.988\ /4.7\right]}{2} = 0.04498\ \mathrm{rad}$$

The reducer loss coefficient is then

$$K_{red} = \frac{\begin{pmatrix} -0.0125\ 0.8494^{\ 4} + 0.0224\ 0.8494^{\ 3} - 0.00723\ 0.8494^{\ 2} \\ +0.00444\ 0.8494 \quad - 0.00745 \end{pmatrix}}{8\ 0.04498^{\ 3} - 8\pi\ 0.04498^{\ 2} - 20\ 0.04498}$$

$$= 1.59 \times 10^{-3}$$

The reducer pressure change is then

$$p_2 - p_{1\ r} = \rho_{vw1}\left(\frac{v_{vw1}^2}{2} - \frac{v_{vw2}^2}{2}\right) - \frac{K_{red}\rho_{vw1}v_{vw2}^2}{2}$$

$$= \frac{1}{2\rho_{vw1}}\ G_{vw1}^2 - G_{vw2}^2\ - \frac{K_{red}G_{vw2}^2}{2\rho_{vw1}}$$

$$= \frac{1}{2 \times 0.1371}\ 6.7899^2 - 10.235^2\ - \frac{1.59 \times 10^{-3} \times\ 10.235^{\ 2}}{2 \times 0.1371}$$

$$= -213.9262 - 0.6075$$

$$= -214.5337\ \mathrm{N/m^2}$$

The pressure at the inlet to the second section of the steam duct can then be determined using equation (2.3),

$$\begin{aligned} p_2 &= p_1 + \left(p_2 - p_1\right)_f + \left(p_2 - p_1\right)_s + \left(p_2 - p_1\right)_r \\ &= 19925.1152 - 3.3153 + 6.3148 - 214.5337 \\ &= 19713.581\,\mathrm{N/m^2} \end{aligned}$$

Equation (A.2.1) can now be used to determine the approximate steam temperature at 2,

$$\begin{aligned} T_{v2} &= 164.630366 + 1.832295\mathrm{x}10^{-3}\ (19713.581) + 4.27215\mathrm{x}10^{-10}\ (19713.581)^2 \\ &\quad + 3.738954\mathrm{x}10^{3}\ (19713.581)^{-1} - 7.01204\mathrm{x}10^{5}\ (19713.581)^{-2} \\ &\quad + 16.161488 \ln (19713.581) - 1.437169\mathrm{x}10^{-4}\ (19713.581) \ln (19713.581) \\ &= 332.9099\,\mathrm{K} \end{aligned}$$

The density at T_{v2} is determined using equation (2.20) with x_1 being used as an approximate for the quality since quality changes are small. The density is then

$$\rho_{vw2} = 0.1357\,\mathrm{kg/m^3}$$

The new quality can now be determined by using equation (2.26)

$$x_2 = \frac{\left[i_1 - i_{w2} + 0.5\left(v_{vw1}^2 - v_{vw2}^2\right) + g\left(z_1 - z_2\right) \right]}{i_{wv2}} \qquad (2.26)$$

where the enthalpies are calculated with equations (2.21), (A.3.5) and (A.3.6),

$$i_1 = 2.4914\times10^6\,\mathrm{J/kg} \qquad (2.21)$$

$$i_{w2} = 2.4973\times10^5\,\mathrm{J/kg} \qquad (A.3.5)$$

$$i_{wv2} = 2.3591\times10^6\,\mathrm{J/kg} \qquad (A.3.6)$$

and the velocities are:

$$v_{vw1} = G_{vw1}/\rho_{vw1} = 6.7899/0.1371 = 49.5312\,\mathrm{m/s}$$

$$v_{vw2} = G_{vw2}/\rho_{vw2} = 10.235/0.1357 = 75.4445\,\mathrm{m/s}$$

and the elevation change is

$$z_1 - z_2 = 4.7\ \mathrm{m}$$

thus

$$x_2 = \frac{\left[2.4914\mathrm{x}10^6 - 2.4973\mathrm{x}10^5 + 0.5\left(49.5312^2 - 75.4445^2\right) + 9.8\ (4.7) \right]}{2.3591\mathrm{x}10^6} = 0.9495$$

As constant properties were not assumed, these values will be the input to the next section. The next section is the length of straight pipe from 2 to 3.

The inlet properties of the steam at T_{v2} with x_2 are as follows:

Steam density: $\rho_{vw2} = 0.1357\ \text{kg/m}^3$ (2.20)

Dynamic viscosity: $\mu_{v2} = 1.1086\times10^{-5}\ \text{kg/ms}$ (2.22)

Enthalpy: $i_2 = 2.4898\times10^{6}\ \text{J/kg}$ (2.21)

The mass flux of the section is

$G_{vw2} = 10.2350\ \text{kg}/\text{m}^2\text{s}$

and the Reynolds number is

$\text{Re} = 4.6050\times10^{6}$

The friction factor for this section is

$f_D = 0.0139$

The frictional pressure differential is then

$$p_3 - p_{2\ f} = -\frac{0.0139\times10.2350^2\times4.350}{2\times0.1357\times4.988} = -4.6788\ \text{N}/\text{m}^2$$

The gravity pressure change is calculated as follows

$p_3 - p_{2\ s} = 0.1357\text{x}9.8\text{x}4.35 = 5.7849\ \text{N}/\text{m}^2$

The new pressure is then calculated to be

$p_3 = p_2 + p_3 - p_{2\ f} + p_3 - p_{2\ s} = 19713.581 - 4.6788 + 5.7849 = 19714.6871\text{N}/\text{m}^2$

The corresponding steam temperature is then

$T_{v3} = 332.9111\text{K}$

and the quality

$x_3 = 0.9488$

At 3 there is a miter bend in the pipe. The loss coefficient of the miter bend is quoted to be 0.28 for a similar type of miter bend (Jorgensen 1961).

The mass flux for this section is the same as for the previous as the mass flow and width of the duct is the same. The physical properties are:

Steam density: $\rho_{vw3} = 0.1358\text{kg}/\text{m}^3$

Enthalpy: $i_3 = 2.4883\times10^{6}\ \text{J}/\text{kg}$

The pressure loss due to the bend is then according to equation (2.11)

$$\Delta p_{b3} = -\frac{K_{mb}G_{vw3}^2}{2\rho_{vw3}} = -\frac{0.28\text{x}10.2350^2}{2\text{x}0.1358} = -107.9951\ \text{N}/\text{m}^2$$

The pressure, temperature and quality after the miter bend is then:

$p_{b3} = p_2 + \Delta p_{b3} = 19714.6871 - 107.9951 = 19606.6920\,\text{N}/\text{m}^2$

$$T_{vb3} = 332.7926\ K$$
$$x_{b3} = 0.9490$$

There are no new calculations until section 5 and therefore only the pressure and temperature change for each section is going to be noted.

$$p_4 - p_{3\ f} = -21.2315\ N/m^2$$
$$\Delta p_{b4} = -108.5643\ N/m^2$$
$$p_5 - p_{4\ f} = -26.1436\ N/m^2$$
$$p_5 - p_{4\ s} = -31.5787\ N/m^2$$
$$\Delta p_{b5} = -109.4391\ N/m^2$$

The pressure after section 5 is then

$$\begin{aligned} p_5 &= p_{b3} + p_4 - p_{3\ f} + \Delta p_{b4} + p_5 - p_{4\ f} + p_5 - p_{4\ s} + \Delta p_{b5} \\ &= 19606.6920 - 21.2315 - 108.5643 - 26.1436 - 31.5787 - 109.4391 \\ &= 19309.7348\ N/m^2 \end{aligned}$$

The temperature and quality for this pressure is

$$T_{v5} = 332.4639K$$
$$x_5 = 0.9483$$

Between 5 and 6 the first of the T-junctions are found. The general correlations found in Kröger(2004) were used to determine an approximate pressure change.

For the ideal case with a uniform steam distribution it was possible to read the square edge pressure loss coefficients for the three T-junctions off the figures given by Kröger(2004). These can then be adjusted to the round edge analogy that is used to get an approximation for the chamfered edge and vanes at the inlet to the branch. Equation (2.17) is used to make this adjustment.

$$K_{31r} = K_{j90°} - 0.45\left(\frac{V_1/V_3}{A_1/A_3}\right)^2 \qquad (2.17)$$

where K_{j90} is the loss coefficient for a square edge junction, V_1 is the volume flow rate in the branch, V_3 is the upstream volume flow rate, A_1 and A_3 are the areas of the previously mentioned pipes, r_j is the bend radius and d_b is the branch diameter. Since the geometry of the T-junctions under consideration by van Heerden(1991) are the same as the ones in this duct system, the same bend radius of 0.5 m will be used.

To determine K_{j90} the following must be known:
The area ratio between the duct and the branch
The volume flow rate between the duct and the branch
These parameters can then be used to determine the loss coefficient using the figures given by Kröger(2004).

Once K_{j90} is determined then the correction can be added to get the approximation of the real loss coefficient of the junction.

For the first of the T-junctions the parameters are as follows:

$$V_1/V_3 = 0.25$$

$$A_1/A_3 = 2.496/4.988^{\,2} = 0.2504$$

From these parameters the loss coefficient is found according to figure 2. 7 to be

$$K_{j90^\circ} = 1.1574$$

The corrected value according to equation (2.17) is then

$$K_{31r} = 1.1574 - 0.45\left(\frac{0.25}{0.2504}\right)^2 = 0.7088$$

The pressure drop into the branch can then be calculated with equation (2.18),

$$p_{br1} - p_{5\ j} = -\frac{K_{jbr1}\rho_{vw5}v_{vw5}^2}{2} + \rho_{vw5}\left(\frac{v_{vw5}^2}{2} - \frac{v_{br1}^2}{2}\right) \qquad (2.18)$$

where the density is

$$\rho_{vw5} = 0.1333\,\mathrm{kg/m^3}$$

and the branch steam speed is

$$v_{br1} = \frac{200/4}{0.1333 \times 2.496^2\,\pi/4} = 76.6586\ \mathrm{m/s}$$

and the steam speed before the branch in the main duct is

$$v_{vw5} = \frac{200}{0.1333 \times 4.988^2\,\pi/4} = 76.7816\ \mathrm{m/s}$$

so

$$p_{br1} - p_{5\ j} = \frac{0.1333}{2}\ \ 1 - 0.7088\ \times 76.7816^2 - 76.6586^2\ \ = -277.2504\,\mathrm{N/m^2}$$

The frictional pressure change between 5 and inlet to the branch is,

$$p_{br1} - p_{5\ f} = -\frac{0.0140 \times 10.2350^2 \times 1.22}{2 \times 0.1333 \times 4.988} = -1.3455\ \mathrm{N/m^2}$$

The pressure just inside the branch is then

$$p_{br1} = p_5 + p_{br1} - p_{5\ j} + p_{br1} - p_{5\ f}$$

$$= 19309.7348 - 277.2504 - 1.3455 = 19031.1389\,\mathrm{N/m^2}$$

with corresponding temperature and quality

$$T_{vb1} = 332.1517\text{K}$$

$$x_{b1} = 0.9483$$

The pressure change between 5 and 6 is calculated in a similar way. The parameters that were evaluated earlier are also used to determine the loss coefficient. The loss coefficient according to figure 2.8 for the pressure change over the branch duct is

$$K_{56} = -0.0167$$

The pressure change is then according to equation (2.19)

$$p_6 - p_{5\ j} = -\frac{K_{56}\rho_{vw5}v_{vw5}^2}{2} + \rho_{vw5}\left(\frac{v_{vw5}^2}{2} - \frac{v_{vw6}^2}{2}\right) \qquad (2.19)$$

where the steam speed after the branch is

$$v_{vw6} = \frac{200 \times 3/4}{0.1333 \times \pi \times 4.988^2/4} = 57.5862\,\text{m/s}$$

so

$$p_6 - p_{5\ j} = \frac{0.1333}{2}\quad 0.0167 + 1\ \times 76.7816^2 - 57.5862^2\ \ = 178.4685\,\text{N/m}^2$$

The frictional pressure change between 5 and 6 is

$$p_6 - p_{5\ f} = -\frac{0.014 \times 10.2350^2 \times 3.7}{2 \times 0.1333 \times 4.988} = -4.0806\ \ \text{N/m}^2$$

The pressure after the branch opening is then

$$p_6 = p_5 - \ p_6 - p_{5\ j} + \ p_6 - p_{5\ f}$$

$$= 19309.7348 + 178.4864 - 4.0806 = 19484.1406\,\text{N/m}^2$$

and the corresponding temperature and quality

$$T_{v6} = 332.6575\text{K}$$

$$x_6 = 0.9479$$

Between 6 and 7 is a conical reducer that accelerates the steam after the first branch. The procedure to find the loss coefficient of the reducer is as follows:
Determine the area ratio between the outlet and the inlet.
Determine the half angle of the reducer.

Find the loss coefficient by using equation (2.13)

$$K_{red} = \ -0.0125\sigma_{76}^4 + 0.0224\sigma_{76}^3 - 0.00723\sigma_{76}^2 + 0.00444\sigma_{76} - 0.00745$$
$$8\theta^3 - 8\pi\theta^2 - 20\theta \qquad (2.13)$$

The loss coefficient is based on the smaller area, so that the outlet conditions must be used when evaluating the loss coefficient. For the current conical diffuser under investigation the area ratio and half angle is:

Area ratio:

$$\sigma_{76} = A_7/A_6 = \left(\frac{\pi 4.292^2/4}{\pi 4.988^2/4} \right) = 0.7404$$

Half angle:

$$\theta = \frac{\tan^{-1}\left[\left. d_7 - d_6 \right/ L_{6\text{-}7} \right]}{2} = \frac{\tan^{-1}\left[\left. 4.292 - 4.988 \right/ 2.6 \right]}{2} = 0.1308 \text{ rad}$$

The loss coefficient is then

$$K_{red} = \begin{pmatrix} -0.0125 \times 0.7404^4 + 0.0224 \times 0.7404^3 - 0.00723 \times 0.7404^2 \\ +0.00444 \times (0.7404) - 0.00745 \end{pmatrix}$$

$$8 \times 0.1308^3 - 8\pi \times 0.1308^2 - 20 \times 0.1308$$

$$= 0.0084$$

The mass fluxes are

$$G_{vw6} = 7.6734 \text{kg/ms}$$

$$G_{vw7} = 10.3677 \text{kg/ms}$$

and the density is

$$\rho_{vl6} = 0.1345 \text{kg/m}^3$$

The pressure change over the reducer can then be calculated with equations (2.14) and (2.7). According to equation (2.14)

$$p_7 - p_{6\ r} = \rho_{vw6} \left(\frac{v_{vw6}^2}{2} - \frac{v_{vw7}^2}{2} \right) - \frac{K_{red} \rho_{vw6} v_{vw7}^2}{2} \qquad (2.14)$$

$$= \frac{1}{2\rho_{vw6}} \left(G_{vw6}^2 - G_{vw7}^2 \right) - \frac{K_{red} G_{vw7}^2}{2\rho_{vw6}}$$

$$= \frac{1}{2 \times 0.1345} \left(7.6734^2 - 10.3677^2 \right) - \frac{0.0084 \times 10.3677^2}{2 \times 0.1345}$$

$$= -184.0559 \text{N/m}^2$$

The friction pressure change is evaluated at the mean diameter of the reducer,

$$d_{m6-7} = \frac{d_6 + d_7}{2} = \frac{4.988 + 4.292}{2} = 4.64 \text{m}$$

The mass flux at the mean diameter is then

$$G_{vlm} = 4 \times 150 / \ \pi \times 4.64^2 \ = 8.8706 \, \mathrm{kg/ms^2}$$

The Reynolds number is

$$\mathrm{Re_m} = 3.7192 \times 10^6$$

and the friction factor

$$f_D = 0.0142$$

The friction pressure change is then according to equation (2.7)

$$p_7 - p_{6\ f} = -\frac{1}{2} \frac{0.0142 \times 2.6}{4.64} \times \frac{8.8706^2}{0.1345} = -2.3275 \, \mathrm{N/m^2}$$

Using equation (2.19) the new pressure is then

$$p_7 = p_6 + \ p_7 - p_{6\ r} + \ p_7 - p_{6\ f}$$

$$= 19484.1406 - 184.0559 - 2.3275 = 19297.7572 \, \mathrm{N/m^2}$$

and the corresponding temperature and quality

$$T_{v7} = 332.4506 \mathrm{K}$$

$$x_7 = 0.9472$$

For the rest of the ducting only the pressure changes will be stated and the reasons for the change i.e. miter bends, reducers or friction losses.

The pressure change between 7 and 8 can is due to friction and the change across the branch mouth. The two changes are

$$p_8 - p_{7\ f} = -10.1458 \, \mathrm{N/m^2}$$

$$p_8 - p_{7\ j} = 227.2378 \, \mathrm{N/m^2}$$

Between 8 and 9 there is a reducer with corresponding pressure loss

$$p_9 - p_{8\ r} = -231.7444 \, \mathrm{N/m^2}$$

$$p_9 - p_{8\ f} = -2.9724 \, \mathrm{N/m^2}$$

From 9 to 10 there is another friction pressure drop and a branch mouth pressure change:

$$p_{10} - p_{9\ f} = -13.2703 \, \mathrm{N/m^2}$$

$$p_{10} - p_{9\ j} = 291.4415 \, \mathrm{N/m^2}$$

Another reducer is found between 10 and 11:

$$p_{11} - p_{10\ r} = -293.0462 \, \mathrm{N/m^2}$$

$$p_{11} - p_{10\ f} = -2.9177 \, \mathrm{N/m^2}$$

There is a friction pressure loss between 11 and 12 with a miter bend at 12:

$$p_{12} - p_{11\ f} = -14.5753 \, \mathrm{N/m^2}$$

$$\Delta p_{12b} = -109.8108\,\mathrm{N/m^2}$$

The pipe now goes up from 12 to 13 so there is a gravity pressure change as well as a friction loss. At 13 there is also a miter bend.

$$p_{13} - p_{12\ f} = -63.9601\,\mathrm{N/m^2}$$

$$p_{13} - p_{12\ s} = -32.5586\,\mathrm{N/m^2}$$

$$\Delta p_{13b} = -110.8378\,\mathrm{N/m^2}$$

The last section of the pipe from 13 to 14 is a straight section with only a friction loss:

$$p_{14} - p_{13\ f} = -12.3597\,\mathrm{N/m^2}$$

The total to total pressure change from 1 to 14 is

$$p_{t1} - p_{t14} = 775.5511\,\mathrm{N/m^2}$$

with corresponding steam density and speed at 14

$$\rho_{vw14} = 0.1307\,\mathrm{kg/m^3}$$

$$v_{vw14} = 78.1835\,\mathrm{m/s}$$

The static to static pressure and temperature change is

$$p_1 - p_{14} = 1006.8778\,\mathrm{N/m^2}$$

$$T_{v1} - T_{v14} = 1.1260\mathrm{K}$$

The total to total pressure change from 1 to 15 is

$$p_{t1} - p_{t15} = 862.6957\,\mathrm{N/m^2}$$

with corresponding steam density and speed at 15

$$\rho_{vw15} = 0.1302\,\mathrm{kg/m^3}$$

$$v_{vw15} = 78.4838\,\mathrm{m/s}$$

The static to static pressure and temperature change is

$$p_1 - p_{15} = 1095.5565\,\mathrm{N/m^2}$$

$$T_{v1} - T_{v15} = 1.2267\mathrm{K}$$

The total to total pressure change from 1 to 16 is

$$p_{t1} - p_{t16} = 857.1455\,\mathrm{N/m^2}$$

with corresponding steam density and speed at 16

$$\rho_{vw16} = 0.1302\,\mathrm{kg/m^3}$$

$$v_{vw16} = 78.4838\,\mathrm{m/s}$$

The static to static pressure and temperature change is

$$p_1 - p_{16} = 1090.0063\,\mathrm{N/m^2}$$
$$T_{v1} - T_{v16} = 1.2204\mathrm{K}$$

The total to total pressure change from 1 to 17 is
$$p_{t1} - p_{t17} = 871.8435\,\mathrm{N/m^2}$$

with corresponding steam density and speed at 17
$$\rho_{vw17} = 0.1301\,\mathrm{kg/m^3}$$
$$v_{vw17} = 78.5441\,\mathrm{m/s}$$

The static to static pressure and temperature change is
$$p_1 - p_{17} = 1105.0125\,\mathrm{N/m^2}$$
$$T_{v1} - T_{v17} = 1.2374\mathrm{K}$$

Shown in table B.1 is the inlet conditions to each of the dividing headers.

Table B.1: Inlet conditions to dividing headers

Section	Static pressure p, N/m^2	Temperature T_v, ℃	Density ρ_{vw}, kg/m^3	Speed v_{vw}, m/s
14	18918.2374	58.874	0.1307	78.1835
15	18829.5587	58.7733	0.1302	78.4838
16	18835.1089	58.7796	0.1302	78.4838
17	18820.1027	58.7626	0.1301	78.5441

It should be noted that the pressure differentials due to the frictional effects in the straight sections of the steam duct are much smaller than those for the miter bends and T-junctions in the steam duct.

Shown in figure B.1 below is the pressure change from 1 to 14 for different inlet steam temperatures. The pressure has been scaled with the inlet pressure to the steam duct. It can be seen that there is a much larger steam pressure drop for the 40°C and 50°C steam temperatures while for the higher steam temperatures the pressure variation is much smaller.

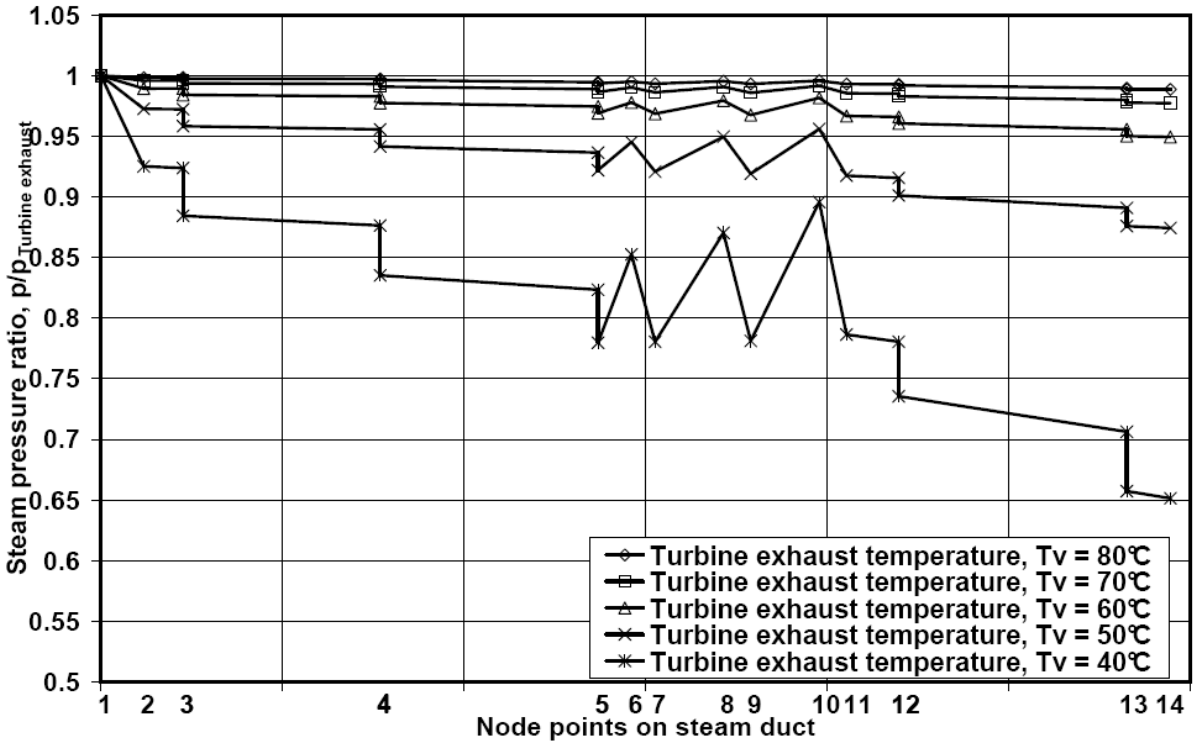

Figure B.1: Scaled pressure distribution in steam duct system

Shown in figure B.2 is the scaled temperature distribution for different turbine exhaust temperatures in degrees Celsius. The same trend is seen as in figure B.1.

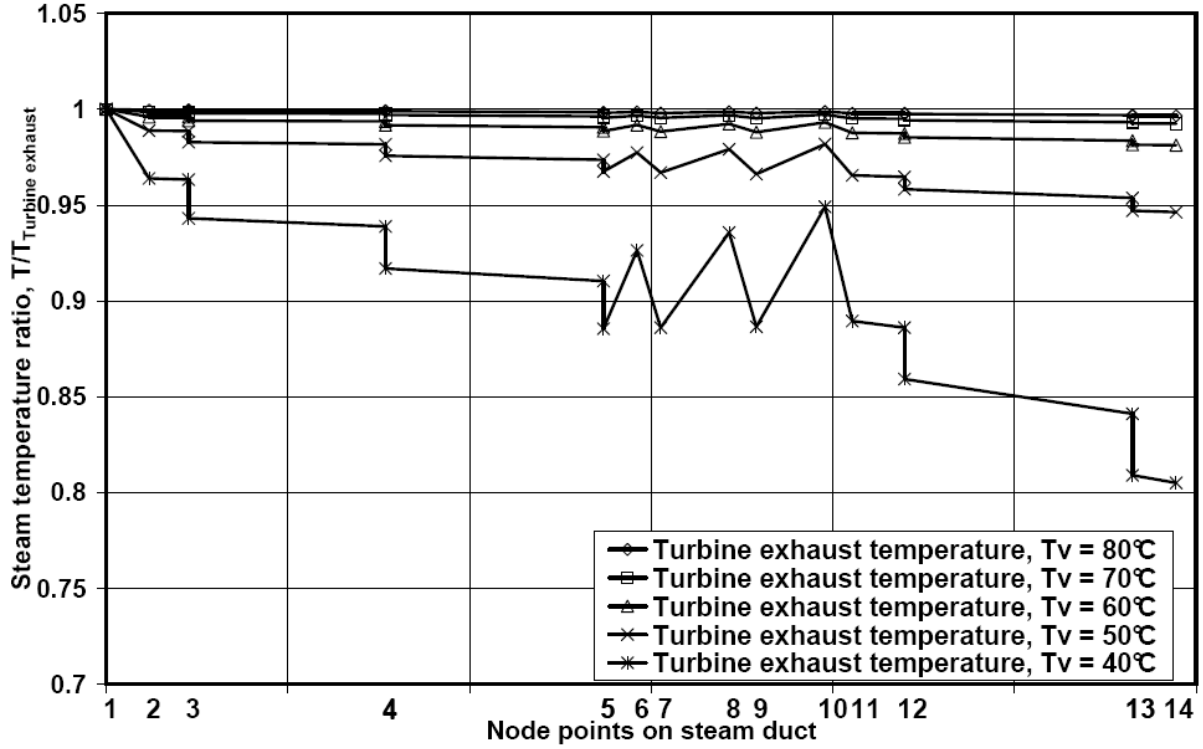

Figure B.2 Scaled steam temperature(ºC) change in steam duct system

The calculation above was repeated with constant properties, where the inlet properties were used throughout the duct, and again with the quality equal to the

inlet quality throughout the duct with variable properties. The resulting steam pressure and temperature changes are shown in figure B.3. It can be seen that the comparison is good with slight deviation at very low steam temperatures. It was decided that a constant quality would be assumed in the steam duct with variable properties to simplify calculations.

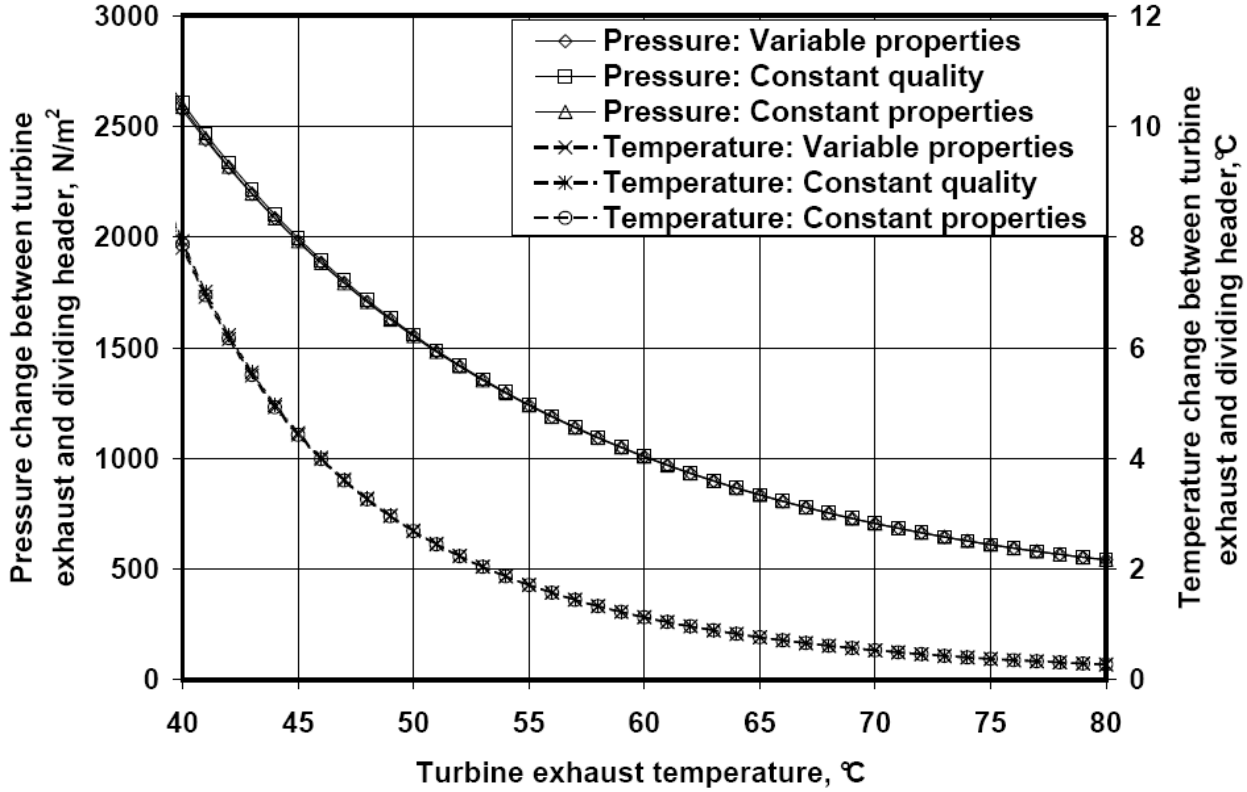

Figure B.3: Comparison of the pressure and temperature change between sections 1 and 14 for constant and variable properties in the steam duct

Appendix C: Sample calculation for pressure and temperature distribution in the dividing header

A schematic of the header configuration is shown in figure 2.10. It can be seen that between points 3 and 5 there is a reducer and a straight section of pipe. No steam exits the dividing header in these sections.

The dividing header is modelled as if there was only one finned tube row and for the purpose of this calculation all the tubes receive the same amount of steam. The amount of steam that leaves the header per fan unit can be calculated and that is used to determine the amount of steam present at any point in the header

Header specifications

Header diameters	$d_{1-3} = 2.496\text{m}$
	$d_{4-8} = 1.970\text{m}$
Header cross-sectional area	$A_{1-3} = 4.8930\text{m}^2$
	$A_{4-8} = 3.0481\text{m}^2$
Surface roughness	$\varepsilon = 1\times10^{-3}\text{m}$
Length of each condenser unit	$L = 11.8\text{m}$
Overall momentum correction factor (Bajura 1971)	$\alpha_d = 1$

Inlet conditions

Vapor quality	$x_1 = 1$
Vapour mass flow rate entering header:	$m_{v1} = 45.0289\,\text{kg/s}$
Vapour drawn off by first condenser fan unit	$\Delta m_{v1-2} = 8.5047\,\text{kg/s}$
Inlet temperature to header	$T_{v1} = 333.15\text{K}\ \ 60°\text{C}$

The inlet steam pressure is calculated with equation (A.2.2),

$$p_1 = 10^{z} \qquad \text{(A.2.2)}$$

where

$$z = 10.79586\ \left(1 - 273.16/T_v\right) + 5.02808\log_{10}\left(273.16/T_v\right)$$
$$+ 1.50474\times10^{-4}\left[1 - 10^{-8.29692\ \left(T_v/273.16 - 1\right)}\right]$$
$$+ 4.2873\times10^{-4}\left[10^{4.76955\ \left(1 - 273.16/T_v\right)} - 1\right] + 2.786118312$$
$$= 10.79586\ \left(1 - 273.16/333.15\right) + 5.02808\log_{10}\left(273.16/333.15\right)$$
$$+ 1.50474\times10^{-4}\left[1 - 10^{-8.29692\ \left\{\left(333.15/273.16\right) - 1\right\}}\right]$$
$$+ 4.2873\times10^{-4}\left[10^{4.76955\left(1 - 273.16/333.15\right)} - 1\right] + 2.786118312$$
$$= 4.2994$$

so

$$p_1 = 10^{4.2994} = 19925.1152\,\mathrm{N/m^2}$$

The vapor density is determined at the inlet to each section and it is assumed to be constant in each section.

According to equation (A.2.3) the density at 1 is

$$\begin{aligned}\rho_{v1} &= -4.062329056 + 0.10277044T_{v1} - 9.76300388\times10^{-4}T_{v1}^2 \\ &\quad + 4.475240795\times10^{-6}T_{v1}^3 - 1.004596894\times10^{-8}T_{v1}^4 + 8.89154895\times10^{-12}T_{v1}^5 \\ &= -4.062329056 + 0.10277044\ \ 333.15\ - 9.76300388\times10^{-4}\ \ 333.15\ ^2 \\ &\quad + 4.475240795\times10^{-6}\ \ 333.15\ ^3 - 1.004596894\times10^{-8}\ \ 333.15\ ^4 \\ &\quad + 8.89154895\times10^{-12}\ \ 333.15\ ^5 \\ &= 0.1302\,\mathrm{kg/m^3}\end{aligned} \qquad \text{(A.2.3)}$$

The viscosity is calculated with equation (A.2.4)

$$\begin{aligned}\mu_{v1} &= 2.562435\times10^{-6} + 1.816683\times10^{-8}T_{v1} + 2.579066\times10^{-11}T_{v1}^2 \\ &\quad - 1.067299\times10^{-14}T_{v1}^3 \\ &= 2.562435\times10^{-6} + 1.816683\times10^{-8}\ \ 333.15\ + 2.579066\times10^{-11}\ \ 333.15\ ^2 \\ &\quad - 1.067299\times10^{-14}\ \ 333.15\ ^3 \\ &= 1.1083\times10^{-5}\,\mathrm{kg/ms}\end{aligned} \qquad \text{(A.2.4)}$$

From equation (2.31) it can be seen that the momentum pressure change is given by

$$p_2 - p_1\ _m = -\frac{\rho_{v1}\alpha_d}{2}\ \ v_{v2}^2 - v_{v1}^2 \qquad \text{(C.1)}$$

The vapor speed at the inlet to the header at 1 is

$$v_{v1} = \frac{m_{v1}}{\rho_{v1}A_{1-3}} = \frac{45.0289}{0.1302\times4.8930} = 70.6814\,\mathrm{m/s} \qquad \text{(C.2)}$$

The steam speed at 2 is

$$v_{v2} = \frac{m_{v1} - \Delta m_{v1-2}}{\rho_{v1}A_{1-3}} = \frac{45.0289 - 8.5047}{0.1302\times4.8930} = 57.3317\,\mathrm{m/s}$$

The momentum pressure change can now be calculated with equation (C.1)

$$p_2 - p_1\ _m = -\frac{0.1302\times1}{2}\ \ 57.3317^2 - 70.6814^2\ \ = 111.2518\,\mathrm{N/m^2}$$

To calculate the frictional pressure change the average mass flux for the section is used. This is done to account for the outflow of steam in the section. Using equation (B.1) the mass flux is

$$G_{12} = \frac{m_1 - \Delta m_{v1-2}/2}{A_{1-3}} = \frac{45.0289 - 8.5047/2}{4.8930} = 8.3337\,\mathrm{kg/m^2 s} \qquad \text{(B.1)}$$

The Reynolds number is calculated with equation (2.10),

$$Re_{v1} = \frac{G_{12} d_{1-3}}{\mu_{m1}} = \frac{8.5717 \times 2.496}{1.1083 \times 10^{-5}} = 1.8768 \times 10^{6}$$

The corresponding friction factor is can be calculated using equation (2.9)

$$f_D = \frac{0.30864}{\left[\log\left\{\left(\frac{6.9}{Re}\right) + \left(\frac{\varepsilon/d_m}{3.7}\right)^{1.11}\right\}\right]^2} \qquad \text{(2.9)}$$

$$= \frac{0.30864}{\left[\log\left\{\left(\frac{6.9}{1.8768 \times 10^{6}}\right) + \left(\frac{1 \times 10^{-3}/2.496}{3.7}\right)^{1.11}\right\}\right]^2}$$

$$f_D = 0.0161$$

The friction pressure change is given by equation (2.7),

$$p_2 - p_{1\ f} = -\frac{1}{2}\frac{f_D L}{d_{1-3}}\frac{G_{12}^2}{\rho_{v1}} = \frac{1}{2}\frac{0.0161 \times 11.8}{2.496}\frac{8.3337^2}{0.1302} = -20.3001\,\mathrm{N/m^2} \qquad \text{(2.7)}$$

The pressure at section 2 can now be calculated

$$p_2 = p_1 + \left(p_2 - p_{1\ m}\right) + \left(p_2 - p_{1\ f}\right) = 19925.1152 + 111.2518 - 20.3001 = 20016.0669\,\mathrm{N/m^2}$$

The corresponding steam temperature can then be calculated with equation (A.2.1) to be

$$T_2 = 333.2388\mathrm{K} \text{ or } 60.0888°\mathrm{C}$$

This procedure is repeated for all the sections where outflow of steam occur. The pressure change in the reducer and straight section is calculated with equations (2.14), (2.7) and (2.6) respectively.

Shown in figure C.1 below is the pressure and temperature distributions for the sample calculation done above.

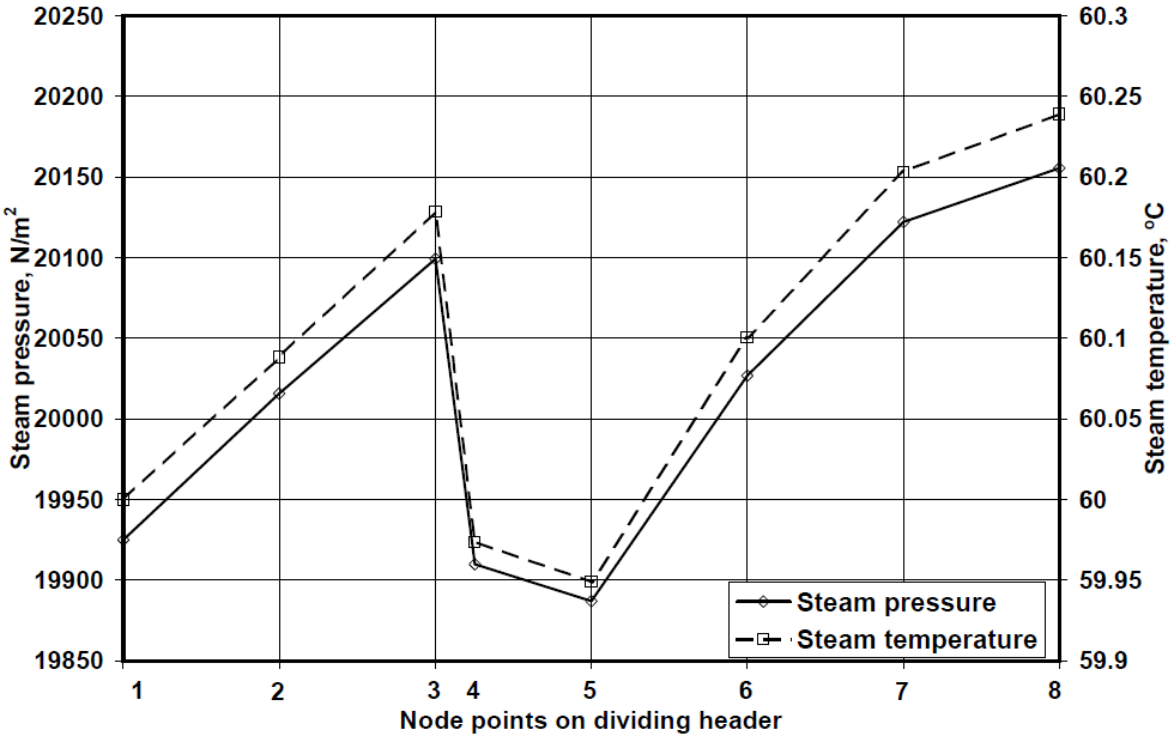

Figure C.1: Steam pressure and temperature distributions in the dividing header

Appendix D: Sample calculation for pressure change in condenser tube

A sample calculation for the pressure change from the dividing header to the combining header and the average pressure and temperature in the condensing tube is presented for a single-row condenser tube. The calculation is for the first tube in the dividing header with the condenser operating under ideal conditions with an ambient ground level temperature of 15.6°C.

Header conditions

Dividing header temperature	$T_{v1} = 60°C \ \ 333.15K$
Dividing header mass flow rate	$m_{hd} = 45.0289 kg/s$
Dividing header steam quality	$x_1 = 1$
Combining header mass flow rate	$m_{hc} = 0 kg/s$

Header specifications

Dividing header diameter	$d_{hd} = 2.496m$
Combining header diameter	$d_{hc} = 0.41m$
Momentum correction factors(Bajura, 1971)	$\alpha_d = 1$ $\alpha_c = 2.6$

Finned tube information

Mass flow rate into finned tube	$m_{vin} = \ 0.01806 kg/s$
Mass flow rate out of finned tube	$m_{vout} = 5.7514 \times 10^{-4} kg/s$
Half apex angle	$\theta = 30°$
Tube length	$L_T = 9.5m$
Cross-sectional area of tube	$A_{ts} = 0.0034m^2$
Hydraulic diameter of finned tube	$d_e = 0.0309m$
Inside width of tube	$W_T = 0.017m$
Inside height of tube	$H_T = 0.2m$
Header tube pitch	$P_t = 0.05m$

Pressure and temperature change calculation

The steam pressure in the header is calculated with equation (A.2.2)

$$
\begin{aligned}
z &= 10.79586\ (1-273.16/T_{v1}) + 5.02808\log_{10}(273.16/T_{v1}) \\
&\quad + 1.50474\times10^{-4}\left[1-10^{-8.29692\,(T_{v1}/273.16\,-1)}\right] \\
&\quad + 4.2873\times10^{-4}\left[10^{4.76955\,(1-273.16/T_{v1})}-1\right] + 2.786118312 \\
&= 10.79586\ (1-273.16/333.15) + 5.02808\log_{10}(273.16/333.15) \\
&\quad + 1.50474\times10^{-4}\left[1-10^{-8.29692\,(333.15/273.16\,-1)}\right] \\
&\quad + 4.2873\times10^{-4}\left[10^{4.76955\,(1-273.16/333.15)}-1\right] + 2.786118312 \\
&= 4.2994 \\
p_1 &= 10^{z} = 10^{4.2994} = 19925.1152\ \mathrm{N/m^2}
\end{aligned}
\qquad \text{(A.2.2)}
$$

The steam density in the header is according to equation (A.2.3)

$$
\begin{aligned}
\rho_{v1} &= -4.062329056 + 0.10277044T_{v1} - 9.76300388\times10^{-4}T_{v1}^2 \\
&\quad + 4.475240795\times10^{-6}T_{v1}^3 - 1.004596894\times10^{-8}T_{v1}^4 + 8.89154895\times10^{-12}T_{v1}^5 \\
&= -4.062329056 + 0.10277044\ (333.15) - 9.76300388\times10^{-4}\ (333.15)^2 \\
&\quad + 4.475240795\times10^{-6}\ (333.15)^3 - 1.004596894\times10^{-8}\ (333.15)^4 \\
&\quad + 8.89154895\times10^{-12}\ (333.15)^5 \\
&= 0.13023\ \mathrm{kg/m^3}
\end{aligned}
\qquad \text{(A.2.3)}
$$

The steam speed in the header is

$$v_{v1} = m_{hd}/(\rho_{v1}\times A_{hd}) = 45.0289/(0.13023\times\pi\times 2.496^2/4) = 70.6641\ \mathrm{m/s}$$

Assuming that the density changes are small the steam speed entering the tube is

$$v_{v2} = m_{vin}/(\rho_{v1}A_{ts}) = 0.01806/(0.13023\times0.0034) = 40.7875\ \mathrm{m/s}$$

In chapter 5 it is shown that the inlet loss coefficients of the finned tubes differ significantly from that of the corrected equation (2.49). The tube inlet pressure change will be larger when the values of chapter 5 are used and therefore the pressure change across the condenser tube will be larger too for the same inlet mass flow rate and condensation rate. The step configuration is for the first finned tube is used here and the 10 experimentally determined inlet loss coefficients is shown in figure D.1. Fitting a third order polynomial trendline through the inlet loss coefficients for the first tube the following equation is calculated,

$$K_i = -0.184\times\left(\frac{v_{hi}}{v_l}\right)^3 + 1.5429\times\left(\frac{v_{hi}}{v_l}\right)^2 - 2.5494\times\left(\frac{v_{hi}}{v_l}\right) + 1.2036 \qquad \text{(D.1)}$$

where

$$\frac{v_{hi}}{v_l} = \frac{v_{v1}}{v_{v2}} = \frac{70.6641}{40.7875} = 1.7325 \qquad \text{(D.2)}$$

so

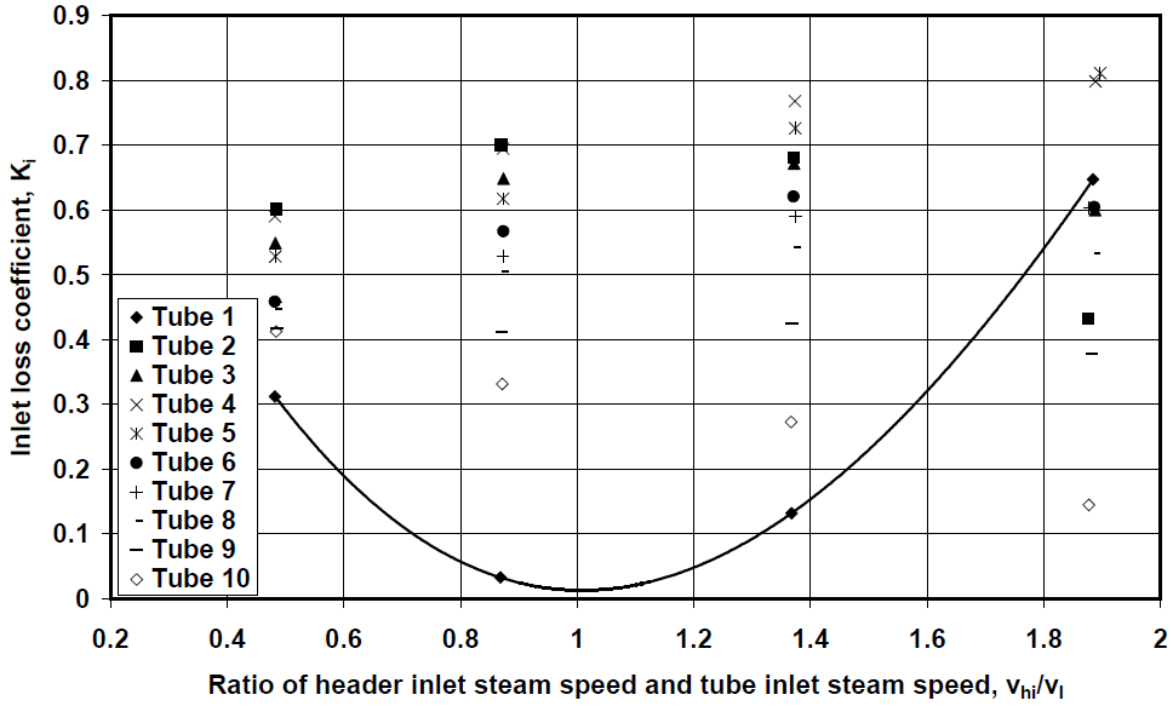

Figure D.1: Experimentally determined inlet loss coefficient for step at inlet to header (see figure 2.20)

$$K_i = -0.184 \times 1.7325^{3} + 1.5429 \times 1.7325^{2} - 2.5494 \times 1.7325 + 1.2036$$
$$= 0.461$$

The pressure change into the condenser tube is calculated with equation (2.48)

$$p_2 - p_1 = -\rho \frac{v_i^2}{2} K_i + 1 \qquad (2.48)$$

The steam pressure just inside the condenser tube is then

$$p_2 = p_1 - \rho \frac{v_i^2}{2} K_i + 1$$
$$= 19925.1152 - 0.13023 \times \frac{40.7875^2}{2} 0.461 + 1$$
$$= 19766.85\,\mathrm{N/m^2}$$

The steam temperature corresponding to p_{v2} is calculated with equation (A.2.1)

$$T_{v2} = 164.630366 + 1.832295\text{x}10^{-3} p_{v2} + 4.27215\text{x}10^{-10} p_{v2}^2 + 3.738954\text{x}10^{3} p_{v2}^{-1} \qquad (A.2.1)$$
$$- 7.01204\text{x}10^{5} p_{v2}^{-2} + 16.161488 \ln p_{v2} - 1.437169\text{x}10^{-4} p_{v2} \ln p_{v2}$$
$$= 164.630366 + 1.832295\text{x}10^{-3} \times 19751.3525 + 4.27215\text{x}10^{-10} \; 19766.85^{2}$$
$$+ 3.738954\text{x}10^{3} \; 19766.85^{-1} - 7.01204\text{x}10^{5} \; 19766.85^{-2} + 16.161488 \ln 19766.85$$
$$- 1.437169\text{x}10^{-4} \; 19766.85 \ln 19766.85$$
$$= 332.9681\,\mathrm{K} \; 59.8181\,^{\circ}\mathrm{C}$$

The steam properties just inside the tube are then according to equations (A.2.3) and (A.2.4)

Density $\rho_{v2} = 0.1292\,\mathrm{kg/m^3}$ (A.2.3)

Dynamic viscosity $\mu_{v2} = 1.1077\times10^{-5}\,\mathrm{kg/sm}$ (A.2.4)

The pressure change in the finned tube consists of three different changes namely the frictional pressure change, the static pressure change and the momentum pressure change.

The Reynolds number at the top of the condenser tube is calculated with equation (2.10)

$$\mathrm{Re}_{v2} = \frac{v_{v2}\rho_{v2}d_e}{\mu_{v2}} = \frac{40.7875\times0.1292\times0.0309}{1.1077\times10^{-5}} = 1.47\times10^{4} \qquad (2.10)$$

The finned tube outlet steam speed is

$$v_{v3} = m_{vout}/\ \rho_{v1}A_{ts}\ = 5.7514\times10^{-4}/\ 0.1292\times0.0034\ = 1.3092\,\mathrm{m/s}$$

and the outlet Reynolds number is then

$$\mathrm{Re}_{v3} = \frac{v_{v3}\rho_{v2}d_e}{\mu_{v2}} = \frac{1.3092\times0.1293\times0.0309}{1.1077\times10^{-5}} = 472.2162$$

The Reynolds number for the steam flow normal to the condensing surface is according to equation (2.62)

$$\mathrm{Re}_{vn} = \mathrm{Re}_{v2}\times\frac{W_T}{2\times L_T} - \mathrm{Re}_{v3}\times\frac{W_T}{2\times L_T} \qquad (2.62)$$

$$= 1.47\times10^{4}\times\frac{0.017}{2\times9.5} - 472.2162\times\frac{0.017}{2\times9.5}$$

$$= 12.73$$

and according to equations (2.55) and (2.56)

$$a_1 = 1.0649 + 1.0411\times10^{-3}\,\mathrm{Re}_{vn} - 2.011\times10^{-7}\,\mathrm{Re}_{vn}^3 \qquad (2.55)$$

$$= 1.0649 + 1.0411\times10^{-3}\times12.73 - 2.011\times10^{-7}\times12.73^3$$

$$= 1.0777$$

$$a_2 = 290.1479 + 59.3153\,\mathrm{Re}_{vn} + 1.5995\times10^{-2}\,\mathrm{Re}_{vn}^3 \qquad (2.56)$$

$$= 290.1479 + 59.3153\times12.73 + 1.5995\times10^{-2}\times12.73^3$$

$$= 1078.2283$$

The frictional pressure change can then be calculated with equation (2.65)

$$p_3 - p_{2\ f} = -\frac{0.1582\mu_{v2}^2 L_t}{\rho_{v2}d_e^3\ \mathrm{Re}_{v3} - \mathrm{Re}_{v2}}\left[\frac{a_1}{2.75}\ \mathrm{Re}_{v3}^{2.75} - \mathrm{Re}_{v2}^{2.75}\ + \frac{a_2}{1.75}\ \mathrm{Re}_{v3}^{1.75} - \mathrm{Re}_{v2}^{1.75}\ \right] \qquad (2.65)$$

$$= -\frac{0.1582 \times \left(1.1077 \times 10^{-5}\right)^2 \times 9.5}{0.1292 \times 0.0309^3 \left(472.2162 - 1.47 \times 10^4\right)}$$

$$\times \left[\begin{array}{l} \frac{1.0777}{2.75} \left(472.2162\right)^{2.75} - \left(1.47 \times 10^4\right)^{2.75} \\ + \frac{1078.2283}{1.75} \left(472.2162\right)^{1.75} - \left(1.47 \times 10^4\right)^{1.75} \end{array} \right]$$

$$= -425.3857 \, \mathrm{N/m^2}$$

The static pressure change is according to equation (2.66)

$$p_3 - p_{2\,s} = \rho_{v2} g L_t \sin\theta = 0.1291 \times 9.8 \times 9.5 \times \sin 30 = 6.0143 \, \mathrm{N/m^2} \quad (2.66)$$

while the momentum pressure change is according to equation (2.67)

$$p_3 - p_{2\,m} = -\rho_{v2} \left(v_{v3}^2 - v_{v2}^2\right) = -0.1292 \times \left(4.7427^2 - 44.0397^2\right) = -214.7183 \, \mathrm{N/m^2} \quad (2.67)$$

The pressure at the section 3 of the condenser tube is then according to equation (2.3)

$$\begin{aligned} p_3 &= p_2 + \left(p_3 - p_{2\,f}\right) + \left(p_3 - p_{2\,s}\right) + \left(p_3 - p_{2\,m}\right) \\ &= 19766.85 - 425.3857 + 6.0143 + 214.7183 \\ &= 19562.1929 \, \mathrm{N/m^2} \end{aligned} \quad (2.3)$$

with corresponding steam temperature according to equation (A.2.1)

$$T_{v3} = 332.7436\mathrm{K} \quad 59.5936°\mathrm{C} \quad (A.2.1)$$

The density at the outlet of the finned tube is

$$\rho_{v3} = 0.1279 \, \mathrm{kg/m^3} \quad (A.2.3)$$

The outlet pressure change is calculated using equation (2.68)

$$p_4 - p_3 = -\frac{\rho_{v3} v_{v3}^2}{2} \left[K_e - 1 + \alpha_c \frac{v_{v4}^2}{v_{v3}^2} \right] \quad (2.68)$$

where

$$K_e = \left(1 - \sigma_{34}\right)^2 \quad (2.69)$$

With $\sigma_{34} = \sigma_{21}$ and $v_{v4} = 0$ the header pressure can be calculated using equation (2.68)

$$\begin{aligned} p_4 &= p_3 - \frac{\rho_{v3} v_{v3}^2}{2} \left[\left(1 - \sigma_{34}\right)^2 - 1 \right] \\ &= 19562.1929 - \frac{0.1279 \times 1.3092^2}{2} \left[\left(1 - 0.34\right)^2 - 1 \right] \\ &= 19562.2548 \, \mathrm{N/m^2} \end{aligned}$$

The corresponding steam temperature in the combining header is

$$T_{v4} = 332.7437\text{K} \;\; 59.5937°\text{C} \qquad \text{(A.2.1)}$$

The pressure change between the headers is

$$p_1 - p_4 = 19925.1152 - 19562.2548 = 362.8604\,\text{N/m}^2$$

and the temperature change is

$$T_{v1} - T_{v4} = 60 - 59.5937 = 0.4063°\text{C}$$

The pressure change inside the condenser tube is

$$p_2 - p_3 = 19766.85 - 19562.1929 = 204.6571\,\text{N/m}^2$$

and the temperature change is

$$T_{v2} - T_{v3} = 59.8181 - 59.5936 = 0.2245°\text{C}$$

The average pressure in the condenser tube is according to equation (2.79)

$$p_{vm} = p_{v2} - \frac{0.1582\mu_{v2}^2 L}{\rho_{v2} d_e^3 \;\; Re_{v3} - Re_{v2}} \left[\begin{array}{l} \dfrac{a_1 \;\; Re_{v3}^{3.75} - Re_{v2}^{3.75}}{10.3125 \;\; Re_{v3} - Re_{v2}} - \dfrac{a_1 Re_{v2}^{2.75}}{2.75} \\ + \dfrac{a_2 \;\; Re_{v3}^{2.75} - Re_{v2}^{2.75}}{4.8125 \;\; Re_{v3} - Re_{v2}} - \dfrac{a_2 Re_{v2}^{1.75}}{1.75} \end{array} \right] \qquad \text{(2.79)}$$

$$- \frac{\rho_{v2}}{3}\left[v_{v3}^2 + v_{v3} v_{v2} - 2v_{v2}^2 \right] + \frac{\rho_{v2} g L \sin\phi}{2}$$

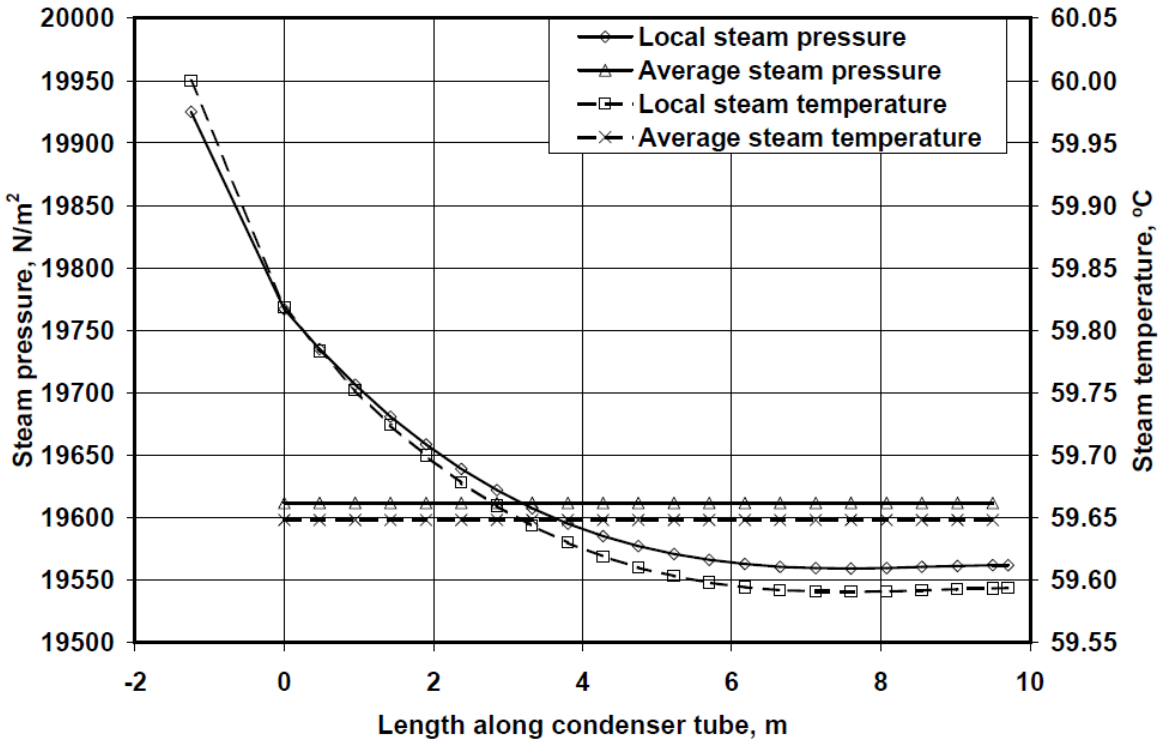

Figure D.2: Local and average steam pressure and temperature values for the first condenser tube row

$$= 19751.3525 - \frac{0.1582 \times \ 1.1077 \times 10^{-5}\ ^{2} \times 9.5}{0.1292 \times \ 0.0309\ ^{3}\ \ 472.2162 - 1.47 \times 10^{4}}$$

$$\left[\frac{1.0777 \times \ \ 472.2162\ ^{3.75} - \ 1.47 \times 10^{4}\ ^{3.75}}{10.3125\ \ 472.2162 - 1.47 \times 10^{4}} \right.$$

$$- \frac{1.0777 \times \ 1.47 \times 10^{4}\ ^{2.75}}{2.75}$$

$$+ \frac{1078.2283 \times \ \ 472.2162\ ^{2.75} - \ 1.47 \times 10^{4}\ ^{2.75}}{4.8125\left(472.2162 - 1.47 \times 10^{4}\right)}$$

$$\left. - \frac{1078.2283 \times \left(1.47 \times 10^{4}\right)^{1.75}}{1.75} \right]$$

$$- \frac{0.1292}{3}\left[1.3092^{2} + 1.3092 \times 40.7875 - 2 \times 40.7875^{2}\right]$$

$$+ \frac{0.1292 \times 9.8 \times 9.5 \sin\left(30\right)}{2}$$

$$= 19606.6152\ \mathrm{N/m^{2}}$$

and the average temperature corresponding to this pressure according to equation (A.2.1) is

$$T_{vm} = 332.7925\mathrm{K}\ \ 59.6425°\mathrm{C} \qquad \text{(A.2.1)}$$

Shown in figure D.2 is the local pressure and temperature in the condenser tube from the dividing to the combining header and the average pressure and temperature in the condenser tube.

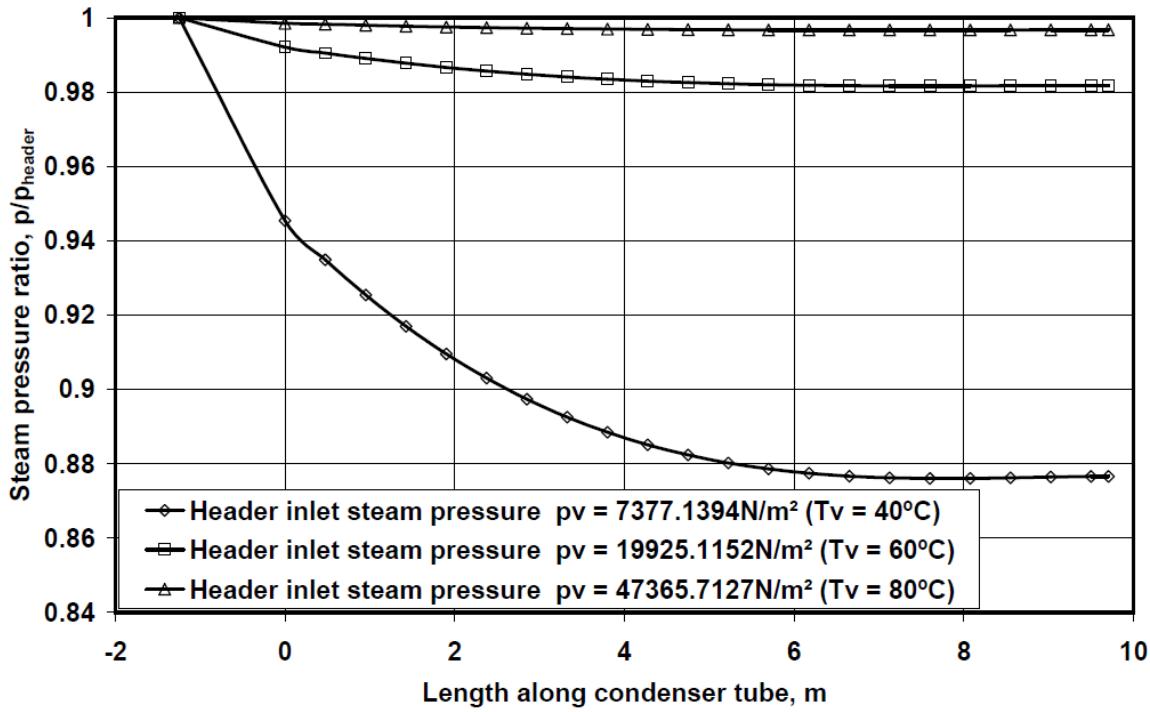

Figure D.3: Scaled pressure distribution for different header steam temperatures

In figures D.3 and D.4 the scaled pressure and temperature distribution for inlet temperatures of 40°C, 60°C and 80°C is shown. It can be seen that the the lower the steam temperature drops the bigger the changes in the pressure and temperature.

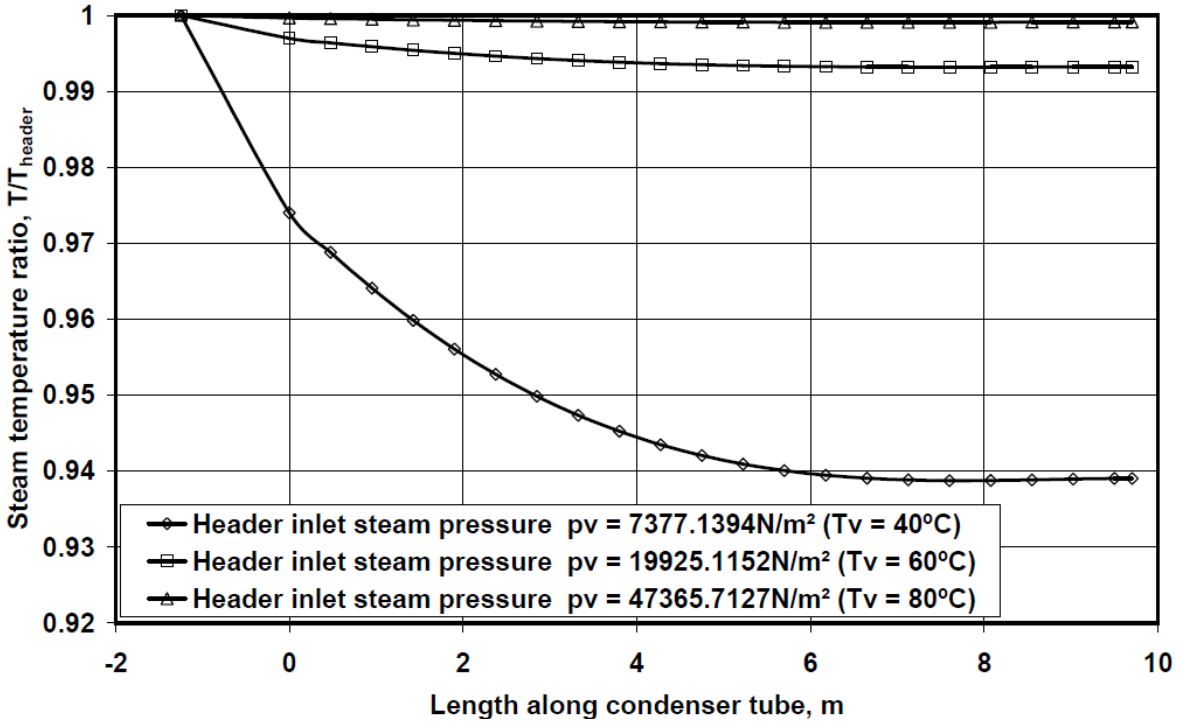

Figure D.4: Scaled temperature distribution(°C) for different header steam temperatures

Appendix E: Sample calculation for ideal air-cooled heat exchanger fan unit

This is a sample calculation to show the method that is used to obtain the performance of an air-cooled condenser. It solves for the amount of heat rejected for both tube rows for a K-type condenser.

Ambient conditions:

Air temperature at ground level	$T_{a1} = 15.6°C(288.75K)$
Wetbulb temperature at ground level	$T_{wb} = 0°C$ (dry air)
Atmospheric pressure at ground level	$p_{a1} = 84600\ N/m2$

Ambient temperature gradient, -0.00975 K/m from ground level

Steam conditions:

Saturated steam supply temperature	$T_v = 60°C$
Steam quality at condenser bundle inlet	$x = 1$
Diameter of steam header	$d_s = 1.25\ m$
Total mean steam ducting loss coefficient based on the steam velocity at the inlet to first tube row	$K_{sd} = 2.5$

Finned tube bundle specifications:

The condenser is made up of two rows of condenser tubes. The characteristics of the two rows are so that approximately the same amount of condensate forms in each row so that there is no build up of noncondensables in the condenser.

Hydraulic diameter of tube	$d_e = 0.02975\ m$
Inside area of tube per unit length	$A_{ti} = 0.21341\ m$
Inside cross-sectional tube flow area	$A_{ts} = 0.00159\ m$
Length of finned tube	$L_t = 9.5\ m$
Inside height of tube	$H_t = 0.097\ m$
Inside width of tube	$W_t = 0.017\ m$
Number of tube rows	$n_r = 2$
Number of tubes per bundle (first row)	$n_{tb(1)} = 57$
Number of tubes per bundle (second row)	$n_{tb(2)} = 58$
Number of steam passes	$n_{vp} = 1$
Number of bundles	$n_b = 8$
Effective frontal area of one bundle (second row)	$A_{fr} = 27.55\ m^2$
Apex angle of A-frame	$2\theta = 60°$
Ratio of minimum to free stream flow area through finned tube bundle	$\sigma = 0.48$
Ratio of minimum to free stream flow area	

at inlet to finned tube bundle	$\sigma_{21} = 0.875$
Steam-side tube inlet loss coefficient	$K_c = 0.6$

The experimentally determined characteristic heat transfer parameter for normal flow through the rows of tubes are given by the following empirical relations(Kröger 2004):

The first row,

$$Ny_{(1)} = 366.007945Ry^{0.433256} \quad \text{(E.1)}$$

and for the second row,

$$Ny_{(1)} = 360.588007Ry^{0.470373} \quad \text{(E.2)}$$

The loss coefficient across both rows is also reported by Kröger (2004) to be:

$$K_{he} = 4177.08481Ry^{-0.4392686} \quad \text{(E.3)}$$

Fan installation specifications:

Fan diameter	$d_F = 9.145$ m
Fan casing diameter	$d_c = 9.17$ m
Fan hub diameter	$d_h = 1.4$ m
Rotational speed	$N = 125$ rpm
Efficiency of fan drive system	$\eta_{Fd} = 0.9$
Inlet screen distance from fan blade (upstream)	$x_{si} = 1.3$ m
Support beam distance from fan blade (upstream)	$x_{bi} = 1.34$ m
Support beam distance from blade (downstream)	$x_{bo} = 0.53$ m
Walkway distance from fan blade (downstream)	$x_{so} = 1.0$ m
Ratio of inlet screen area to fan casing are	$\sigma_{si} = 0.125$
Ratio of support beam area to fan casing area (upstream)	$\sigma_{bi} = 0.15$
Ratio of support beam area to fan casing area (downstream)	$\sigma_{bo} = 0.05$
Ratio of walkway area to fan casing area	$\sigma_{so} = 0.1$
Height of fan above ground level	$H_3 = 25$ m
Width of walkway between heat exchanger bundle and windwall	$L_w = 0.2$ m
Heat exchanger inlet support loss coefficient (based on frontal area of heat exchanger)	$K_{ts} = 1.5$

For more information to how the ratios above is calculated refer to Kröger(2004).

The following correlations are given by Kröger(2004) for the fan static pressure rise and fan power at a reference density of 1.2 kg/m^3:

Fan static pressure:

$$\Delta p_{Fs} = 320.0451719 - 0.2975215484V + 6.351486\times10^{-4}V^2 - 8.14\times10^{-7}V^3,\ \mathrm{N/m^2} \quad \text{(E.4)}$$

Fan power

$$P_F = 186645.2333 - 59.413863388V + 0.476168398V^2 - 5.08308\times10^{-4}V^3,\ \mathrm{W} \quad \text{(E.5)}$$

The performance of the system was determined by an iterative procedure. The energy and draft equations were seen to be satisfied at an air mass flow of $m_a = 604.46\ \mathrm{kg/s}$. For this mass flow rate the inlet air temperature to the first row is found to be $T_{ai(1)} = 15.614°C\ \ 288.7640K$. The mean outlet air temperature after the first row is $T_{ao(1)} = 33.3248°C\ \ 306.4748K$ which is also the inlet temperature to the second row. The outlet temperature of the second row is $T_{ao(2)} = 47.8586°C\ \ 321.0086K$. The inlet steam velocities of the two rows is $v_{vi(1)} = 49.4168\,\mathrm{m/s}$, $\rho_{vi(1)} = 0.1275\,\mathrm{kg/m^3}$, and $v_{vi(2)} = 39.8824\ \mathrm{m/s}$ respectively.

Solution:

The density immediately upstream of the heat exchanger bundle is calculated by using equation (A.1.1),

$$\rho_{a5} \approx \frac{p_{a1}}{RT_{ai(1)}} = \frac{84600}{287.08\times288.7640} = 1.0205\ \mathrm{kg/m^3} \quad \text{(A.1.1)}$$

Neglecting the pressure changes through the bundle, the outlet air density is

$$\rho_{a5} \approx \frac{p_{a1}}{RT_{ai(1)}} = \frac{84600}{287.08\times321.0086} = 0.9180\ \mathrm{kg/m^3} \quad \text{(A.1.1)}$$

The mean air temperature through the first row of finned tubes is

$$T_{a(1)} = \frac{15.614 + 33.3248}{2} = 24.4694°C\ \ 297.6194K$$

The air properties are obtained by the correlations given in appendix A

Density	$\rho_{a(1)} = 0.9902\,\mathrm{kg/m^3}$	(A.1.1)
Specific heat	$c_{pa(1)} = 1006.8702\,\mathrm{J/kgK}$	(A.1.3)
Dynamic viscosity	$\mu_{a(1)} = 1.8359\times10^{-5}\,\mathrm{kg/ms}$	(A.1.2)
Thermal conductivity	$k_{a(1)} = 0.0260\,\mathrm{W/mK}$	(A.1.4)
Prandtl number	$Pr_{a(1)} = 0.7100$	

The mean temperature through the second row of finned tubes is

$$T_{a(2)} = \frac{33.3248 \ + \ 47.8586}{2} = 40.5917°C \ \ 313.7417K$$

The air properties for the second row are:

Density	$\rho_{a(2)} = 0.9393 kg/m^3$	(A.1.1)
Specific heat	$c_{pa(2)} = 1007.5319 J/kgK$	(A.1.3)
Dynamic viscosity	$\mu_{a(2)} = 1.9097 \times 10^{-5} kg/ms$	(A.1.2)
Thermal conductivity	$k_{a(2)} = 0.0273 W/mK$	(A.1.4)
Prandtl number	$Pr_{a(2)} = 0.7053$	

The rate of heat transfer from the first row of finned tubes is according to equation (2.29)

$$\begin{aligned} Q_{a(1)} &= m_a c_{pa(1)} \ \ T_{ao(1)} - T_{ai(1)} \\ &= 604.46 \times 1006.8702 \times \ 33.3248 - 15.6140 \ \ = 10.7790 \ MW \end{aligned} \qquad (2.29)$$

Similarly for the second row:

$$\begin{aligned} Q_{a(2)} &= m_a c_{pa(2)} \ \ T_{ao(2)} - T_{ai(2)} \\ &= 604.46 \times 1007.5319 \times \ 47.8586 - 33.3248 \ \ = 8.8513 \ MW \end{aligned} \qquad (2.29)$$

The total heat transfer rate is then:

$$Q_a = Q_{a(1)} + Q_{a(2)} = 19.6303 MW$$

The air-side characteristic flow parameter for the first row is given by equation (2.36). Assuming that there is no by-pass air and taking into consideration the reduced frontal area due to the smaller amount of tubes,

$$Ry_{(1)} = \frac{m_a}{\mu_{a(1)} A_{fr} \, n_{tb(1)} / n_{tb(2)}} = \frac{604.46}{1.8359 \times 10^{-5} 27.55 \times 57/58} = 152005.8521 m^{-1} \qquad (2.36)$$

The characteristic heat transfer parameter is according to eqaution (E.1),

$$\begin{aligned} Ny_{(1)} &= 366.007945 Ry^{0.433256} \\ &= 366.007945 (152005.8521)^{0.433256} \\ &= 64352.0791 m^{-1} \end{aligned} \qquad (E.1)$$

The effective heat transfer coefficient is then calculated using equation (2.34)

$$\begin{aligned} h_{ae(1)} A_{a(1)} &= k_{a(1)} \, Pr_{a(1)}^{0.333} \, n_b A_{fr} Ny_{(1)} \, n_{tb(1)} / n_{tb(2)} \\ &= 0.0260 \times \ 0.71 \ ^{0.333} \times 8 \times 27.55 \times 64352.0791 \times 57/58 \\ &= 323795.1495 W/K \end{aligned} \qquad (2.34)$$

There will be a pressure loss from where the steam enters the steam duct to the entrance to the condenser tubes. This loss is given by

$$\Delta p_{sd} = \frac{K_{sd}\rho_{vi(1)}v_{vi(1)}^2}{2} = \frac{2.5\rho_{vi(1)}v_{vi(1)}^2}{2} \qquad \text{(E.1)}$$

As the steam enters the finned tube it experiences a contraction loss. Equation (2.47) is not used so that the values calculated can be compared with that of Kröger (2004) so that the model could be validated.

$$\Delta p_i = (1-\sigma_s^2 + K_c)\frac{\rho_{vi(1)}v_{vi(1)}^2}{2} \qquad \text{(E.2)}$$

where σ_s is the area contraction ratio for the flattened tube

$$\sigma_s = \frac{W_t}{P_t} = \frac{W_t L_t n_{tb(2)}}{A_{fr}} = 0.34 \qquad \text{(E.3)}$$

The inlet pressure drop is then calculated using equation (E.2) and (E.3) and found to be

$$\Delta p_i = \left(1-\left(0.017\times 9.5\times\frac{58}{27.55}\right)^2 + 0.6\right)\frac{\rho_{vi(1)}v_{vi(1)}^2 2}{2} = 1.4844\frac{\rho_{vi(1)}v_{vi(1)}^2}{2}$$

The pressure drop from the inlet to the steam duct to just inside the condenser tube is then given by adding equations (E.1) and (E.2) to find

$$\Delta p_{sd} + \Delta p_i = 2.5 + 1.4844 \times \frac{0.1275\times 49.4168^2}{2} = 620.0579 \ \mathrm{N/m^2}$$

The mean saturation pressure at the inlet to the condenser tubes will therefore be the inlet pressure minus the pressure drop between the steam duct and the inlet of the tube. This gives $19925.113 - 620.0579 = 19305.0551 \mathrm{N/m^2}$. The saturation temperature for this pressure is then calculated by using the following correlation,

$$T_{vi} = \frac{5149.6889682}{\ln 1.020472843\mathrm{x}1011/p_v} - 273.15 \qquad \text{(E.4)}$$

$$= \frac{5149.6889682}{\ln 1.020472843\mathrm{x}1011/19305.0551} - 273.15 = 59.5048°\mathrm{C}$$

The steam temperature in the second row of tubes will equal to that in the first row if the condensation rates are similar.

The properties of saturated steam at this temperature are calculated using the correlations given in appendix A,

Density	$\rho_{vi} = 0.1275 \mathrm{kg/m^3}$	(A.2.3)
Specific heat	$c_{pvi} = 1926.0643 \mathrm{J/kgK}$	(A.2.5)
Dynamic viscosity	$\mu_{vi} = 1.1067\times 10^{-5} \mathrm{kg/ms}$	(A.2.4)

Thermal conductivity $k_{vi} = 0.0210\,W/mK$ (A.2.6)

Due to condensation the pressure in the tube will not stay constant and therefore the process will not take place at a constant temperature. A mean pressure can however be used to simplify the analysis. It is assumed that the density in the tube does not change significantly and that no steam exits at the bottom of the finned tubes. Under these conditions equation (2.79) reduces to

$$p_{vm(1)} = p_{vi} - \frac{0.1582\mu_{vi}^2 L_t}{\rho_{vi(1)} d_e^3 Re_{vi(1)}}\left[0.267 a_1 Re_{vi(1)}^{2.75} + 0.364 a_2 Re_{vi(1)}^{1.75}\right] + \frac{2\rho_{vi(1)} v_{vi(1)}^2}{3} + \frac{\rho_{vi(1)} g L_t \cos\theta}{2} \quad \text{(E.5)}$$

where according to equation (2.60)

$$Re_{vi(1)} = \frac{\rho_{vi(1)} v_{vi(1)} d_e}{\mu_{vi}} = \frac{0.1275 \times 49.4168 \times 0.02975}{1.1067 \times 10^{-5}} = 16931.2706$$

and equations (2.65), (2.58),(2.59)

$$Re_{vn(1)} = \frac{Re_{vi(1)} W_t}{2L_t} = \frac{16931.2706 \times 0.017}{2 \times 9.5} = 15.1490 \quad \text{(2.62)}$$

$$\begin{aligned} a_{1(1)} &= 1.0649 + 1.041 \times 10^{-3} Re_{vn(1)} - 2.011 \times 10^{-7} Re_{vn(1)}^3 \\ &= 1.0649 + 1.041 \times 10^{-3} \times 15.1490 - 2.011 \times 10^{-7} \times (15.1490)^3 \quad \text{(2.55)} \\ &= 1.0800 \end{aligned}$$

$$\begin{aligned} a_{2(1)} &= 290.1479 + 59.3153 Re_{vn(1)} + 1.5995 \times 10^{-2} Re_{vn(1)}^3 \\ &= 290.1479 + 59.3153 \times 15.1490 + 1.5995 \times 10^{-2} \times (15.1490)^3 \quad \text{(2.56)} \\ &= 1244.3254 \end{aligned}$$

Substituting all required values back into equation (E.5) to find the mean pressure in the tube

$$\begin{aligned} p_{vm(1)} &= 19305.0551 - \frac{0.1582 \times (1.1067 \times 10^{-5})^2 \times 9.5}{0.1275 \times 0.02975^3 \times 16931.2706} \times \\ &\left[\begin{array}{l} 0.267 \times 1.0800 \times \ 16931.2706\ ^{2.75} + \\ 0.364 \times 1244.3254 \times \ 16931.2706\ ^{1.75} \end{array}\right] \\ &+ \frac{2 \times 0.1275 \times 49.4168^2}{3} + \frac{0.1275 \times 9.8 \times 9.5 \times \cos(30)}{2} \\ &= 19083.3570\,N/m2 \end{aligned}$$

The corresponding steam temperature is then

$$T_{vi} = \frac{5149.6889682}{\ln\ 1.020472843x1011/19083.3570} - 273.15 = 59.2568°C \qquad \text{(E.4)}$$

The thermal properties of condensate at $T_{vm(1)}$ was evaluated using appendix A.4 of Kröger(2004).

Density	$\rho_{c(1)} = 983.6061 kg/m^3$	(A.3.1)
Specific heat	$c_{pc(1)} = 4183.6192 J/kgK$	(A.3.2)
Dynamic viscosity	$\mu_{c(1)} = 4.6837 \times 10^{-4}\ kg/ms$	(A.3.3)
Thermal conductivity	$k_{c(1)} = 0.6525 W/mK$	(A.3.4)
Latent heat of vaporization	$i_{fg(1)} = 2360.4362 \times 10^3 J/kg$	(A.3.6)

The condensate flow rate in the first row of tubes can be calculated using equation (2.31) to find

$$m_{c(1)} = \frac{Q_{a(1)}}{i_{fg(1)}} = \frac{10.7790 \times 10^6}{2360.4362 \times 10^3} = 4.5665 kg/s \qquad \text{(2.29)}$$

The condensation heat transfer coefficient is calculated using equation (2.37)

$$h_{c(1)} = 0.9245 \left[\frac{L_t k_{c(1)}^3 \rho_{c(1)}^2 g \cos\ \phi\ i_{fg(1)}}{\mu_{c(1)} m_{al(1)} c_{pa(1)}\ \ T_{vm(1)} - T_{ai(1)} \left[1 - \exp\ -\ U_{c(1)} H_t L_t\ /\ m_{al(1)} c_{pa(1)} \right]} \right]^{0.333} \qquad \text{(2.37)}$$

The inside tube area for the first row of tubes is calculated using equation (2.40),

$$A_{c(1)} = n_{tb(1)} n_b A_{ti} L_t = 57 \times 8 \times 0.21341 \times 9.5 = 924.4921 m^2 \qquad \text{(2.40)}$$

The overall heat transfer coefficient for the condensation if the film resistance is neglected and the effective height over which condensation takes place is equal to H_t, then according to equation (2.39)

$$U_{c(1)} H_t L_t = \frac{h_{ae(1)} A_{a(1)}}{2 n_{tb(1)} n_b} = \frac{323795.1495}{2 \times 57 \times 8} = 355.0385 W/K \qquad \text{(2.39)}$$

The air mass flow rate of the air on one side of the finned tube is calculated using equation (2.38).

$$m_{a1(1)} = \frac{m_a}{2 n_{tb(1)} n_b} = \frac{604.46}{2 \times 57 \times 8} = 0.6628 kg/s \qquad \text{(2.38)}$$

Substitute these values back into equation (2.37) to find

$$h_{c(1)} = 0.9245\left[\frac{9.5\times 0.6525^3\times 983.6061^2\times 9.8\times\cos(90-30)\times 2360.4362\times 10^3}{4.6837\times 10^{-4}\times 0.6628\times 1006.8702\ \ 59.2568-15.6140\ \times \left[1-\exp\ -355.0385/\ 0.6628\times 1006.8702\ \right]}\right]^{0.333}$$

$$= 15907.8010\,\mathrm{W/m^2K}$$

The overall heat transfer coefficient for the first row is then calculated using equation (2.32)

$$UA_{(1)} = \left[\frac{1}{h_{ae}A_{a\ (1)}} + \frac{1}{h_cA_{c\ (1)}}\right]^{-1} \qquad (2.32)$$

$$= \left[\frac{1}{323795.1495} + \frac{1}{15907.8010*924.4921}\right]^{-1} = 316819.7479\,\mathrm{W/K}$$

The effectiveness for the first row of the condenser tubes is calculated using equation (2.31)

$$e_{(1)} = 1-\exp\left[-\frac{UA_{(1)}}{m_ac_{pa(1)}}\right] \qquad (2.31)$$

$$= 1-\exp\left[-\frac{316819.7479}{604.46\times 1006.8702}\right] = 0.4058$$

From equation (2.34) it follows that the heat transfer rate from the first row is

$$Q_{a(1)} = m_ac_{pa(1)}\ \ T_{vm(1)}-T_{ai(1)}\ \ e_{(1)} \qquad (2.30)$$

$$= 604.46\times 1006.8702\times(59.2568-15.6140)\times 0.4058 = 10.779\mathrm{MW}$$

This value compares well with the previous value of $10.779\ \mathrm{MW}$

The same procedure is now used to determine the heat transfer rate of the second row of condenser tubes.

The inlet steam velocity of the second row is $v_{vi(2)} = 39.8824\,\mathrm{m/s}$ and the steam properties are approximately the same as for the first row of tubes. So

$$Ry_{(2)} = \frac{604.46}{1.9097\times 10^{-5}\times 8\times 27.55} = 143616.8882\mathrm{m^{-1}}$$

$$Ny_{(2)} = 360.588007\times 143616.8882^{0.470373} = 96121.712\mathrm{m^{-1}}$$

$$h_{ae(2)}A_{a(2)} = 0.0273\times 0.7053^{0.333}\times 8\times 27.55\times 96121.712 = 514479.5906\ \ \mathrm{W/K}$$

$$Re_{vi(2)} = \frac{0.1275\times 39.8824\times 0.02975}{1.1067\times 10^{-5}} = 13664.5710$$

$$Re_{vn(2)} = \frac{13664.5710 \times 0.017}{2 \times 9.5} = 12.2262$$

$$a_{1(2)} = 1.0773$$

$$a_{2(2)} = 1044.5803$$

With these values the mean steam pressure in the second row can be determined in the same way as for the first tube row

$$p_{vm(2)} = 19305.0551 - \frac{0.1582 \times (1.1067 \times 10^{-5})^2 \times 9.5}{0.1275 \times 0.02975^3 \times 13664.5710} \times \left[\begin{array}{l} 0.267 \times 1.0773 \times \ 13664.5710 \ ^{2.75} + \\ 0.364 \times 1044.5803 \times \ 13664.5710 \ ^{1.75} \end{array} \right] + \frac{2 \times 0.1275 \times 39.8824^2}{3} + \frac{0.1275 \times 9.8 \times 9.5 \times \cos(30)}{2} = 19083.3570 \, N/m2$$

The corresponding steam temperature is then

$$T_{vi} = \frac{5149.6889682}{\ln \ 1.020472843x1011/19146.5387} - 273.15 = 59.3277°C$$

The thermophysical properties of the steam condensate at $T_{vm(2)}$ are:

Density	$\rho_{c(2)} = 983.5691 kg/m^3$
Specific heat	$c_{pc(2)} = 4183.6634 J/kgK$
Dynamic viscosity	$\mu_{c(2)} = 4.6791 \times 10^{-4} kg/ms$
Thermal conductivity	$k_{c(2)} = 0.6525 W/mK$
Latent heat of vaporization	$i_{fg(2)} = 2360.2629 \times 10^3 J/kg$

The condensate flow rate in the second tube row is

$$m_{c(2)} = \frac{Q_{a(2)}}{i_{fg(2)}} = \frac{8.8513 \times 10^6}{2360.2629 \times 10^3} = 3.7501 kg/s$$

The effective condensation heat transfer area on the inside of the tubes is

$$A_{c(2)} = A_{c(1)} \times 58/57 = \ 924.4921 \times 58/57 = \ 940.7113 m^2$$

and the approximate overall heat transfer coefficient based on $A_{c(2)}$ is

$$U_{c(2)} H_t L_t = \frac{h_{ae(2)} A_{a(2)}}{2 n_{tb(2)} n_b} = \frac{514479.5906}{2 \times 58 \times 8} = 554.3963 W/K$$

The mass flow rate of air on one side of a finned tube in the second row is

$$m_{al(2)} = \frac{m_a}{2n_{tb(2)}n_b} = \frac{604.46}{2\times 58\times 8} = 0.6514\,kg/s$$

The condensation heat transfer coefficient is then

$$h_{c(2)} = 0.9245\left[\frac{9.5\times 0.6526^3\times 983.6061^2\times 9.8\times\cos(90-30)\times 2360.2629\times 10^3}{4.6791\times 10^{-4}\times 0.6514\times 1007.5319\ \ 59.3277-33.3248\ \times \left[1-\exp\ -554.3963/\ 0.6514\times 1007.5319\ \right]}\right]^{0.333}$$

$$= 17071.5323\,W/m^2K$$

The actual overall heat transfer coefficient for the second row is then

$$UA_{(2)} = \left[\frac{1}{514478.5766} + \frac{1}{17071.5323\times 940.7114}\right]^{-1} = 498509.502\,W/K$$

The effectiveness is then

$$e(2) = 1-\exp\left[-\frac{498509.502}{604.46\times 1007.5319}\right] = 0.5589$$

And the heat transfer rate is

$$Q_{a(2)} = 604.46\times 1007.5319\times\ 59.3277-33.3248\ \times 0.5589\ = 8.8513MW$$

This value compares well with the previous of $8.8513MW$.

Evaluation of the draft equation:

To evaluate the draft equation the fan operating point has to be determined. The approximate air temperature on the fan suction side is

$$T_{a3} \approx T_{a1} - 0.00975H_3 = 15.6 - 0.00975\times 25 = 15.3563℃\ \ 288.5063K$$

and the density is then

$$\rho_{a3} = \frac{84600}{287.08\times 288.5063} = 1.0214\,kg/m^3$$

The specific heat of the air is $c_{pa3} = 1006.474\,J/kgK$ and the volume flow rate through the fan is

$$V = \frac{m_a}{\rho_{a3}} = \frac{604.46}{1.0214} = 591.7733m^3/s \qquad \text{(E.6)}$$

This value is above the 573.148 m^3/s at the point of maximum efficiency for the fan, the fan will therefore operate effectively.

The fan static pressure rise at a reference density of $1.2\,\mathrm{kg/m^3}$ is then

$$\begin{aligned}\Delta p_{Fs(1.2)} &= 320.0451719 - 0.2975215484V \\ &\quad + 6.351486\times10^{-4}V^2 - 8.14\times10^{-7}V^3 \\ &= 320.0451719 - 0.2975215484\times591.7733 \\ &\quad + 6.351486\times10^{-4}(591.7733)^2 - 8.14\times10^{-7}(591.7733)^3 \\ &= 197.7157\,\mathrm{N/m^2}\end{aligned} \qquad \text{(E.4)}$$

Using the fan laws the real pressure rise at a density of $1.0214\,\mathrm{kg/m^3}$ can be calculated as

$$\Delta p_{Fs} = \Delta p_{Fs(1.2)}\ \rho_{a3}/\rho_r\ = 197.7157\times\ 1.0214/1.2\ = 168.2953\,\mathrm{kg/m^3} \qquad \text{(E.7)}$$

The corresponding fan coefficient is then defined as

$$K_{Fs} = 2\Delta p_{Fs}\rho_{a3}\left(\frac{A_c}{m_a}\right)^2 = 2\times168.2953\times1.0214\times\left(\frac{4\times604.46}{\pi\times9.1702}\right)^2 = 4.1043 \qquad \text{(E.8)}$$

Applying the fan laws to equation (E.5) the required shaft power at a density of 1.0214 kg/m^3 is

$$\begin{aligned}P_F &= \rho_{a3}/\rho_r \times\begin{pmatrix}186645.2333 - 59.413863388V \\ +0.476168398V^2 - 5.08308\times10^{-4}V^3\end{pmatrix} \qquad \text{(E.9)} \\ &= 1.0214/1.2\ \times\begin{pmatrix}186645.2333 - 59.413863388\times591.7733 \\ +0.476168398\times\ 591.7733\ ^2 - 5.08308\times10^{-4}\times\ 591.7733\ ^3\end{pmatrix} \\ &= 181.2183\mathrm{kW}\end{aligned}$$

The approximate air temperature directly upstream of the heat exchangers is

$$T_{a5} = T_{ai(1)} = T_{a1} + P_F/\ m_a\times c_{pa3}\ - 0.00975H_5 \qquad \text{(E.10)}$$

where $H_5 = H_3 + 0.5L_t\cos\theta\ = 25 + 9.5\times\cos\ 30\ = 29.1136\mathrm{m}$

Thus

$$T_{a5} = 15.6 + 181.2183\times10^3/\ 604.46*1006.474\ - 0.00975\times29.1136 = 15.6140^{\circ}\mathrm{C}$$

For the ratios and dimensionless distances that were given with the fan specifications heading the loss coefficients for the beams and screens are read from figures given by Kröger(2004).

The safety screen inlet loss coefficient $K_{si} = 0.1317$

The safety screen support beams loss coefficient $K_{bi} = 0.16523$

The total upstream loss coefficient is then

$$K_{up} = 0.1317 + 0.16523 = 0.29693$$

Similarly the downstream loss coefficients are found to be
$K_{do} = 0.2324 + 0.1584 = 0.3908$

The sum of the upstream and downstream loss coefficients is then
$K_{up} + K_{do} = 0.29693 + 0.3908 = 0.68773$

The heat exchanger loss coefficient under normal isothermal flow conditions is specified i.e.

$$K_{he} = 4177.08481 Ry^{-0.4392686} \qquad \text{(E.3)}$$

The characteristic flow parameter, Ry, is evaluated by using a mean dynamic viscosity, μ_{a56}, which is found at $T_{a56} = 0.5 \times (15.614 + 47.8586) = 31.7436°C$. The dynamic viscosity is then $\mu_{a56} = 1.8693 \times 10^{-5}\ kg/ms$. The characteristic flow parameter according to equation (2.39) is then

$$Ry = \frac{m_a}{A_{fr}\mu_{a56}\ \ n_{tb(1)}/n_{tb(2)}} = \frac{604.46}{27.55 \times 8 \times 1.8693 \times 10^{-5}\ \ 58/57} = 149290.7253 m^{-1}$$

Thus
$K_{he} = 4177.08481 \times 149290.7253^{-0.4392686} = 22.2886$

The contraction coefficient is

$$\begin{aligned} \sigma_{ci} &= 0.6144517 + 0.04566493\sigma_{21} - 0.336651\sigma_{21}^2 + 0.4082743\sigma_{21}^3 \\ &\quad + 2.672041\sigma_{21}^4 - 5.963169\sigma_{21}^5 + 3.558944\sigma_{21}^6 \\ &= 0.6144517 + 0.04566493 \times 0.875 - 0.336651 \times 0.875^2 + 0.4082743 \times 0.875^3 \\ &\quad + 2.672041 \times 0.875^4 - 5.963169 \times 0.875^5 + 3.558944 \times 0.875^6 \\ &= 0.77515 \end{aligned} \qquad \text{(E.11)}$$

The entrance contraction loss coefficient is then

$$K_{ci} = \left[\left(\frac{1}{\sigma_{21}}\right)\left(\frac{1}{\sigma_{ci}} - 1\right)\right]^2 = \left[\left(\frac{1}{0.875}\right)\left(\frac{1}{0.77515} - 1\right)\right]^2 = 0.1099 \qquad \text{(E.12)}$$

The effective mean inlet flow angle is

$$\begin{aligned} \theta_m &= 0.0019\theta^2 + 0.9133\theta - 3.1558 \\ &= 0.0019 \times 30^2 \ + \ 0.9133 \times 30 - 3.1558 = 25.95315° \end{aligned} \qquad \text{(E.13)}$$

The downstream loss coefficient, K_d, is composed of two parts, a jetting loss and a turning loss. There is also a loss of kinetic energy to the atmosphere. The jetting loss coefficient is

$$K_{dj} = \left[\begin{array}{l} -2.8919\ L_w/L_t + 2.9329(L_w/L_t)^2 \times \sin\theta - d_s/2L_t + L_w/L_t \ ^{-1} \\ \times\left[1 - 0.5 d_s/\ L_t\ \sin\theta\ +\ L_w/L_t\ \right]^{-1} \times (28/\theta)^{0.4} \\ +\left\{ \begin{array}{l} \exp\ 2.36987\ +\ 5.8601\times10^{-2}\theta - 3.3797\times10^{-3}\theta^2\ \times \\ \left[1 - 0.5\times d_s/\ L_t\ \sin\theta + L_w/L_t\ \right] \end{array} \right\}^{0.5} \\ \times\ 1 + L_w/(L_t \sin\theta)\ ^{-1} \end{array} \right]^2 \qquad \text{(E.14)}$$

$$= \left[\begin{array}{l} -2.8919\ 0.2/9.5\ + 2.9329(0.2/9.5)^2\ \times \sin 30 - 1.25/\ 2\times 9.5\ + 0.2/9.5\ ^{-1} \\ \times\left[1 - 0.5\times 1.25/\ 9.5\ \sin 30\ +\ 0.2/9.5\ \right]^{-1} \times (28/30)^{0.4} \\ +\left\{ \begin{array}{l} \exp\ 2.36987\ +\ 5.8601\times10^{-2}30 - 3.3797\times10^{-3}30^2\ \times \\ \left[1 - 0.5\times 1.25/\ 9.5\ \sin 30 + 0.2/9.5\ \right] \end{array} \right\}^{0.5} \\ \times\ 1 + 0.2/(9.5\times\sin 30)\ ^{-1} \end{array} \right]^2$$

$$= 1.9551$$

and the outlet loss coefficient

$$K_o = \left[\begin{array}{l} -2.89188\ L_w/L_t\ + 2.93291\ L_w/L_t\ ^2 \times\left[1 - 0.5 d_s/\ L_t\ \sin\theta + L_w/L_t\ \right]^3 \\ +1.9874 - 3.02783\ 0.5 d_s/\ L_t\ \sin\theta + L_w/L_t \\ +2.0817\ 0.5 d_s/\ L_t\ \sin\theta + L_w/L_t\ ^2 \end{array} \right]$$

$$\times\ \sin\theta - d_s/(2L_t) + L_w/L_t\ ^{-2} \qquad \text{(E.15)}$$

$$= \left[\begin{array}{l} -2.89188\ 0.2/9.5\ + 2.93291\ 0.2/9.5\ ^2 \\ \times\left[1 - 0.5\times 1.25/\ 9.5\ \sin 30 + 0.2/9.5\ \right]^3 \\ +1.9874\ - 3.02783\ 0.5\times 1.25/\ 9.5\ \sin 30 + 0.2/9.5 \\ +2.0817\ 0.5\times 1.25/\ 9.5\ \sin 30 + 0.2/9.5\ ^2 \end{array} \right]$$

$$\times\ \sin 30 - 1.25/(2\times 9.5) + 0.2/9.5\ ^{-2}$$

$$= 7.7126$$

Thus

$$K_d = 1.955121 + 7.70772 = 9.6677$$

The total loss coefficient for the heat exchanger taking into account kinetic energy loss at the outlet and the non-isothermal flow, is

$$K_{\theta t} = K_{he} + \left(2/\sigma^2\right) \times \frac{\rho_{a5} - \rho_{a6}}{\rho_{a5} + \rho_{a6}} + \frac{2\rho_{a6}}{\rho_{a5} + \rho_{a6}} \times \left(1/\sin\theta_m - 1\right)$$
$$\times \left[\left(1/\sin\theta_m - 1\right) + 2K_{ci}^{0.5} \right] + \frac{2K_d\rho_{a5}}{\rho_{a5} + \rho_{a6}} \qquad \text{(E.16)}$$
$$= 22.2886 + \left(2/0.48^2\right) \times \frac{1.0205 - 0.9180}{1.0205 + 0.9180} + \frac{2 \times 0.9180}{1.0205 + 0.9180} \times \left(1/\sin 25.9532 - 1\right)$$
$$\times \left[\left(1/\sin 25.9532 - 1\right) + 2 \times 0.1099_{ci}^{0.5} \right] + \frac{2 \times 9.6677 \times 1.0205}{1.0205 + 0.9180}$$
$$= 35.2974$$

The draft equation, given by equation (2.45) can now be evaluated. The equation has the following form

$$p_{a1}\left[\left(1 - 0.00975 \times 0.5 \times \cos\theta \times L_t/T_{a6}\right)^{3.5} - \left(1 - 0.00975 \times 0.5 \times \cos\theta \times L_t/T_{a1}\right)^{3.5} \right]$$
$$= K_{ts}/\left(2\rho_{a5}\right) \times \left(m_a/\left(n_b \times A_{fr}\right)\right)^2 + \left(K_{up} + K_{do}\right)/\left(2\rho_{a3}\right) \times \left(m_a/A_e\right)^2 \qquad \text{(2.45)}$$
$$- K_{Fs}/\left(2\rho_{a3}\right) \times \left(m_a/A_c\right)^2 + K_{\theta t}/\left(2\rho_{a56}\right) \times \left(m_a/\left(n_b A_{fr}\right)\right)^2$$

The harmonic mean density through the bundle is

$$\rho_{a56} = 2/\left(1/\rho_{a5} + 1/\rho_{a6}\right) = 2/\left(1/1.0205 + 1/0.9180\right) = 0.9666\,\text{kg/m}^3 \qquad \text{(E.17)}$$

The areas that will be needed in the draft equation are the following

$$A_c = \pi d_c^2/4 = \pi \times (9.170)^2/4 = 66.0433\text{m}^2 \qquad \text{(E.18)}$$

and

$$A_e = \pi\left(d_e^2 - d_h^2\right)/4 = \pi\left(9.170^2 - 1.4^2\right)/4 = 64.5039\text{m}^2 \qquad \text{(E.20)}$$

The left hand side of the draft equation is then

$$p_{a1}\left[\left(1 - 0.00975 \times 0.5 \times \cos\theta \times L_t/T_{a6}\right)^{3.5} - \left(1 - 0.00975 \times 0.5 \times \cos\theta \times L_t/T_{a1}\right)^{3.5} \right]$$
$$= 84600\left[\left(1 - 0.00975 \times 0.5 \times \cos 30 \times 9.5/321.0086\right)^{3.5} - \left(1 - 0.00975 \times 0.5 \times \cos 30 \times 9.5/288.75\right)^{3.5} \right]$$
$$= 4.1317\ \text{N/m}^2$$

and the right hand side

$$K_{ts} / \ 2\rho_{a5} \ \times \ m_a / \ n_b \times A_{fr} \ ^2 + \ K_{up} + K_{do} \ / \ 2\rho_{a3} \ \times \ m_a / A_e \ ^2$$
$$- K_{Fs} / \ 2\rho_{a3} \ \times \ m_a / A_c \ ^2 + K_{\theta t} / \ 2\rho_{a56} \ \times \ m_a / \ n_b A_{fr} \ ^2$$
$$= 1.5 / \ 2 \times 1.0205 \ \times \ 604.46 / \ 8 \times 27.55 \ ^2 + \ 0.68773 \ / \ 21.0214 \ \times \ 604.46 / 64.5039 \ ^2$$
$$- 4.1043 / \ 2 \times 1.0214 \ \times \ 604.46 / 66.0433 \ ^2 + 35.2974 / \ 2 \times 0.9666 \ \times \ 604.46 / \ 8 \times 27.55 \ ^2$$
$$= 4.1340 \, N / m^2$$

There is agreement between the two sides of the draft equation.

Appendix F: Sample calculation for the pressure and temperature distribution in the combining header

A schematic of the combining header is shown in figure 2.10. The combining header pressure distribution must be solved iteratively. The steam must be distributed in such a way that there are no discontinuities in the pressure distribution in the header and between the outlet pressures and the header pressures.

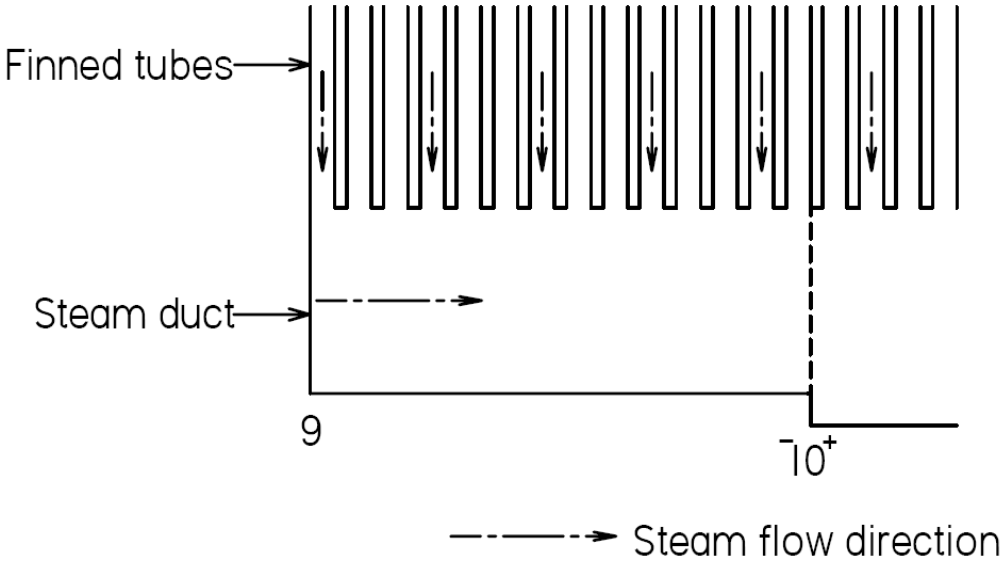

Figure F.1: Schematic of section of combining header

The combining header differs from the dividing header in two ways, the pressure decreases in the direction of the flow and the flow direction is not the same everywhere in the header. It is assumed that the condensate volume is small enough to ignore.

Header specifications

Header diameters:	$d_{9-10} = 0.41\text{m}$
	$d_{10-11} = 0.58\text{m}$
	$d_{11-12} = 0.71\text{m}$
	$d_{12-13} = 0.71\text{m}$
	$d_{13-14} = 0.58\text{m}$
	$d_{14-15} = 0.41\text{m}$
Length of fan unit:	$L = 11.8\text{m}$
Surface roughness:	$\varepsilon = 1\times10^{-3}\text{m}$

Inlet conditions

Divding header inlet steam temperature	$T_{vd} = 60°\text{C}$
Steam outlet quality	$x = 1$

There is no outflow out of the first tube of the first fan unit in figure 2.10. The pressure at 9 in figure F.1 is given as

$$p_9 = 19562.7437\,\mathrm{N/m^2}$$

and the corresponding steam temperature is according to equation (A.2.1)

$$\begin{aligned} T_{v9} &= 164.630366 + 1.832295x10^{-3}p_{v9} + 4.27215x10^{-10}p_{v9}^2 + 3.738954x10^{3}p_{v9}^{-1} \\ &\quad - 7.01204x10^{5}p_{v9}^{-2} + 16.161488\ln\ p_{v9} - 1.437169x10^{-4}p_{v9}\ln\ p_{v9} \\ &= 164.630366 + 1.832295x10^{-3}\ 19562.7437\ + 4.27215x10^{-10}\ 19562.7437\ ^2 \\ &\quad + 3.738954x10^{3}\ 19562.7437\ ^{-1} - 7.01204x10^{5}\ 19562.7437\ ^{-2} \\ &\quad + 16.161488\ln\ 19562.7437\ - 1.437169x10^{-4}\ 19562.7437\ \ln\ 19562.7437 \\ &= 59.5942°\mathrm{C}\ (332.7442\mathrm{K}) \end{aligned} \tag{A.2.1}$$

Under ideal conditions for a single row condenser the combining header receives excess steam. From the first condenser fan unit the combining header receives

$$m_{v9-10} = 0.196\mathrm{kg/s}$$

The steam pressure distribution is calculated in the following way:

The steam properties at 9 are used to calculate the pressure and temperature change under the first fan unit. The density is calculated with equation (A.2.3),

$$\begin{aligned} \rho_{v9} &= -4.062329056 + 0.10277044T_{v9} - 9.76300388\times10^{-4}T_{v9}^2 \\ &\quad + 4.475240795\times10^{-6}T_{v9}^3 - 1.004596894\times10^{-8}T_{v9}^4 + 8.89154895\times10^{-12}T_{v9}^5 \\ &= -4.062329056 + 0.10277044\ 332.7442\ - 9.76300388\times10^{-4}\ 332.7442\ ^2 \\ &\quad + 4.475240795\times10^{-6}\ 332.7442\ ^3 - 1.004596894\times10^{-8}\ 332.7442\ ^4 \\ &\quad + 8.89154895\times10^{-12}\ 332.7442\ ^5 \\ &= 0.1280\,\mathrm{kg/m^3} \end{aligned} \tag{A.2.3}$$

The dynamic viscosity is according to equation (A.2.4)

$$\begin{aligned} \mu_{v9} &= 2.562435\times10^{-6} + 1.816683\times10^{-8}T_{v9} + 2.579066\times10^{-11}T_{v9}^2 \\ &\quad - 1.067299\times10^{-14}T_{v9}^3 \\ &= 2.562435\times10^{-6} + 1.816683\times10^{-8}\ 332.7442\ + 2.579066\times10^{-11}\ 332.7442\ ^2 \\ &\quad - 1.067299\times10^{-14}\ 332.7442\ ^3 \\ &= 1.1070\times10^{-5}\,\mathrm{kg/ms} \end{aligned} \tag{A.2.4}$$

Since the combining header is closed at 9, there is no steam in the pipe. At 10 all the excess steam has entered the header and the mass flow rate is

$$m_{v10} = 0.196\mathrm{kg/s}$$

Since the mass flow rate in the header changes with position along the header the average mass flow rate between 9 and 10 was calculated to determine the frictional pressure change. The average mass flow rate is

$$m_{vm} = m_{v10^-}/2 = 0.196/2 = 0.098\,kg/s$$

The average steam speed for this section is then

$$v_{vm} = \frac{m_{vm}}{\rho_{v9} A_{cs}} \qquad (F.1)$$

where

$$A_{cs} = \frac{\pi d_{9-10}^2}{4} = \frac{\pi\ 0.41^{\ 2}}{4} = 0.13203 m^2$$

so from equation (F.1) the average steam speed is

$$v_{vm} = \frac{0.098}{0.1280 \times 0.13203} = 5.7989 m/s$$

The Reynolds number is calculated with equation (2.10)

$$Re = \frac{\rho_{v9} v_{vm} d_{8-9}}{\mu_{v9}} = \frac{0.1280 \times 5.7989 \times 0.41}{1.1070 \times 10^{-5}} = 2.7491 x 10^4 \qquad (2.10)$$

According to equation (2.9) the friction factor is

$$f_D = \frac{0.30864}{\left[\log\left\{\left(\frac{6.9}{Re}\right) + \left(\frac{\varepsilon/d_{9-10}}{3.7}\right)^{1.11}\right\}\right]^2} \qquad (2.9)$$

$$= \frac{0.30864}{\left[\log\left\{\left(\frac{6.9}{2.749 \times 10^4}\right) + \left(\frac{1 \times 10^{-3}/0.41}{3.7}\right)^{1.11}\right\}\right]^2}$$

$$f_D = 0.0289$$

The frictional pressure change in the section of combining header is calculated with equation (2.7)

$$p_9 - p_{10\ f} = \frac{1}{2} \frac{f_D L/2}{d_{9-10}} \rho_{v9} v_{vm}^2 \qquad (2.7)$$

$$= \frac{1}{2}\left(\frac{0.0289 \times 11.8}{0.41}\right) \times 0.1280 \times 5.7989^2 = 1.7901 N/m^2$$

The momentum pressure change for the section is calculated with the momentum pressure change term in equation (2.31).

$$p_9 - p_{10\ m} = -\frac{\rho_{v9}}{2} \alpha_c \left(v_{v9} - v_{v10^-}^2 \right) \qquad (F.2)$$

Bajura(1971) gives a graphic representation for α_c, the overall momentum correction factor, for different diameter ratios between the tube diameter and the diameter of the header. The diameter ratio is calculated as

$$\frac{d_l}{d_h} = \frac{0.0309}{0.41} = 0.075$$

and it was found that

$$\alpha_C \approx 2.6$$

From equation (F.2) it follows that

$$p_9 - p_{10\ m} = -\frac{0.1280}{2}\ 2.6\quad 0 -\ 2 \times 5.7989^{\ 2}\ = 22.3823\,\mathrm{N/m^2}$$

The pressure at 9 is then

$$p_{10^-} = p_9 -\ p_{v9} - p_{v10\ f} -\ p_{v9} - p_{v10\ m}$$
$$= 19562.7437 - 1.7901 - 22.3823 = 19538.5713\,\mathrm{N/m^2}$$

and the steam temperature is according to equation (A.2.1)

$$T_{v9} = 59.5676°\mathrm{C}\ \ 332.7176\mathrm{K}$$

At 10 there is a expansion pressure change due to the sudden increase in duct diameter. The steam density at 10^- is

$$\rho_{v10^-} = 0.1278\,\mathrm{kg/m^3} \qquad \text{(A.2.3)}$$

According to equation (2.68) the expansion pressure change is

$$\Delta p_{ve10} = \frac{\rho_{v10^-}}{2} v_{v10^-}^2\ \ \sigma_{9-10}^2 - \sigma_{9-10} \qquad \text{(2.68)}$$
$$= 0.1278 \times\ 11.5978^{\ 2} \left[\left(\frac{0.41^2}{0.58^2} \right)^2 - \left(\frac{0.41^2}{0.58^2} \right) \right]$$
$$= -4.2976\,\mathrm{N/m^2}$$

The pressure after the expansion is then

$$p_{10^+} = p_{10^-} - \Delta p_{ve10} = 19538.5713 + 4.2976 = 19542.8689\,\mathrm{N/m^2}$$

and the steam temperature is

$$T_{v10^+} = 59.5723°\mathrm{C}\ \ 332.7223\mathrm{K}$$

Shown in figure F.2 below is the pressure and temperature distribution in the combining header for the case described above.

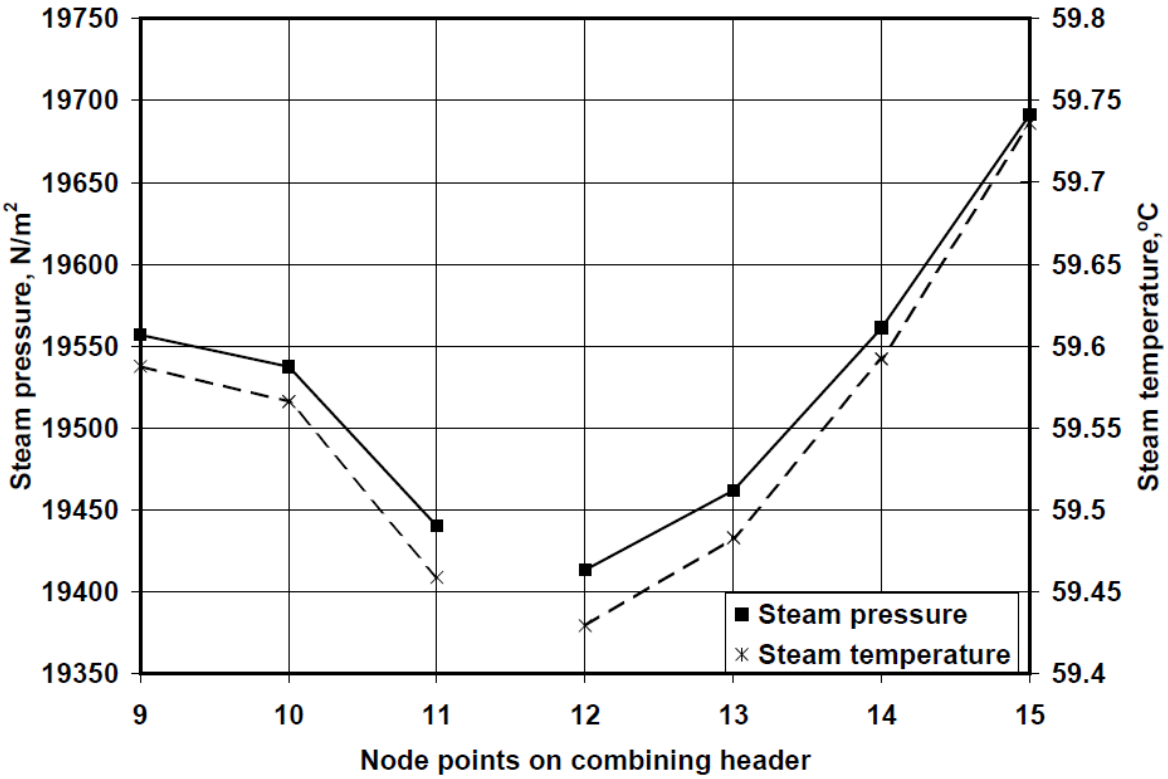

Figure F.2: Pressure and temperature distribution in combining header

Appendix G: Ambient pressure at different elevations for a given temperature distribution and ground level pressure

In figure 3.3 it is shown that each fan in the condenser receives air from different elevations. When the air temperature distribution is not uniform the fan inlet air temperatures will differ from fan to fan. The heat transfer of each condenser tube is a function of the difference in temperature between the air on the outside of the finned tube and the steam inside the finned tube and therefore the fan inlet air temperature must be determined.

To determine the inlet temperature and pressure for each fan in the condenser, the ambient temperature and pressure distributions must be known. The pressure at ground level and the temperature distribution is known, this information can be used to calculate the pressure at the different elevations. Equation (3.1) is used to approximate the temperature distribution

$$T_z = T_1 + 273.15\left(\frac{z}{z_r}\right)^{b_T} - 0.00975z$$

$$\approx T_1 + 273.15\left(\frac{z}{z_r}\right)^{b_T} \qquad (3.1)$$

where T_1 is in °C and measured close to ground level (typically 1 to 2 meters above ground) and z_1 is the elevation corresponding to T_1. The temperature distribution is known and therefore b_T can be solved for by an optimizing algorithm.

The pressure gradient of the air is given by

$$\frac{dp}{dz} = -\rho g \qquad (G.1)$$

For an isentropic change in air conditions

$$\frac{p}{\rho^{\gamma}} = \text{constant} \qquad (G.2)$$

Air can be assumed to be an ideal gas and therefore the density can be given as

$$\rho = \frac{p}{RT} \qquad (G.3)$$

Substitute equation (G.3) into equation (G.2) to find

$$p^{1-\gamma}RT = \text{constant} \qquad (G.4)$$

Differentiate equation (G.4) in term of z and simplify to find

$$\frac{(-\gamma)}{\gamma p}\frac{dp}{dz}+\frac{1}{T}\frac{dT}{dz}=0 \qquad \text{(G.5)}$$

By combining equations (G.1), (G.3) and (G.5) the temperature gradient can be found to be

$$\frac{dT}{dz}=-\frac{g(\gamma-1)}{\gamma R} \qquad \text{(G.6)}$$

For dry air with $\gamma = c_p/c_v = 1.4$, R = 287.08 J/kg K and g = 9.8 m/s^2 find

$$\frac{dT}{dz}=-0.00975\,K/m \qquad \text{(G.7)}$$

Equation (G.7) is known as the dry adiabatic lapse rate(DALR) and after integration an equation to generate the temperature distribution is found.

$$T_z = T_1 - 0.00975z \qquad \text{(G.8)}$$

Substitute equation (3.1) into equation (G.3) to find

$$\rho=\frac{p}{R\left(T_1+273.15\left(\frac{z}{z_r}\right)^{b_T}\right)} \qquad \text{(G.9)}$$

Substitute equation (G.9) into (G.1) to find

$$\frac{dp}{dz}=-\frac{pg}{R\left(T_1+273.15\left(\frac{z}{z_r}\right)^{b_T}\right)} \qquad \text{(G.10)}$$

Integrate and find

$$p_z = p_0 \exp\left[\frac{-g\ z^{1-b_T}-z_r^{1-b_T}}{T_1+273.15\ R\ 1-b_T\ z_r^{-b_T}}\right] \qquad \text{(3.2)}$$

where p_0 is the ground level pressure.

In figure G.1, the equation (G.8) is compared with two different temperature distributions. The one is a day time temperature distribution, while the other is a night-time air temperature distribution (inversion). Equation (G.8) is not accurate for these two distributions. For the day time distribution it predicts temperatures that are too high. The DALR is not applicable to temperature inversions, as can be seen from the figure. It can thus be seen that equation (G.8) can not be used for

inversions and a different method must be used to describe the distribution. The assumption that the process is isentropic is also rejected on grounds of figure G.1 and equation (3.1b) is used to describe the temperature distributions. Equation (3.2) can be used to calculate the pressure at different elevations for different temperature distributions.

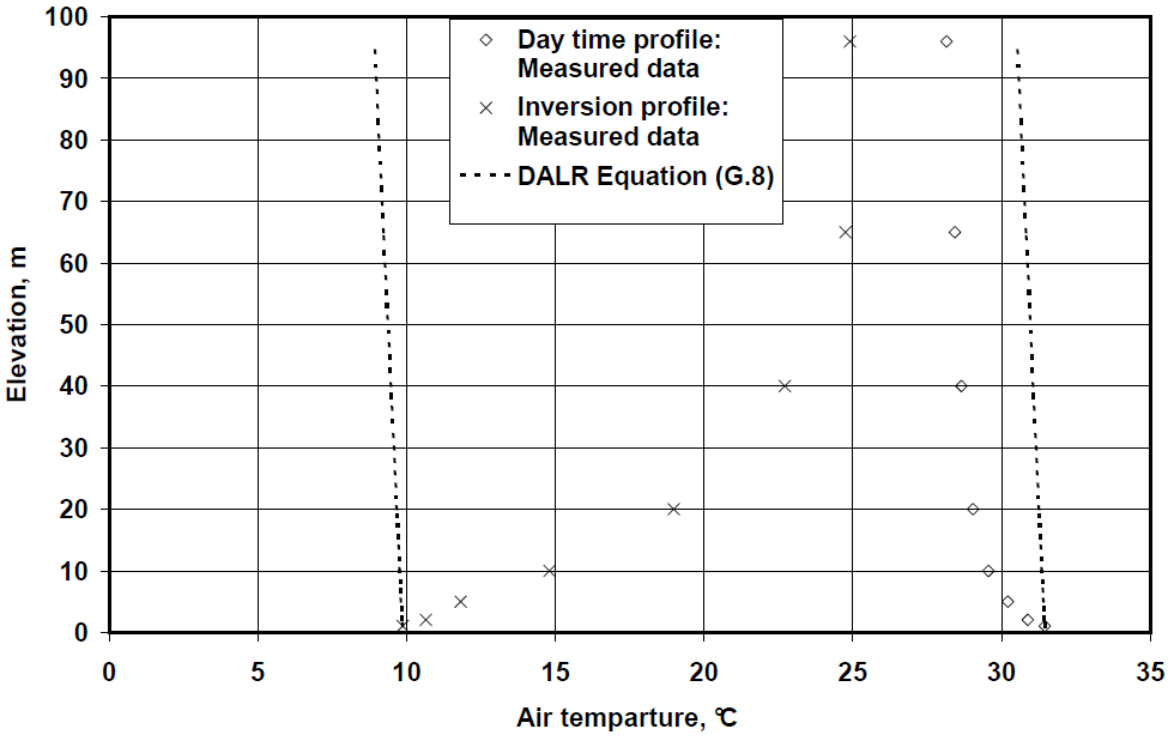

Figure G.1: Comparison measured data and equation (G.8) for a day time and inversion temperature distribution (also see figures 3.4 and 3.5)

To calculate the pressure change from ambient conditions to the inlet of the fan it is necessary to make a few assumptions. Firstly it is assumed that the ambient air is stationary and then accelerates to the fan and frictional effects in the air are ignored as these will be negligible.

Refering to figure 3.3 it can be seen that there will be elevation changes as the air is sucked into the fan, therefore there will be elevation pressure change:

$$p_{amb} - p_{Fi\ s} = \rho g \Delta z \qquad \text{(G.11)}$$

where Δz is measured from the centre of the intake elevation for each fan to the platform height. The speed of the air changes so there will be a momentum pressure change:

$$p_{amb} - p_{Fi\ m} = \frac{1}{2}\rho\ v_{amb}^2 - v_{Fi}^2$$

$$= -\frac{1}{2}\rho\ v_{Fi}^2 \qquad \text{(G.12)}$$

It is now possible to calculate the inlet pressure to the fan,

$$p_{Fi} = p_{amb} + \rho g \Delta z - \frac{1}{2}\rho\ v_{Fi}^2 \qquad \text{(G.13)}$$

where p_{amb} is the average ambient pressure for each intake elevation, p_{Fi} is the inlet pressure to the fan and v_{Fi} is the speed at the fan inlet

$$v_{Fi} = m_a / \rho A_c \qquad \text{(G.14)}$$

where m_a is the air mass flow through the fan and A_c is the fan inlet area.

It is necessary to calculate the average pressure for each fan inlet elevation. The average was calculated as follows:

$$p_{amb} = \frac{\sum_{j=1}^{n} p_{\ j} \times \Delta z}{\left| z_{\ i+1} - z_i \right|} \qquad \text{(3.4)}$$

where $\Delta z = |z_{(i+1)} - z_i|/n$ and n is the number of points taken between $z_{(i+1)}$ and z_i.

The process as the air is sucked into the fans is assumed to be isentropic. The isentropic relation between temperature and pressure can be used to calculate the air temperature at the inlet to the fan from the pressure at the inlet and the starting conditions. The relation is:

$$Tp^{(-\gamma)/\gamma} = \text{constant} \qquad \text{(G.15)}$$

therefore

$$T_{Fi} = T_{iamb}\left(\frac{p_{iamb}}{p_{Fi}}\right)^{\frac{1-\gamma}{\gamma}} \qquad \text{(G.16)}$$

where T_{amb} is the starting temperature, T_{Fi} is the fan inlet temperature and γ is the specific heat ratio. The specific heat ratio is assumed to be constant while the air is sucked into the fan. The specific heat ratio is calculated from the ambient conditions for each of the fans. T_{iamb} is the average temperature for the intake elevation range of the i^{th} fan. It is calculated as follows:

$$T_{iamb} = \frac{1}{z_{\ i+1\ a} - z_{ia}} \int_{z_{ia}}^{z_{\ i+1\ a}} \left(T_1 + 273.15 \left(\frac{z}{z_1} \right)^{b_T} \right) dz$$

$$T_{iamb} = \frac{T_1 + 273.15 \quad z_{(i+1)a}^{\ b_T+1} - z_{ia}^{\ b_T+1}}{z_{(i+1)a} - z_{ia} \quad z_1^{b_T} \quad b_T + 1} \qquad \text{(3.3)}$$

where T_{iamb} is the average temperature the between $z_{(i+1)}$ and z_i, z_1 is the elevation of T_1,the ground level temperature, which is at 1m.

Figures 3.4 and 3.5 show the temperature distributions for a day time temperature distribution and a night time temperature distribution(inversion). Tables G.1 and G.2 show the ambient and inlet conditions for each of the fans in the air-cooled condenser for the day time and night time temperature distributions repectively.

Table G.1: Ambient and inlet fan conditions for day time distributions

Fan	Ambient conditions		Inlet conditions	
	Pressure, N/m^2	Temperature, ^oC	Pressure, N/m^2	Temperature, ^oC
1	90928.3270	30.0059	90499.1897	29.5971
2	90779.7581	29.1028	90503.9555	28.8406
3	90625.9961	28.7076	90503.9976	28.5917
4	90472.3290	28.4513	90503.9593	28.4814
5	90318.8089	28.2609	90503.7474	28.4367
6	90165.4623	28.1092	90503.3266	28.4307

From the values in table G.1 it can be seen that the inlet temperature changes very little from the ambient condition, to the inlet temperature. It is interesting to note that the inlet pressure for each fan is almost identical even though the ambient pressure varies for each fan.

Figure 3.5 shows the temperature distribution for a night time temperature inversion. Equation (3.1) is not as accurate as for the day time temperature distribution. The uncertainty for the prediction of the temperature shown in figure 3.5 is greater than the change in temperature from the ambient condition to fan inlet condition. It was therefore decided to use the ambient conditions as inlet conditions for the fan units. Shown below is the ambient and inlet conditions for the distribution in figure 3.5.

Table G.2: Ambient and inlet fan conditions for night time distributions

Fan	Ambient conditions		Inlet conditions	
	Pressure, N/m^2	Temperature, ^oC	Pressure, N/m^2	Temperature, ^oC
1	90924.8637	16.0369	90479.2748	15.6320
2	90770.4429	19.9678	90488.8343	19.7082
3	90612.4801	21.7118	90489.7089	21.5978
4	90455.5619	22.8500	90489.4618	22.8816
5	90299.4407	23.6993	90488.5406	23.8765
6	90143.9894	24.3779	90487.1162	24.7004

It would seem that the inlet pressure is more dependant on the ambient ground level pressure and platform height than on the ambient temperature distribution. It must however be noted that it was assumed that all the fans deliver the same mass flow rate for the inlet conditions in tables G.1 and G.2. A sample calculation for each of the distributions in included in the appendix.

Appendix H: Sample calculation for inlet conditions to air-cooled condenser fan units

In this section the inlet conditions to the fans will be calculated for a temperature distribution. The temperature distribution is shown in figure 3.4, while figure H.1 shows the air pressure distribution. First the ambient temperature and pressure for each fan will be calculated and then the pressure changes to the fan inlets. The inlet conditions of the fans can then be calculated. The ground level pressure, p_0, is assumed to be 91 000 N/m^2.

The pressure profile for the air temperature distribution shown in figure 3.4 can be calculated using equation (3.2). The pressure profile is shown in figure H.1.

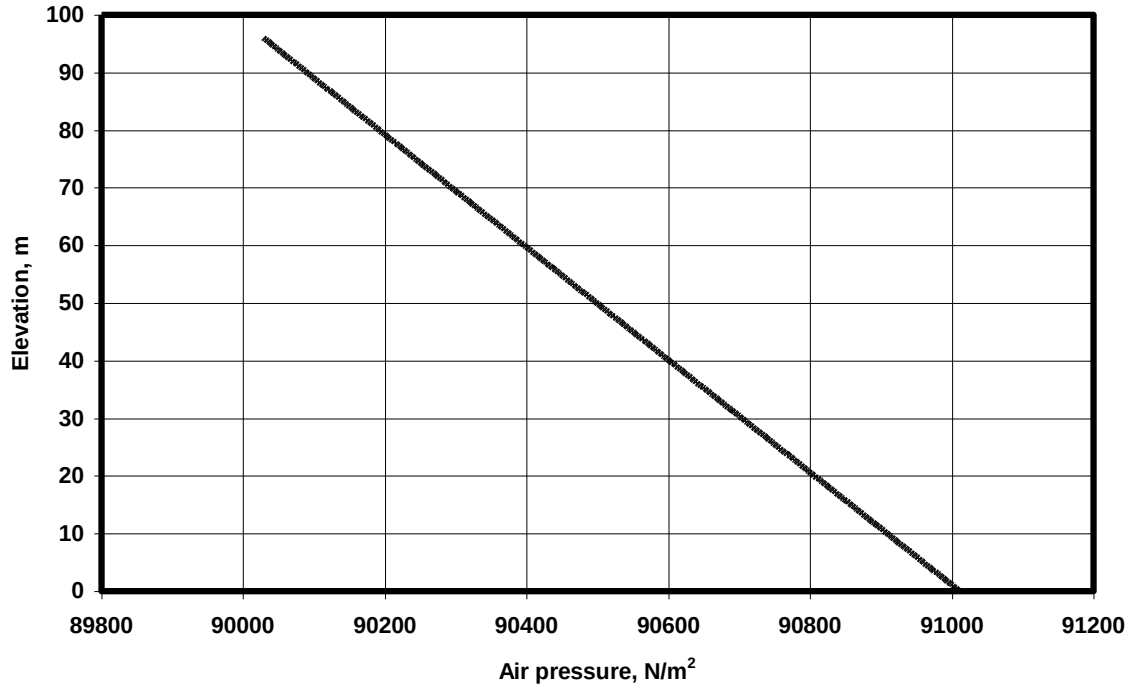

Figure H.1: Day time pressure profile

The following constants are used in this calculation in the calculation of the inlet conditions the fans

Temperature at one meter:	$T_{a1} = 304.6\text{K}$
Elevation of T_1:	$z_1 = 1\text{m}$
Ground level air pressure:	$p_{a0} = 91000\,\text{N/m}^2$
Exponent in equation (3.1)	$b_T = -0.0025$
Fan mass flow rate:	$m_a = 641.67\,\text{kg/s}$
Fan casing diameter:	$d_c = 9.17\text{m}$

It is assumed that the air-cooled condenser is free standing and essentially two-dimensional. Equation (3.3) is used to calculate the average ambient temperature for each of the fans.

Fan 1: $z_{1a} = 1\text{m}$ and $z_{2a} = 15\text{m}$

$$T_{F1a} = \frac{T_1\left(z_{2a}^{b_T+1} - z_{1a}^{b_T+1}\right)}{\left(z_{2a} - z_{1a}\right)z_1^{b_T}\left(b_T+1\right)} \tag{3.3}$$

$$T_{F1a} = \frac{304.6\left(15^{-0.0025+1} - 1^{-0.0025+1}\right)}{\left(15-1\right)^{-0.0025}\left(-0.0025+1\right)} = 303.156\text{K}\left(30.006°\text{C}\right)$$

Equation (3.4) is used to calculate the average ambient pressure for each fan. The calculation was done numerically and only the final step will be shown:

Fan 1:

$$p_{F1a} = \frac{1272996.522}{15-1} = 90928.323\,\text{N/m}^2$$

The inlet fan conditions can now be calculated from the ambient conditions using equations (G.13) and (G.16). The density of the air is assumed to be constant and the ambient pressure and temperature of each fan is used to calculate the density. For the elevation pressure change, the difference in elevation between the platform and the centre of each range from which a fan draws in air was used. The inlet conditions for fan 1 are calculated below.

The air density for fan 1 is according to equation (G.3)

$$\rho_{F1a} = \frac{p_{F1a}}{RT_{F1a}} = \frac{90928.323}{287.08 \times 303.1559} = 1.0448\,\text{kg/m}^3 \tag{G.3}$$

The momentum pressure change is calculated with equation (G.12)

$$\left(p_{amb} - p_{Fi1}\right)_m = -\frac{1}{2}\rho_{F1a}v_{Fi1}^2 \tag{G.12}$$

where

$$v_{Fi1} = \left(\frac{m_a}{\rho_{F1a}\left(\pi d_c^2/4\right)}\right) = \frac{641.67}{1.0448\left(\pi 9.17^2/4\right)} = 9.2993\,\text{m/s} \tag{G.14}$$

so

$$\left(p_{amb} - p_{Fi1}\right)_m = -\frac{1.0448}{2}\left(9.2993^2\right) = -45.1756\,\text{N/m}^2$$

The static pressure change is calculated with equation (G.11)

$$\left(p_{amb} - p_{Fi1}\right)_s = \rho_{F1a}g\Delta z_1 = 1.0448 \times 9.8 \times -37.5 = -383.964\,\text{N/m}^2 \tag{G.11}$$

The inlet air pressure to fan 1 is then according to equation (G.13)

$$p_{Fi1} = p_{F1a} + p_{amb} - p_{Fi1\ m} + p_{amb} - p_{Fi1\ s} \quad \text{(G.13)}$$
$$= 90928.323 - 45.1756 - 383.964$$
$$= 90479.27\ \mathrm{N/m^2}$$

The inlet air temperature for fan 1 is calculated with equation (G.16)

$$T_{Fi1} = T_{F1a}\left(\frac{p_{F1a}}{p_{Fi1}}\right)^{\frac{1-\gamma}{\gamma}} \quad \text{(G.16)}$$

where the specific heat ratio is calculated at T_{F1a} is found to be

$$\gamma = \frac{c_{pa}}{c_{va}} = \frac{1007.002}{719.922} = 1.399$$

so

$$T_{f1i} = 301.34\left(\frac{90928.323}{91267.1114}\right)^{\frac{1-1.399}{1.399}} = 303.4776\mathrm{K}$$